ORNL/TM-2007/079

Monte Carlo Simulation for LINAC Standoff Interrogation of Nuclear Material

June 2007

Prepared by

Shaun Clarke
Marek Flaska
Thomas Miller
Vladimir Protopopescu
Sara Pozzi

ORNL/TM-2007/079

Nuclear Science and Technology Division

MONTE CARLO SIMULATION FOR LINAC STANDOFF INTERROGATION OF NUCLEAR MATERIAL

S.D. Clarke[*,1], M. Flaska[2], T.M. Miller[2], V. Protopopescu[2], and S.A. Pozzi[2]

[1]*School of Nuclear Engineering, Purdue University, West Lafayette, IN 47907*
[2]*Oak Ridge National Laboratory, Oak Ridge, TN 37831*

Date Published: June 2007

Prepared by
OAK RIDGE NATIONAL LABORATORY
P.O. Box 2008
Oak Ridge, Tennessee 37831-6285
managed by
UT-BATTELLE, LLC
for the
U.S. DEPARTMENT OF ENERGY
under contract DE-AC05-00OR22725

[*] On research assignment at Oak Ridge National Laboratory.

CONTENTS

Page

LIST OF FIGURES

Figure **Page**

Figure **Page**

Figure **Page**

Figure **Page**

LIST OF TABLES

Table **Page**

ABSTRACT

The development of new techniques for the interrogation of shielded nuclear materials relies on the use of Monte Carlo codes to accurately simulate the entire system, including the interrogation source, the fissile target and the detection environment. The objective of this modeling effort is to develop analysis tools and methods—based on a relevant scenario—which may be applied to the design of future systems for active interrogation at a standoff. For the specific scenario considered here, the analysis will focus on providing the information needed to determine the type and optimum position of the detectors. This report describes the results of simulations for a detection system employing gamma rays to interrogate fissile and nonfissile targets. The simulations were performed using specialized versions of the codes MCNPX and MCNP-PoliMi. Both prompt neutron and gamma ray and delayed neutron fluxes have been mapped in three dimensions. The time dependence of the prompt neutrons in the system has also been characterized

For this particular scenario, the flux maps generated with the Monte Carlo model indicate that the detectors should be placed approximately 50 cm behind the exit of the accelerator, 40 cm away from the vehicle, and 150 cm above the ground. This position minimizes the number of neutrons coming from the accelerator structure and also receives the maximum flux of prompt neutrons coming from the source. The lead shielding around the accelerator minimizes the gamma-ray background from the accelerator in this area. The number of delayed neutrons emitted from the target is approximately seven orders of magnitude less than the prompt neutrons emitted from the system. Therefore, in order to possibly detect the delayed neutrons, the detectors should be active only after all prompt neutrons have scattered out of the system. Preliminary results have shown this time to be greater than 5 μs after the accelerator pulse.

This type of system is illustrative of a host of real-world scenarios of interest to nonproliferation and homeland security. Due to the multistep procedure of the MCNPX/MCNP-PoliMi code system, the analysis of somewhat modular – meaning that changing details such as the detector type, position, or surroundings does not require a re-calculation of the source-target interactions. This feature allows for efficient parametric analysis of numerous system parameters without recomputing the constant source-target behavior. Such efficient analysis mechanisms could prove invaluable in the design and future deployment of an active interrogation detection system.

1. INTRODUCTION

1.1. Project Description

Active measurements based on the use of photon sources from accelerators to induce fission show promise in many applications in nuclear nonproliferation, international safeguards, nuclear material control and accountability, national security, and counter-terrorism programs. A complete active interrogation system may be understood as a series of the following steps:

1. A linear electron accelerator (LINAC) produces an electron beam.
2. The electron beam strikes a target producing photons. Secondary neutrons are also produced.
3. The photons are collimated into a beam which strikes the target to be interrogated producing neutrons and gamma rays.
4. This radiation is transported to the detectors.
5. A specific detector response is produced through interactions within the detector material.
6. The timing and energy of the detected particles may be used to discriminate radiation created in the target and other sources of background radiation.

This report describes the results for steps 1 through 3 performed with specialized versions of the codes MCNP-X [1] and MCNP-PoliMi [2]. The objective of these simulations was to study the prompt and delayed response of unshielded fissile material to interrogation with a portable linear electron accelerator (LINAC) source of high energy photons. The LINAC source is assumed to be transportable on a small vehicle, and photon collimation is obtained with a portable lead collimator. This type of system is illustrative of a host of real-world scenarios of interest to nonproliferation and homeland security, namely active interrogation at a standoff.

Numerous simulations were performed to compute the neutron and photon flux inside the vehicle, fissile material, and surroundings. Initial simulations were performed to determine the bremsstrahlung photon source in energy and angular distribution using electrons as source particles. Subsequent simulations were used to determine the distribution and type of photonuclear events occurring in the target. Prompt, or "beam on," neutron and photon fluxes and delayed, or "beam off," neutron fluxes were then simulated for the system under consideration. These results are useful for the selection and/or development of a neutron and gamma ray detector system that could be used to detect prompt and delayed radiation emissions following the interrogation of a fissile sample.

The analysis has been carried out in four primary steps: (1) LINAC source modeling and characterization, (2) steady-state mapping of the neutron and photon fields, (3) time-dependant behavior of the neutron and photon fields, and (4) evaluation of the delayed neutron source.

1.2. MCNP Model Description

These analyses were performed using the MCNPX/MCNP-PoliMi code system [2]. Figure 1 shows the conceptual system with the LINAC being contained inside a vehicle and the detectors mounted on the sides (hypothetically). The objective of this modeling effort is to develop analysis tools and methods based on a relevant scenario which may be applied to the design of future systems for active interrogation at a standoff. For the specific scenario considered here, the

analysis will focus on providing the information needed to determine the type, and optimum position of the detectors.

Several assumptions were necessary to create a MCNP model of this system. The walls of the vehicle were assumed to be 0.63-cm-thick stainless steel. The LINAC was assumed to occupy an air-filled volume of 150 × 50 × 50 cm. The shielding around the LINAC was 7.62 cm of natural lead on all sides except for the front, which was 15.24 cm. The collimator opening was conical in shape with its diameter decreasing from 2.54 cm to 1.905 cm. All air was modeled at a relative humidity of 45% and the soil contained 20% water. The target material was a 5-kg (3.9979-cm radius) sphere of depleted uranium (100% ^{238}U) placed 5 m from the LINAC along the beamline, 1.5 m above the ground. This target size and shape is the design standard used in active interrogation systems.

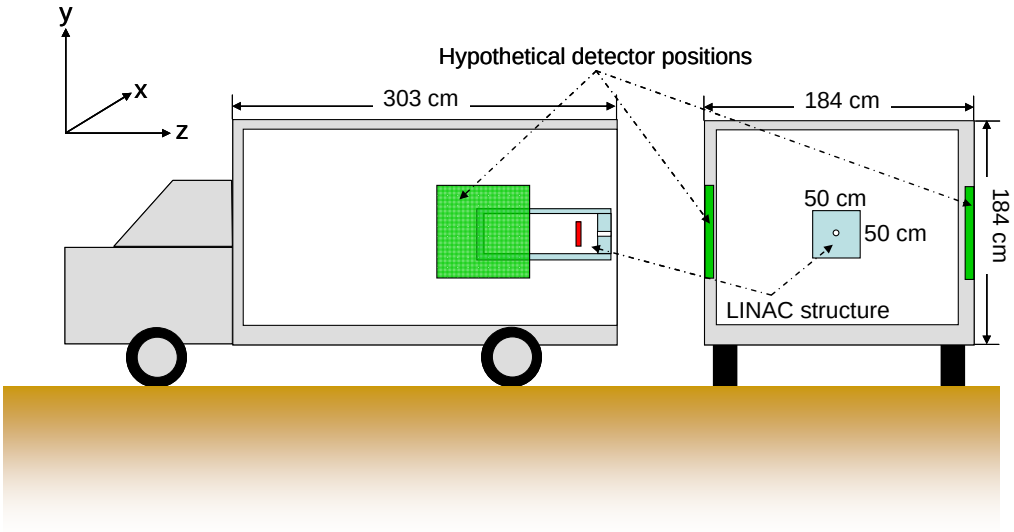

Figure 1. Illustration of the conceptual system including the LINAC and containment vehicle. The detectors shown were not modeled and are for illustrative purposes only.

The model was used to calculate flux maps in the *x*-*y* and *x*-*z* planes at various *z* and *y* locations, respectively. In order to compute the fluxes in the *x*-*y* plane, a series of tally volumes was added to the model; each of the planes shown extends 3 m in both the ±*x* and ±*z* directions. A fixed grid of 10 × 10 × 10 cm^3 was used to compute the volume-averaged flux in the *x*-*y* plane. The space behind the LINAC was the primary region of interest in the model—based on both physics and geometric considerations—and is the most likely location for the detectors. Therefore, a higher concentration of tally volumes was applied in this area. Figure 2 shows these regions.

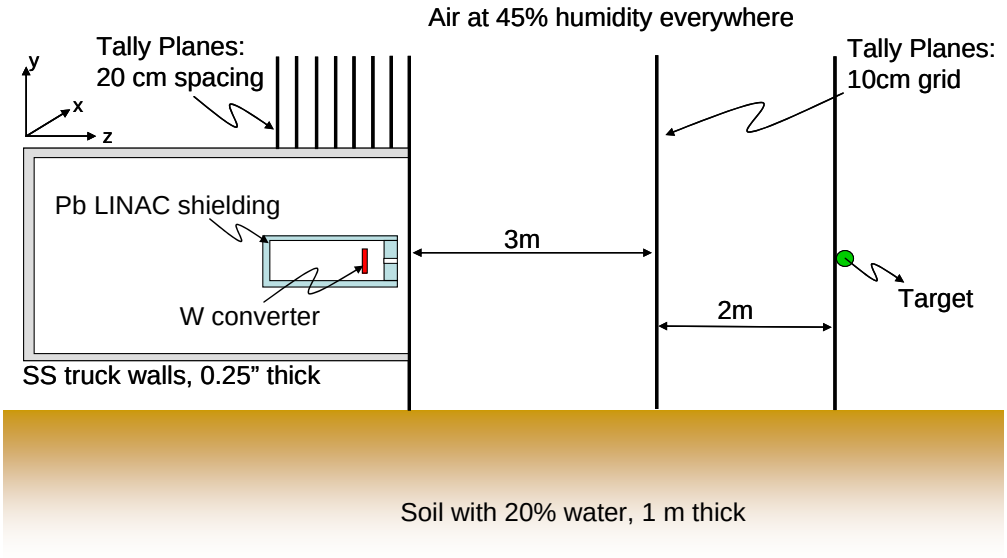

Figure 2. MCNP model illustration showing the location of the *x*-*y* plane tally regions.

The flux in the *x*-*z* plane was computed using a 2 × 2 × 2-cm^3 grid at several positions of interest in the *y*-direction:

1. below the vehicle (y = -149 cm)
2. just inside the vehicle (y = -90.44 cm)
3. half-way between the shielding and vehicle wall (y = -62 cm)
4. just outside the LINAC shielding (y = -33.62)
5. just inside the LINAC shielding (y = ±24 cm)
6. the geometric mid-plane (y = 0 cm)

The remainder of this report is organized as follows: Section 2 describes the specification of a photon source generated by the LINAC. Section 3 presents the results from the attenuation and angular spread of the photon beam. Section 4 describes the neutron and photon fluxes in the model geometry. Section 5 describes the time and energy-dependence of the neutron flux distributions. Section 6 presents the modeling of photonuclear events in the target material. Section 7 describes the delayed neutron production. Finally, Section 8 summarizes our results to date and indicates possible research directions. Appendixes A–H contain input files and map error data.

2. SOURCE MODELING DESCRIPTION

2.1. Source Model

The proposed source of this active interrogation system is a compact portable LINAC. The characteristics of this accelerator were assumed:

- Electron energy of 25 MeV ± 5%
- Repetition rate of 120 Hz
- Pulse time width between 500 and 2500 ns

- Charge per pulse of 25 nC

These characteristics result in approximately 1.872e13 electrons per second:

$$\frac{25nC}{pulse}\cdot\frac{120\,pulse}{s}\cdot\frac{C}{10^{9}nC}\cdot\frac{electron}{1.602\cdot10^{-19}C}=1.872e13\ \ electrons/s$$

In order to make the source model more realistic, variations in three of the beam parameters were simulated using typical values seen at electron accelerator facilities. First, the electron energy was sampled with a variation of plus-or-minus 5%. Secondly, the beam direction was sampled with a variation of ±1º with respect to the beam axis. Finally, the electron position was sampled inside of a 0.25-cm radius around the beam axis. In all simulations utilizing an electron source (input file shown in Appendix A), these three parameters were sampled uniformly between the maximum and minimum allowable values, the particles always start on the upstream side of the tungsten converter, and the beam axis passes through the radial center of the opening in the beam collimator as shown in Figure 1.

2.2. Photon Source

Beginning the simulations with a bremsstrahlung photon source directly, instead of an electron source, significantly reduces the computational time required for each calculation. Charged particle transport in Monte Carlo is computationally inefficient due to the continuous slowing down model that is applied; transporting only photons and electrons is an inherently simpler problem. By performing one coupled neutron-electron-photon simulation of the bremsstrahlung spectrum exiting the electron accelerator, a position-, energy-, and angular-dependent photon spectrum may be generated. This source—which is valid only for the specific set of LINAC properties applied here—can then be used directly as a source in subsequent calculations of the photonuclear spectrum in the target.

There are two possible methods to calculate the desired bremsstrahlung spectrum. The most accurate method is to have MCNPX write a surface crossing file that can be read as a source by other MCNPX calculations. The second is to create a surface tally in MCNPX that has a sufficiently large number of energy, angular, and spatial bins to accurately represent the photons leaking from the accelerator shielding. The second method was chosen because the first requires writing a binary file, which can become very large and also be platform- and/or compiler-dependent.

The surface tally that was created in MCNPX tallied all photons crossing the plane on the outside surface of the accelerator shielding. This surface is the closest to the target area and perpendicular to the beam axis as shown in Figure 1. The position, energy, and angular segmentation of the tally are listed below:

- The surface was divided into 27 radial rings centered on the beam axis. The outside radii of each ring (the first being a disc not a ring) in centimeters are 0.47625, 0.9525 (this corresponds to the radius at the exit of the beam collimator), 1.27 (this corresponds to the radius at the entrance of the beam collimator), 2.27 to 5.27 by steps of 1; 7.27, 9.27 to 18.27 by steps of 3; 20.27, 22.86 to 46.86 by steps of 2, and 50. The area outside of the 50-cm radius was tallied as one large bin.

- The energy range was divided into 104 equally spaced bins from 4 MeV to 30 MeV in steps of 0.25 MeV.
- The angles were divided into 45 bins, where the direction parallel to the beam axis moving from the accelerator towards the target was the 0º angle. The upper angles of these bins in degrees are: 0.1 to 3 in steps of 0.1, 5, 7.5; 10 to 40 in steps of 5; 50 to 90 in steps of 10; and 180.

In order to test the equivalence of this position, energy, and angular-dependent photon source, tally results in the target were compared to those obtained directly using the electron source. The current of photons entering a 5-cm radius spherical target and with zero importance was tallied in the MCNPX calculation. The importance was set to zero inside the sphere to be certain that only photons entering the sphere were counted. The photon current was calculated with the sphere in three different locations along the beam axis: 1 m, 5 m, and 10 m from the beam collimator. Table 1 shows a comparison of the photon current on this sphere for the electron and photon sources at these locations.

Table 1. First comparison of photon source to electron source

Distance of sphere from collimator (m)	Photon current with electron source (γ/s)	Photon current with photon source (γ/s)	Ratio of photon source to electron source
1	1.2410e11	1.2392e11	0.9985
5	1.9552e10	2.3082e10	1.1805
10	5.2819e9	5.7262e9	1.0841

The results in Table 1 are encouraging; however, it is unexpected that the comparison at 10 m is better than at 5 m. One possibility is that the current at 10 m, relative to the current at 5 m, consists of photons closer to the beam axis with very small scattering angles. The areas closest to the beam axis and the smallest scattering angles have been modeled with the finest detail. Thus, if the current at 5 m is dominated by photons in coarse position or angular bins, then a larger difference is expected. With this in mind, the tally bins were modified as follows:

- The surface was divided into 45 rings where the outside radius of each in centimeters is 0.15875 to 1.27 in steps of 0.15875; 1.77 to 7.27 in steps of 0.5; 8.27 to 14.27 in steps of 1; 16.27 to 48.27 in steps of 2; and 50. Again, the area outside of the 50-cm radius was tallied as one large bin.
- The energy bins were unchanged.
- The angles were divided into 112 bins where the upper angle of each bin in degrees is 0.1 to 10 in steps of 0.1; 15 to 40 in steps of 5; 50 to 90 in steps of 10; and 180.

Unfortunately, this increase in the spatial and angular resolution had no significant effect on the comparison of the photon current tallies. Table 2 shows the comparison of the photon current tallies with the electron source and this new photon source.

Table 2. Second comparison of photon source to electron source

Distance of sphere from collimator (m)	Photon current with electron source (γ/s)	Photon current with photon source (γ/s)	Ratio of photon source to electron source
1	1.2410e11	1.2399e11	0.9991
5	1.9552e10	2.3044e10	1.1786
10	5.2819e9	5.7319e9	1.0852

At this point, there are two options for improving the agreement of the photons source: either the MCNPX surface crossing file can be used or even finer resolution is needed in the photon current tally bins. Finer resolution is most likely not needed for the energy or spatial bins, but it may be needed in the angular bins. However, the exact region of the angular distribution requiring the finer resolution is not known. Three possibilities exists.

1. The bin size above 10º needs to be decreased.
2. The bin size below 10º needs to be decreased.
3. Both regions require finer resolution.

In the future, each of these possibilities should be considered in detail. However, considering that the majority of the photons crossing the tally surface pass through the collimator opening, it seems likely that the angular resolution needs to be refined for angles less than 10 º. Finer resolution is probably only needed for angles less than a few degrees. It is important to note that

at some point, the resolution can become so fine that it becomes difficult to obtain convergence of the statistical tally solution in MCNPX.

The following six figures (Figures 3–8) display the photon current tally results used to construct a picture of what the photon source looks like. Figure 3 shows the current and flux as a function of radius from the beam axis. The blue curve in Figure 3 is the current in each radial zone and the red curve is the flux or the current normalized to the area of each radial zone. Since the size of the radial zones varies, nonphysical increases in the current are present. However, the flux, which has been normalized to the area of each radial zone, does not show any of these nonphysical increases. The increase in the flux in Figure 3 around 32 cm occurs because this is the edge of the LINAC shielding. Figure 4 shows the current in the inner-most spatial tally region (circle) as a function of energy. The current is only shown in Figure 4 because all the energy tally bins were 0.25-MeV wide. Figure 5 shows the current in the inner-most spatial tally region and energy group from 4 MeV to 4.25 MeV as a function of angle. Figure 6 shows the current as a function of angle for this same inner-most spatial tally region, but for the energy group from 19.75 MeV to 20 MeV. Like Figure 3, Figure 5 and Figure 6 show the current with a blue curve and the flux or the current normalized to the width of the angular bins with a red curve. Figure 7 and Figure 8 are the same as Figure 5 and Figure 6, respectively, but show more detail from 0 to 10º (in Figure 7) and from 0 to 1º (in Figure 8). However, note that in Figure 7 and Figure 8 only the flux is shown along with the one-sigma standard deviation. In Figure 5 and Figure 6 the peak flux is less than 1º. This peak is due to the photons created in the tungsten converter that pass directly through the collimator opening. In Figure 5, the number of photons at broader angles increases due to photon build up in the LINAC shielding. In Figure 6, there is no photon build up because the energy is close to the electron beam energy (19.75 to 20 MeV). In Figure 7, the flux minimum between about 0.7 and 4.2º is suffering from poor statistical convergence. In fact, some parts of the curves are missing (i.e., there were no tallies in that angular bin), and in some cases, the minus-one-sigma curve only is missing, which is due to a relative error of 1.0.

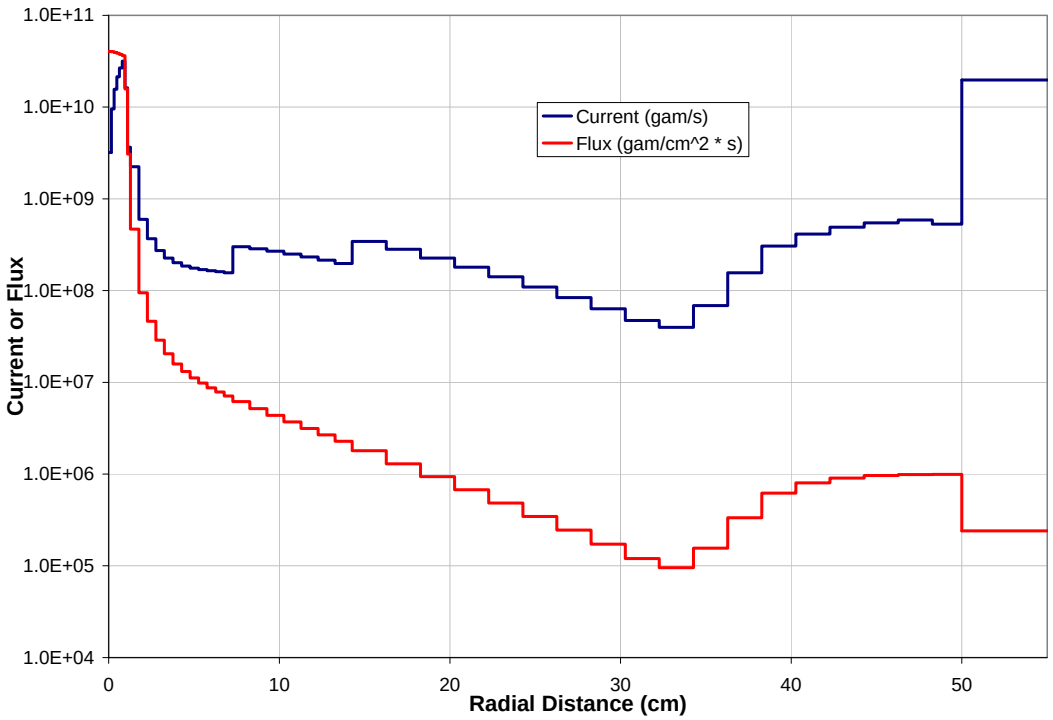

Figure 3. Photon source intensity and flux vs. radial distance from beam axis.

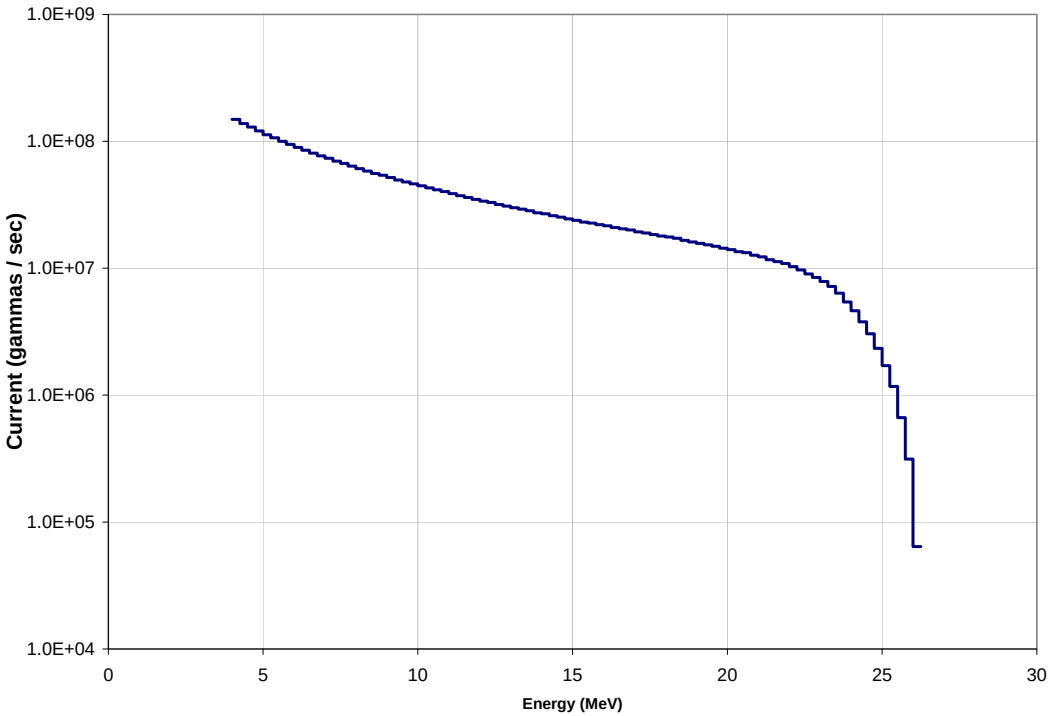

Figure 4. Photon source current for the first radial region (R < 0.15875 cm) vs. energy.

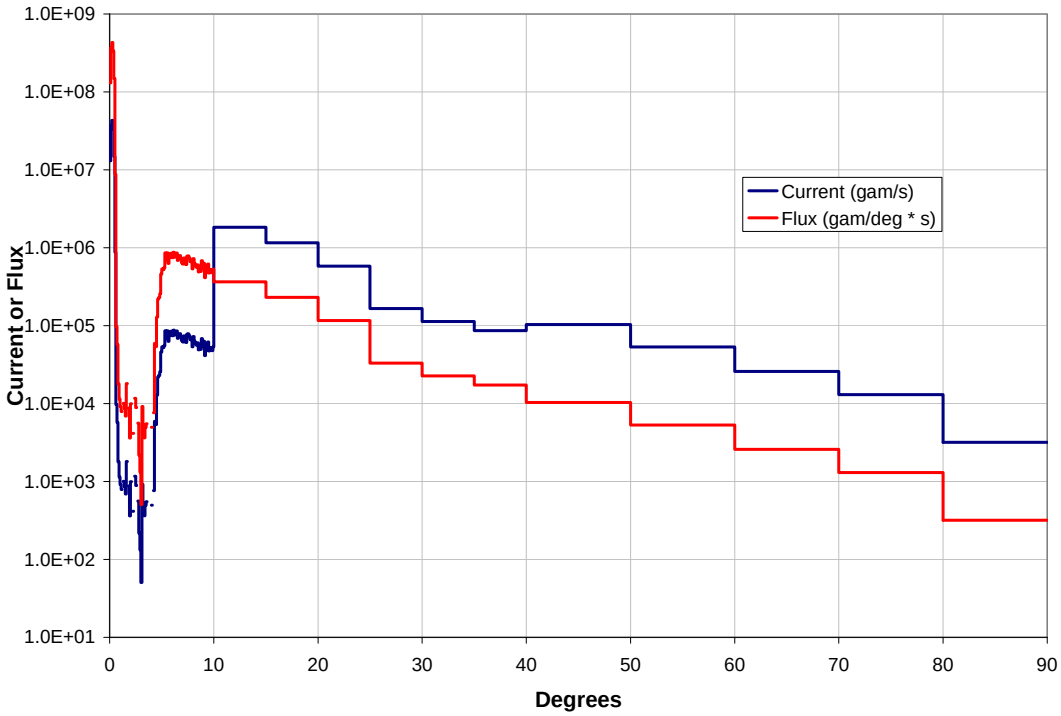

Figure 5. Photon source current and flux for the first radial region (R < 0.15875 cm) and first energy group (4 MeV < E < 4.25 MeV) vs. degrees from the beam axis.

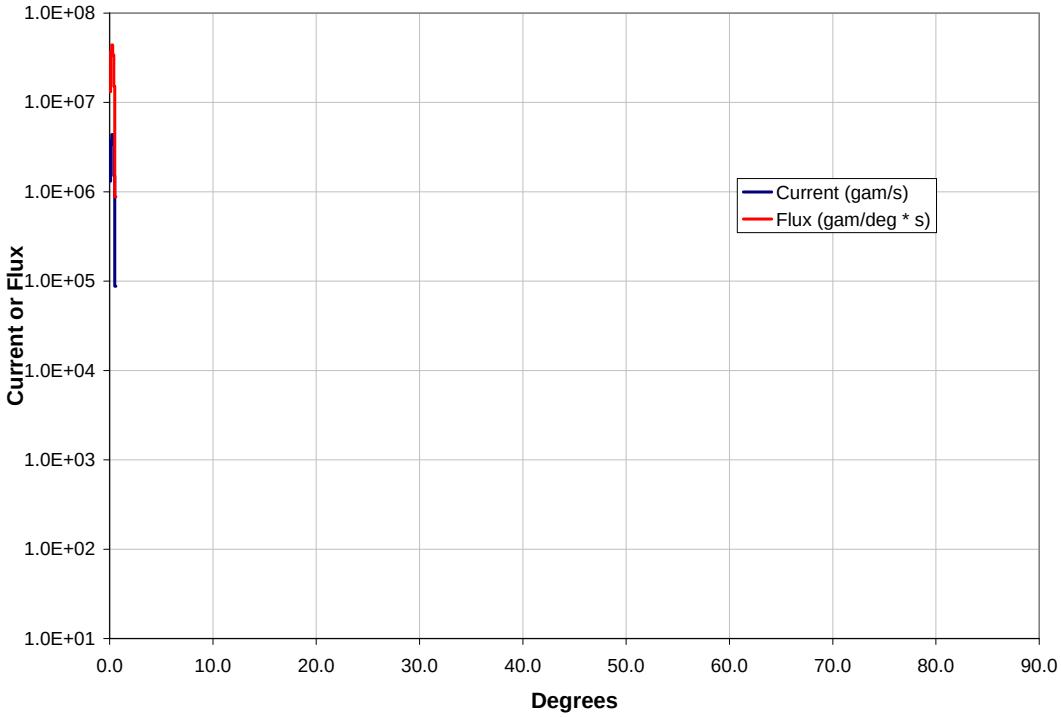

Figure 6. Photon source current and flux for the first radial region (R < 0.15875 cm) and 64th energy group (19.75 MeV < E < 20 MeV) vs. degrees from the beam axis.

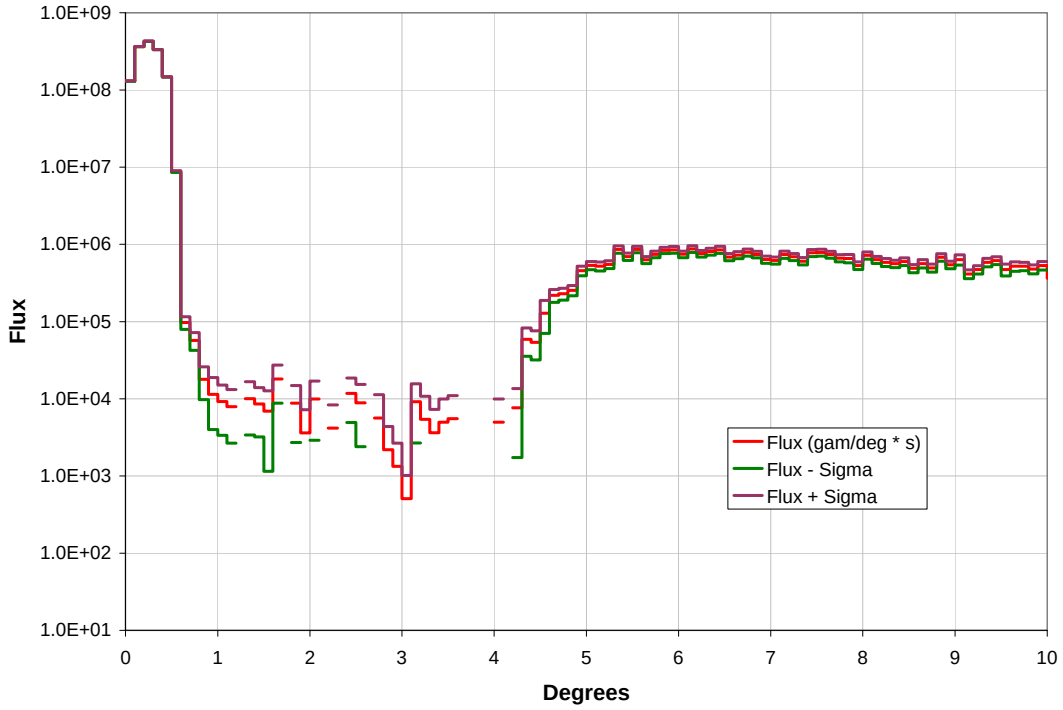

Figure 7. Photon source current and flux for the first radial region (R < 0.15875 cm) and first energy group (4 MeV < E < 4.25 MeV) vs. degrees from the beam axis, 0 to 10º.

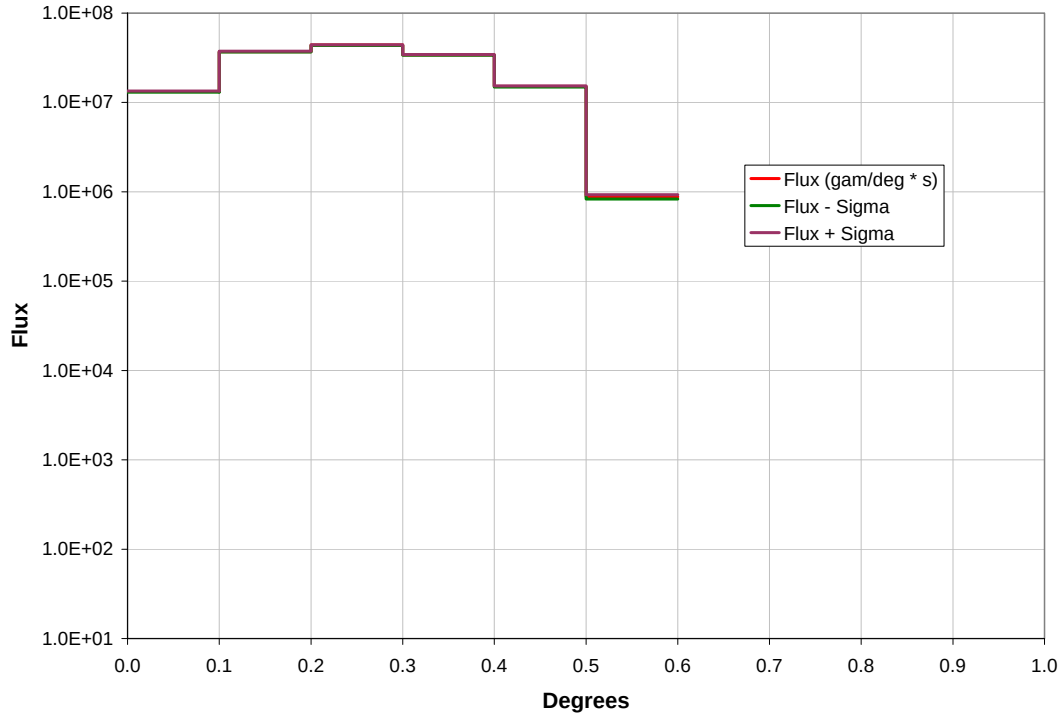

Figure 8. Photon source current and flux for the first radial region (R < 0.15875 cm) and 64th energy group (19.75 MeV < E < 20 MeV) vs. degrees from the beam axis, 0 to 10º.

3. LINAC BEAM CHARACTERIZATION

3.1. Angular Spread and Attenuation of Photon Beam

The photon beam discussed in the previous section was modeled in air both with and without the ground. Then the flux of photons at different distances from the accelerator was calculated to determine how many photons would enter the target at a given location. Using this flux, and the photonuclear cross sections, one can estimate the number of photonuclear interactions that would occur in the target as well as calculate the photoneutron production rate.

3.2. Photon Beam in Air

The angular spread and attenuation of the photon beam was modeled in air only (the input file is shown in Appendix B). Tallies in MCNPX are used to compute the photon flux at six planes, from 5 to 30 m in steps of 5 m, all of which were downstream from the collimator and perpendicular to the beam. This is similar to the geometry shown in Figure 2; however, the system was extended to 30 m, and the vehicle and ground were not modeled. The tally at each plane was segmented into 20 different radial regions (i.e., rings—the first region is simply a disc). The outside radii of the rings in centimeters are 10 to 100 by steps of 10, and 120 to 300 by steps of 20. The peak of the photon fluxes on these six planes can be seen in Figure 9 through Figure 14. The relative errors for Figure 9 through Figure 14 are all less than 0.05.

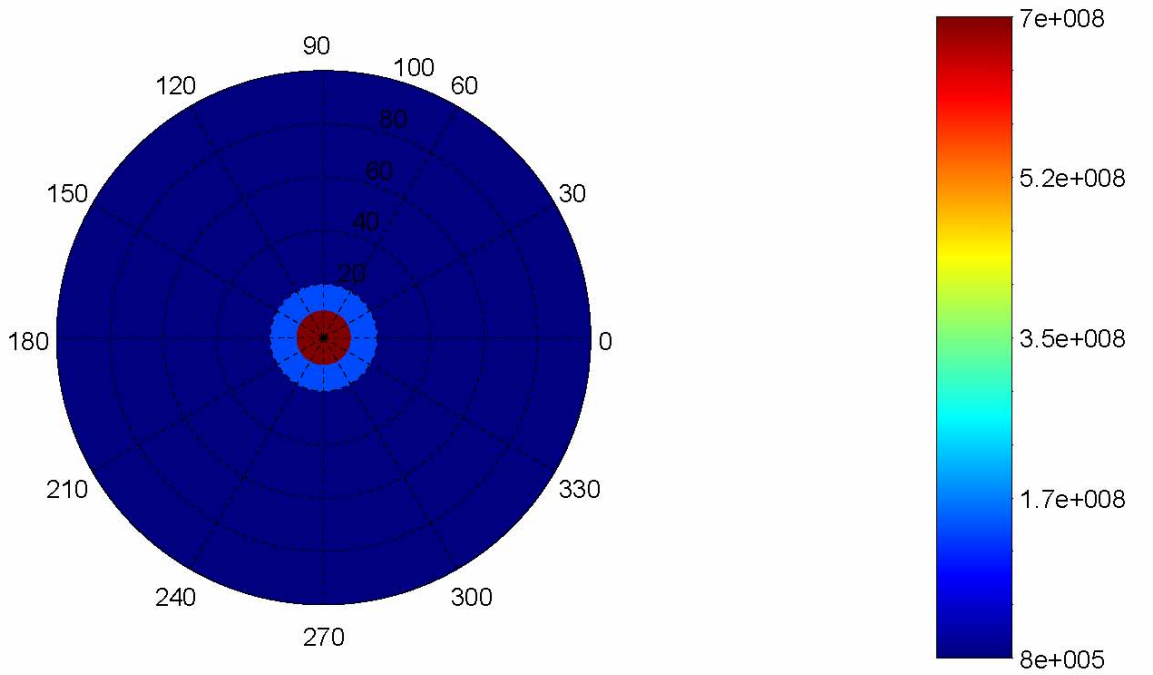

Figure 9. Peak photon flux ($cm^{-2}sec^{-1}$) 5 m from exit of collimator.

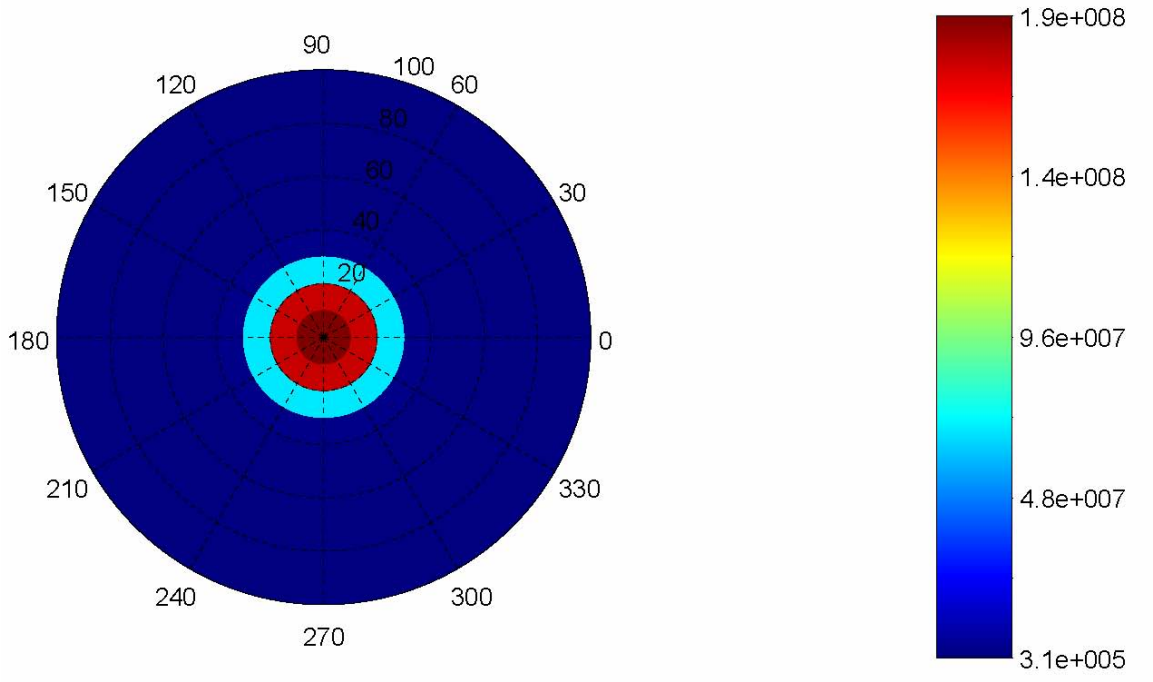

Figure 10. Peak photon flux ($cm^{-2}sec^{-1}$) 10 m from exit of collimator.

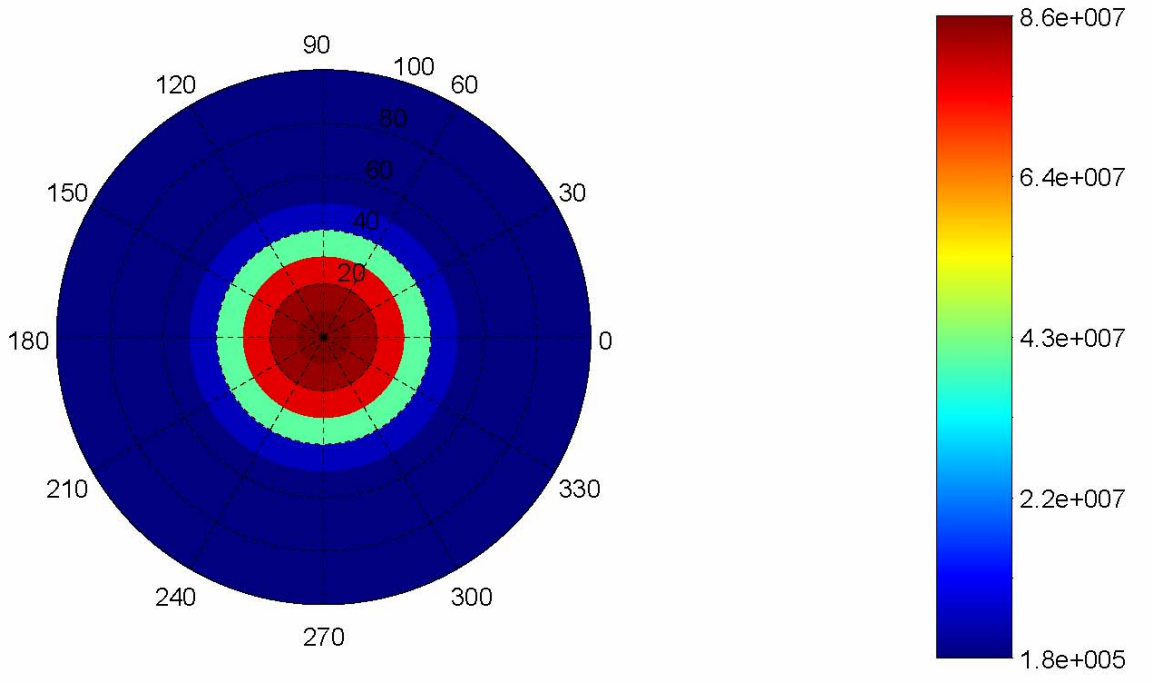

Figure 11. Peak photon flux ($cm^{-2}sec^{-1}$) 15 m from exit of collimator.

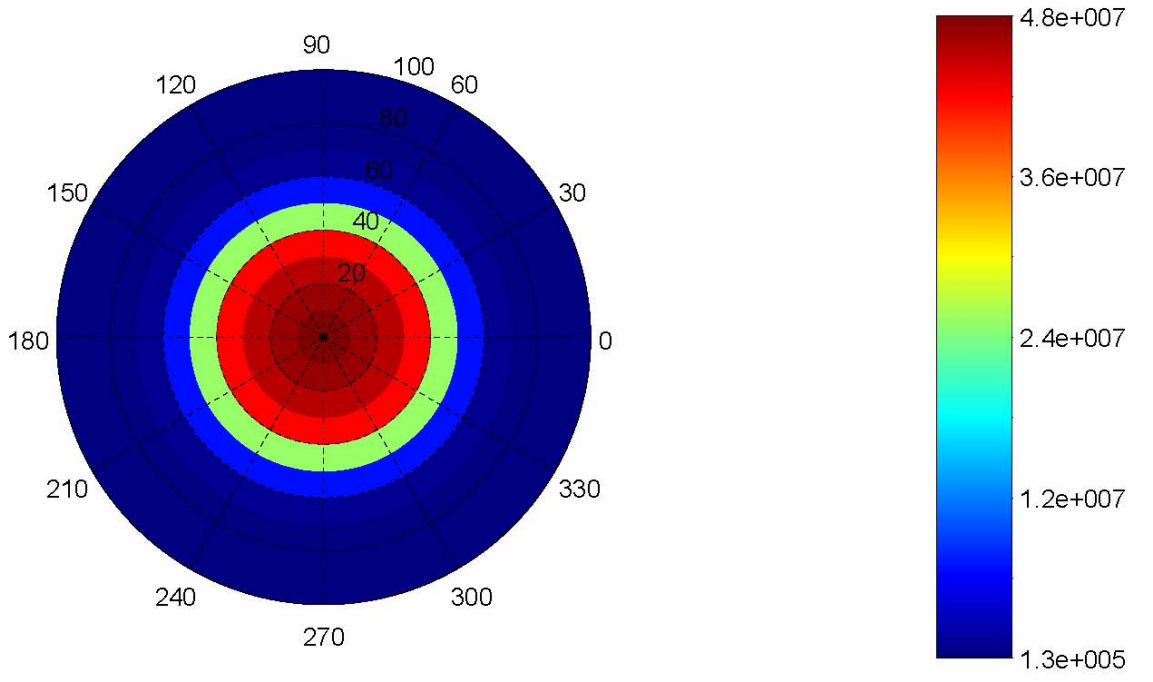

Figure 12. Peak photon flux ($cm^{-2}sec^{-1}$) 20 m from exit of collimator.

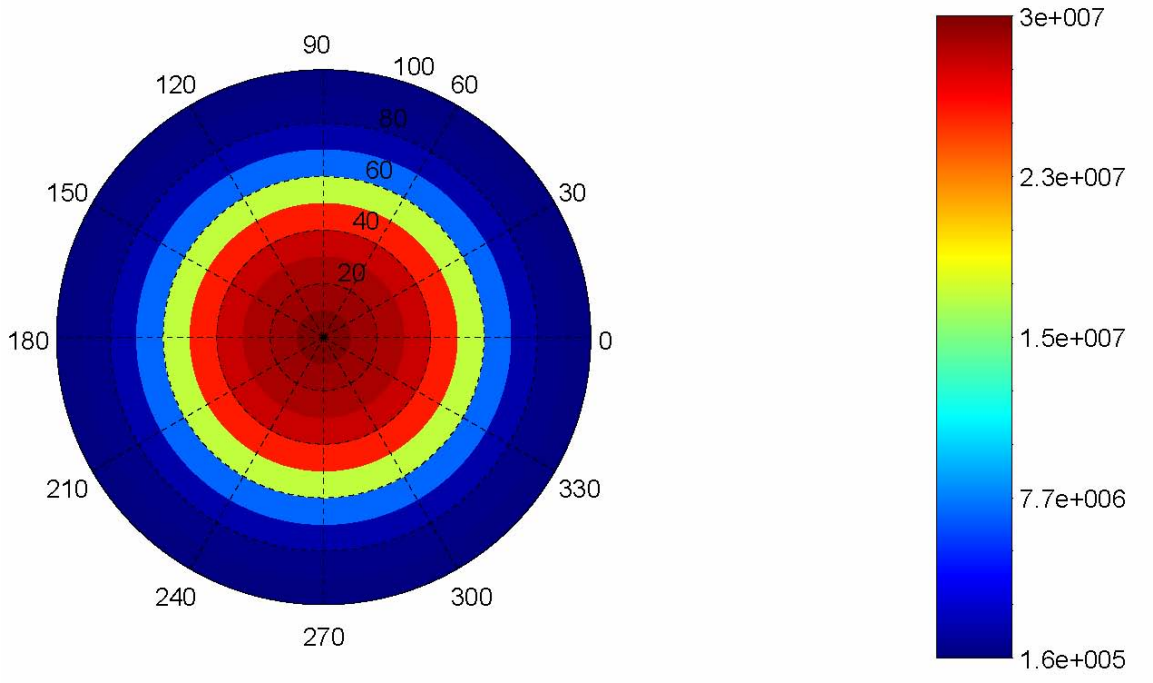

Figure 13. Peak photon flux ($cm^{-2}sec^{-1}$) 25 m from exit of collimator.

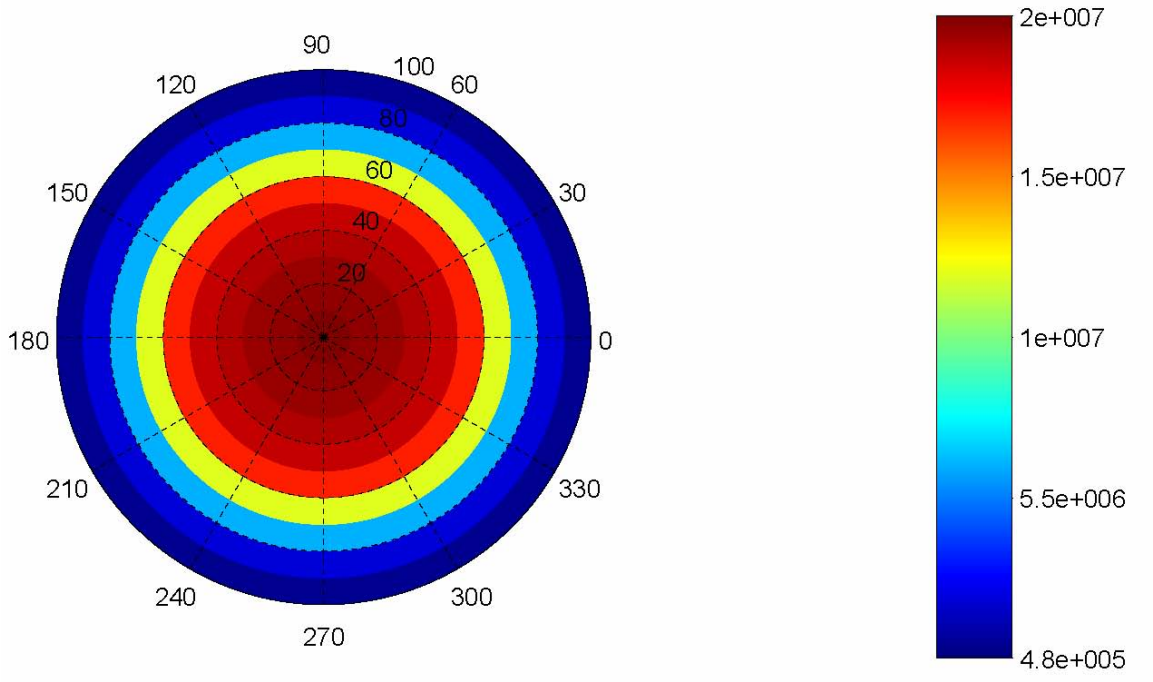

Figure 14. Peak photon flux ($cm^{-2}sec^{-1}$) 30 m from exit of collimator.

The peak photon flux downstream from the collimator shown in Figure 9 through Figure 14 is inside a cone that has a half angle between 1.75 and 2.25 degrees. As a result, a target can be placed at some arbitrary distance from the collimator, and the location of the photon peak with respect to the beam axis is well defined. Table 3 shows the half cone angle of the photon peak at the six tally locations. The exact edge of the photon peak is obscured by the segmenting of the tally flux plane.

Table 3. Half cone angle of peak photon flux

Distance from collimator (cm)	Radius of peak photon flux (cm)	Half cone angle (degrees)
500	20	2.29
1000	30	1.72
1500	50	1.91
2000	60	1.72
2500	80	1.83
3000	90	1.72

3.3. Photon Beam in Air with Soil

Next, the angular spread and attenuation of the photon beam was modeled in air and above 1-m-thick soil (the input file is shown in Appendix B). The beam axis of the electron accelerator was 1.5 m above the soil. Unlike the previous calculations, this geometry is not symmetric due to the soil. Therefore, the tallies in MCNPX were segmented into rectangular regions. The photon flux was calculated at the same six planes. The tally at each plane was segmented into 1400 different rectangular regions. Along the *x*-axis (from left to right) the tally had mesh lines from -300 cm to

-100 cm by steps of 20 cm; from -100 to 100 by steps of 10 cm; and from 100 to 300 cm by steps of 20 cm. Along the *y*-axis (bottom to top) the tally had mesh lines from -150 to 100 cm by steps of 10 cm and from 100 to 300 cm by steps of 20 cm. The peak of the photon fluxes on these six planes can be seen below in Figure 15 through Figure 20. The relative errors for Figure 15 through Figure 20 are less than 0.1 in the cells where the photon peak is located and in the cells surrounding the photon peak. Outside the area immediately surrounding the photon peak the relative errors can be as large as 0.8 close to the boundaries of the tally but most are less than 0.2. The occurrence of these large relative errors explains why the minimum flux labeled in Figures 15 and 16 is approximately 7 $\gamma/cm^2/sec$. This value is far less than the other minimum flux levels in Figures 12, 13, 14, and 17 and is nonphysical. The minimum flux values in Figures 15 and 16 should be on the order of 1e3.

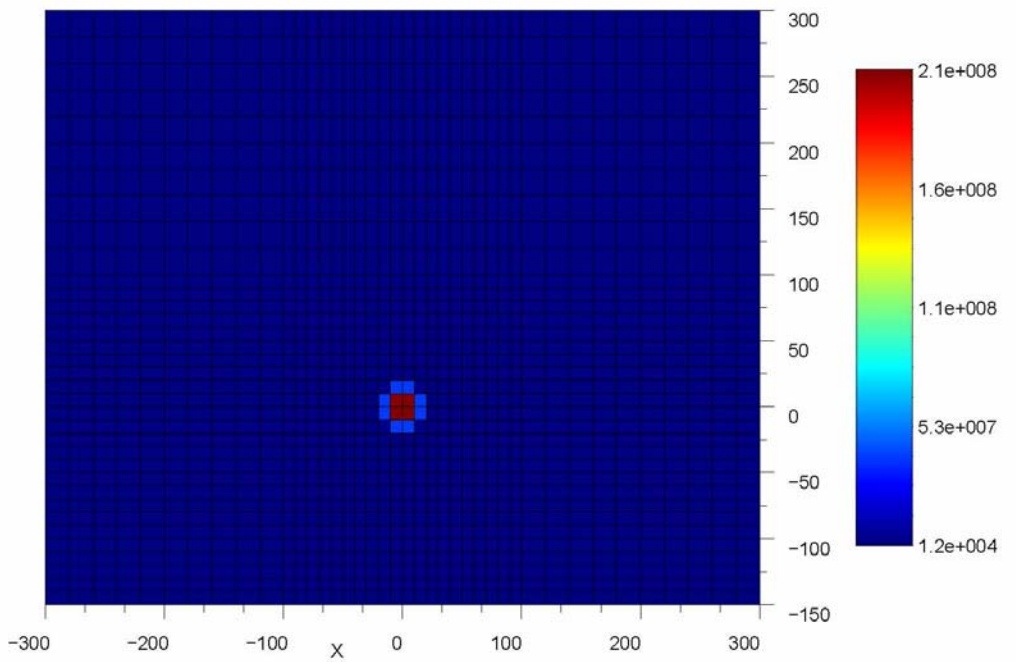

Figure 15. Peak photon flux ($cm^{-2}sec^{-1}$) above the soil 5 m from exit of collimator.

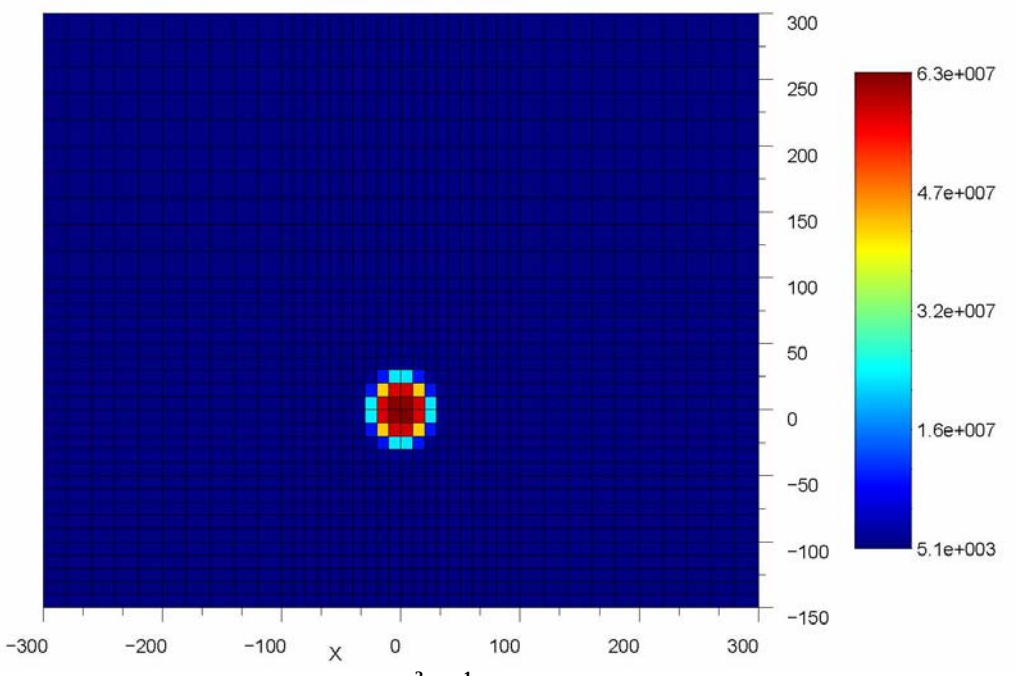

Figure 16. Peak Photon flux ($cm^{-2}sec^{-1}$) above the soil 10 m from exit of collimator.

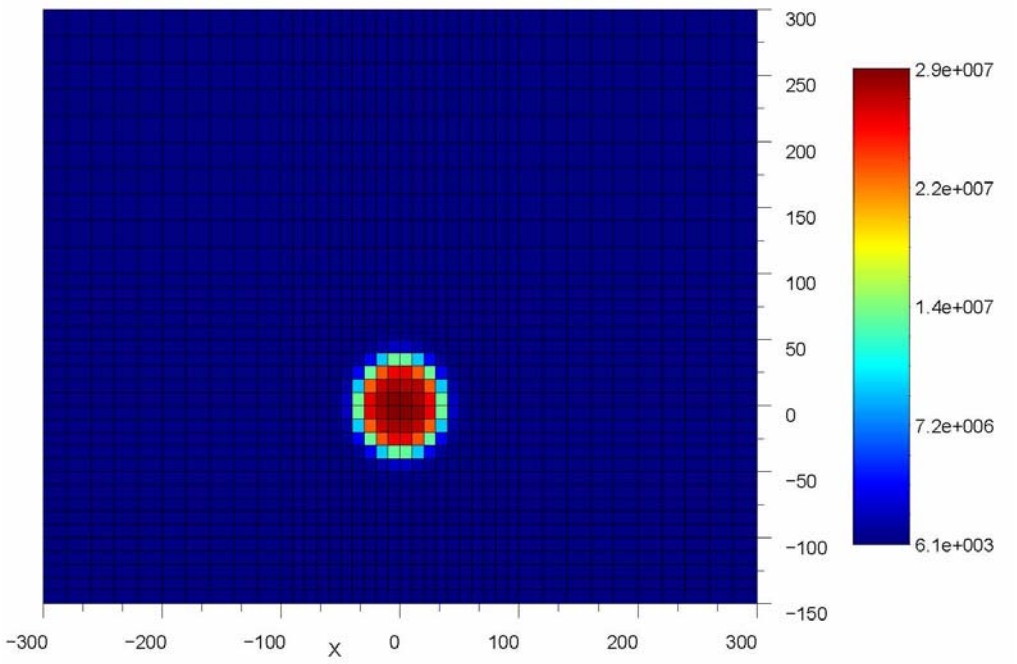

Figure 17. Peak photon flux ($cm^{-2}sec^{-1}$) above the soil 15 m from exit of collimator.

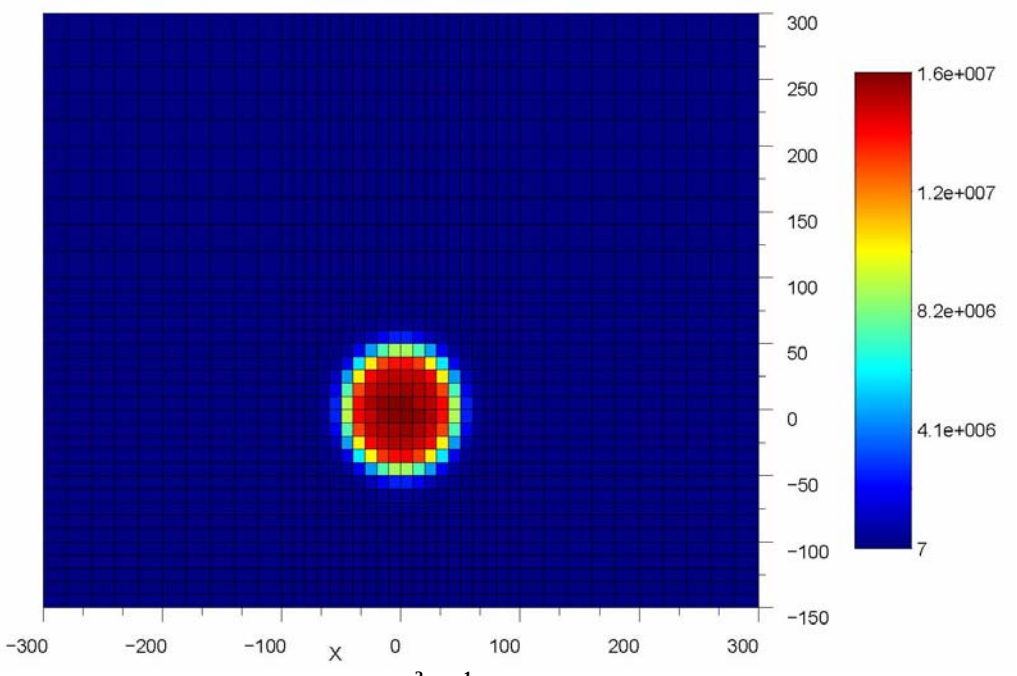

Figure 18. Peak Photon flux ($cm^{-2}sec^{-1}$) above the soil 20 m from exit of collimator.

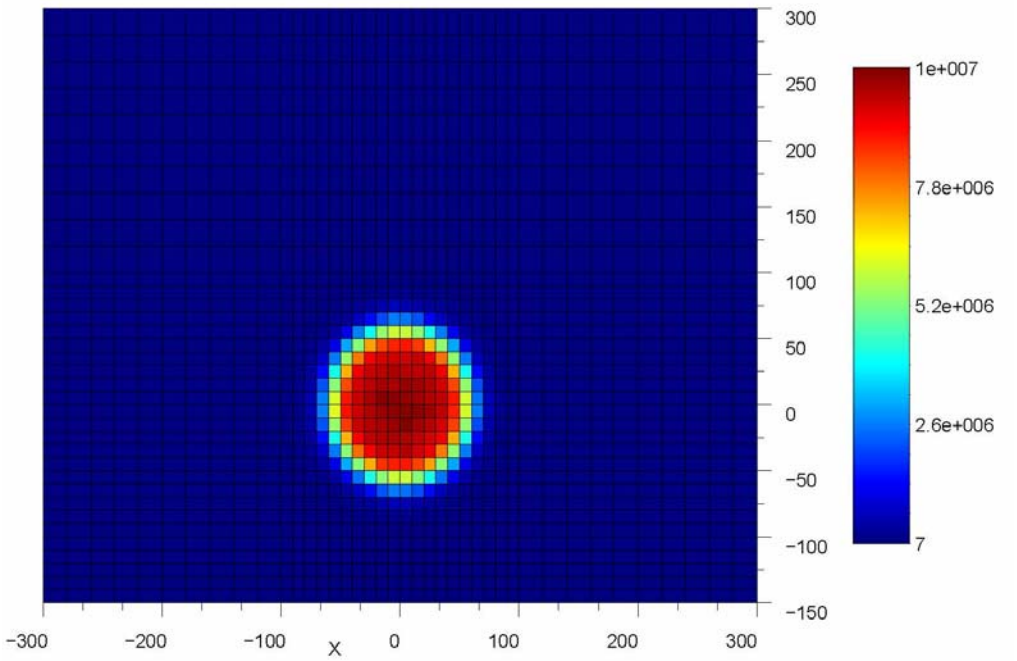

Figure 19. Peak photon flux ($cm^{-2}sec^{-1}$) above the soil 25 m from exit of collimator.

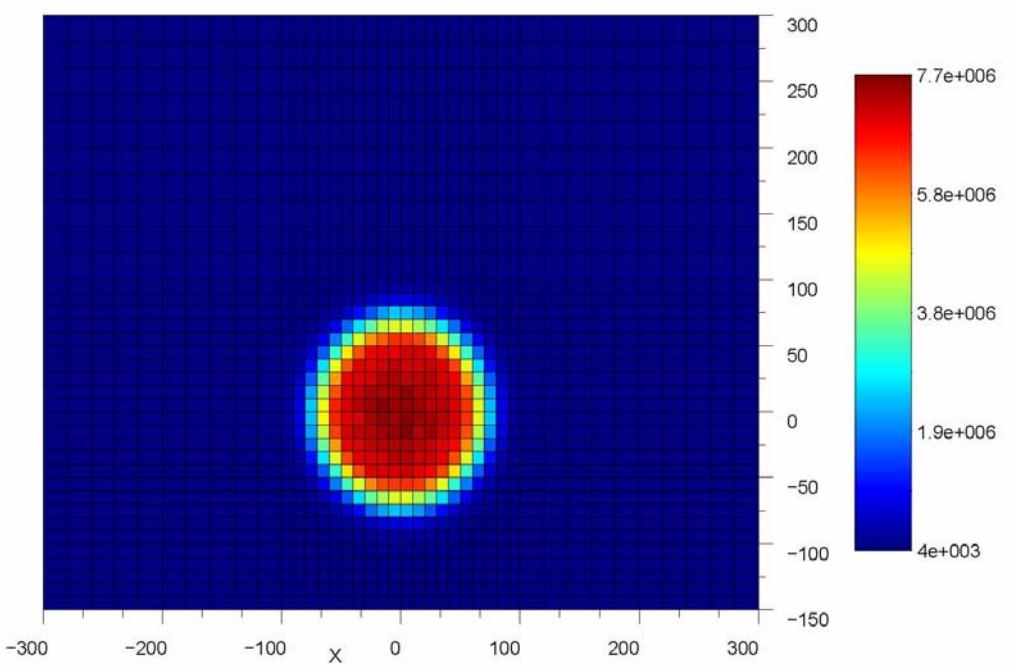

Figure 20. Peak photon flux ($cm^{-2}sec^{-1}$) above the soil 30 m from exit of collimator.

In Figure 15 through Figure 20 the peak photon flux downstream from the collimator is still inside a cone that has a half angle between 1.75 and 2.25º. The presence of the ground had practically no effect on the photon flux, at least when compared to the peak flux. This may suggest that it is not necessary to model the ground in these simulations; however, this ultimately is not the case. Indeed, when the neutrons produced in these simulations are considered, the ground will play a more important role.

4. PROMPT NEUTRON AND PHOTON FLUX MAPS IN MODEL GEOMETRY

The MCNPX code ver. 2.5 was used for prompt neutron and gamma ray fluence simulations at various horizontal planes in the geometry shown in Figure 2. For the neutron fluence simulations, the mesh cells had a size of $2 \times 2 \times 2$ cm^3, while for the gamma-ray simulations, the mesh cells were $10 \times 10 \times 10$ cm^3 in size. The fluence values were averaged over the volume of the mesh cells.

The neutron production relies on photonuclear reactions occurring in the tungsten converter, the collimator, the LINAC shielding, and the depleted uranium target. However, the prompt neutron contribution of the latter is negligible. The primary source of high-energy gamma rays that are required to produce neutrons is bremsstrahlung in the tungsten converter. Bremsstrahlung can also occur in the collimator and shielding; however, many photons produced in these materials will not have sufficient energy to produce photoneutrons.

In order to expedite the simulations, appropriate particle energy cut-offs were applied, identical for both electrons and gamma rays. Specifically, for the neutron fluence simulation the cut-off was set to 4 MeV, while for the gamma ray fluence simulations, it was 0.1 MeV.

Figure 21 through Figure 27 show the neutron fluences over horizontal planes at different elevations. The lead collimator, together with the LINAC shielding and the tungsten converter, produce the highest number of prompt neutrons (see Figure 21). This is expected considering the photonuclear cross sections for lead and tungsten. As expected, the neutron fluence decreases with decreasing plane elevation. The minimum values are reached at an elevation of -149 cm (see Figure 27); this plane is located next to the ground. Appendix D shows the relative errors corresponding to the neutron fluence maps in Figure 21 through Figure 27. The errors reach relatively high values (~30%) only on the periphery of the geometry where statistical accuracy is not important. The values in the central part of the geometry are extremely low.

The flux maps generated with the Monte Carlo model indicate that the detectors should be placed approximately 50 cm behind the exit of the accelerator (see Figure 22). This position minimizes the number of neutrons coming from the accelerator structure as these neutrons must undergo some scattering collisions first.

Figure 28 through Figure 31 show the gamma ray fluences computed in a similar manner to neutron fluences discussed earlier. However, the mesh cell size was increased to 10 × 10 × 10 cm^3. The converter and collimator are the main sources of gamma rays. It is clear from the results that the LINAC shielding made of 3 in. of lead is very efficient in eliminating of gamma rays in the directions perpendicular to the primary electron beamline. On the other hand, the collimator efficiently focuses the gamma ray beam towards the target. Appendix D shows the relative errors corresponding to the neutron fluences shown in Figure 28 through Figure 31. As expected, the largest errors (~80%) are reached in the corners of the geometry at negative *z*-values where accuracy is of low importance. On the other hand, the error values in the central part of the geometry are extremely low.

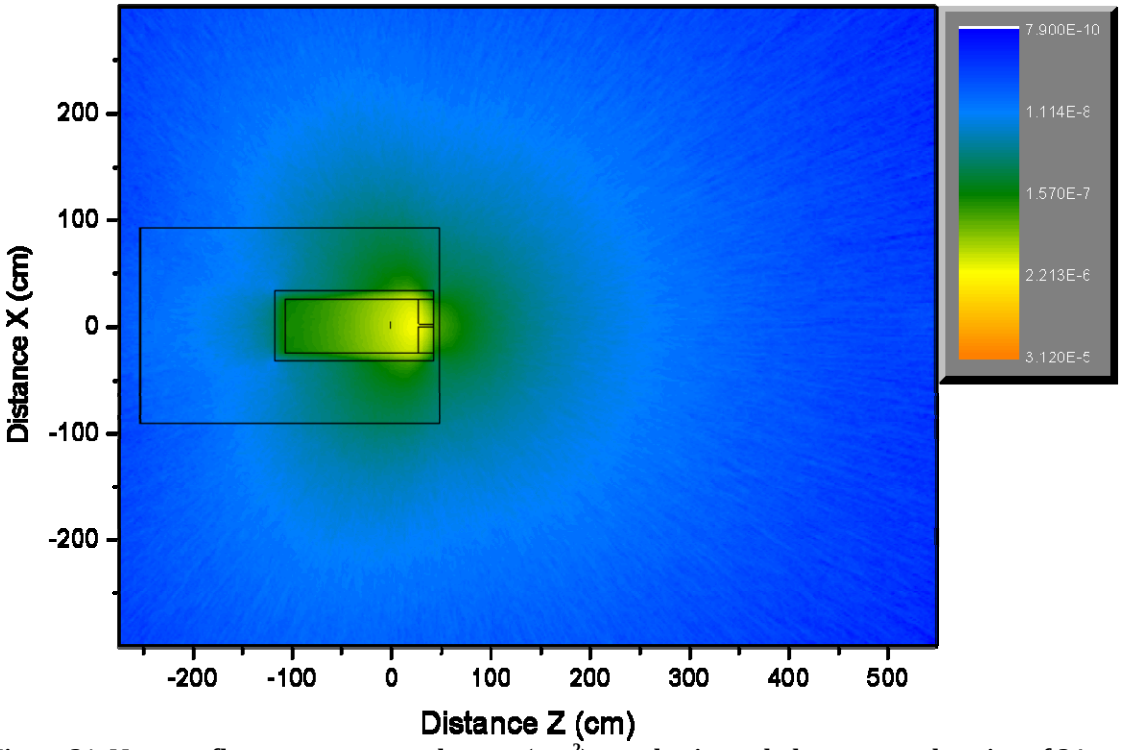

Figure 21. Neutron fluence per source electron (cm^{-2}) over horizontal planes at an elevation of 24 cm.

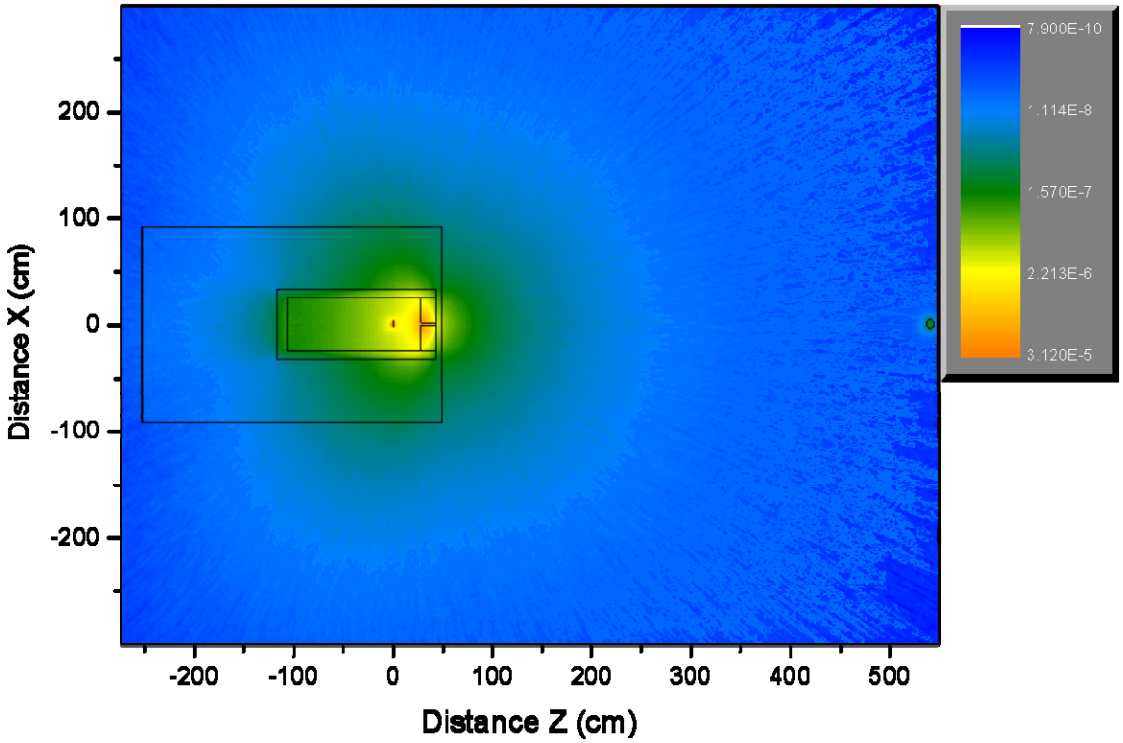

Figure 22. Neutron fluence per source electron (cm^{-2}) over horizontal planes at an elevation of 0 cm.

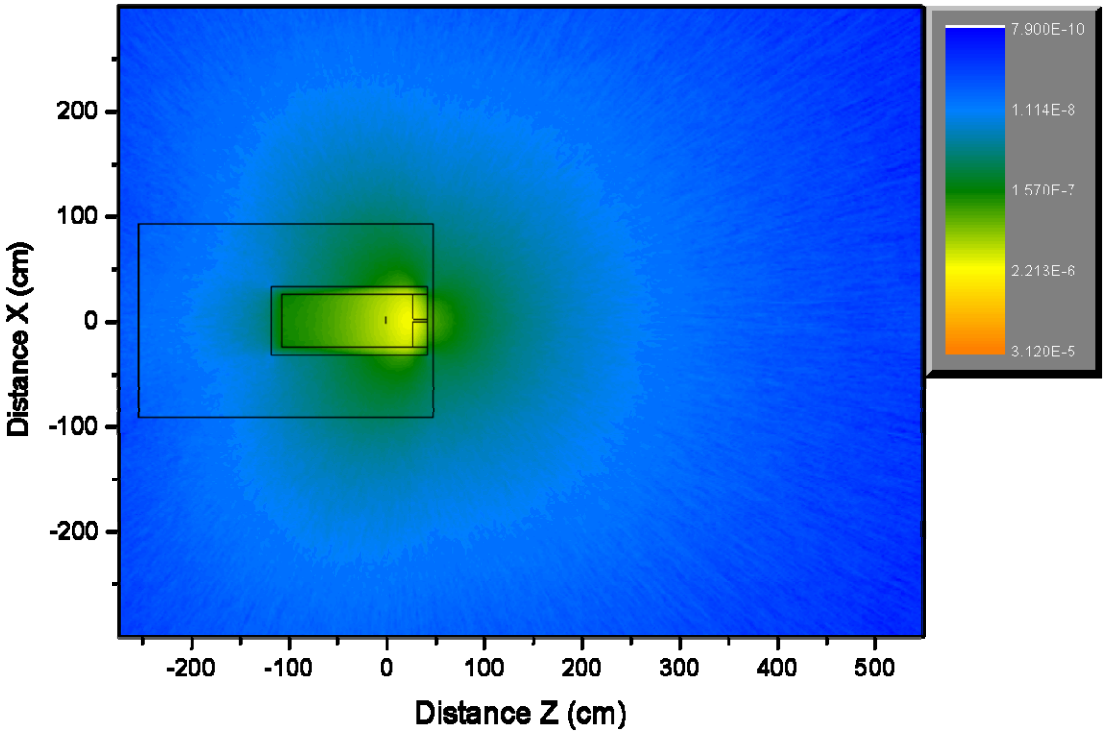

Figure 23. Neutron fluence per source electron (cm^{-2}) over horizontal planes at an elevation of -24 cm.

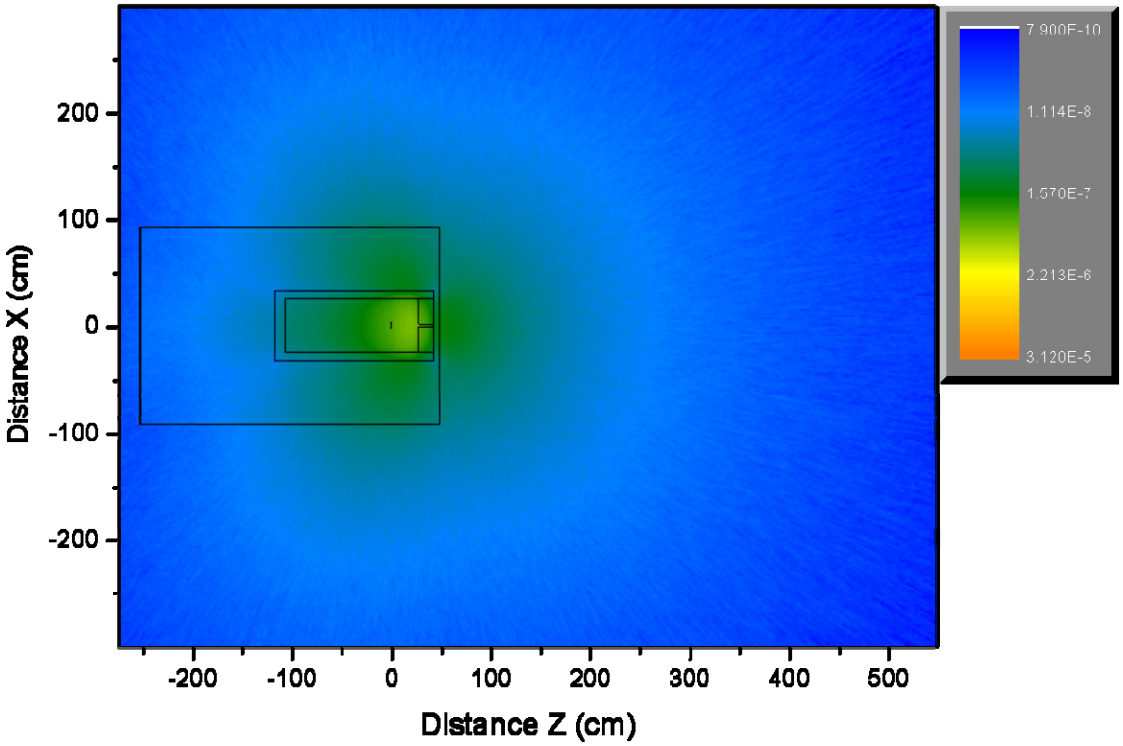

Figure 24. Neutron fluence per source electron (cm^{-2}) over horizontal planes at an elevation of -33.62 cm.

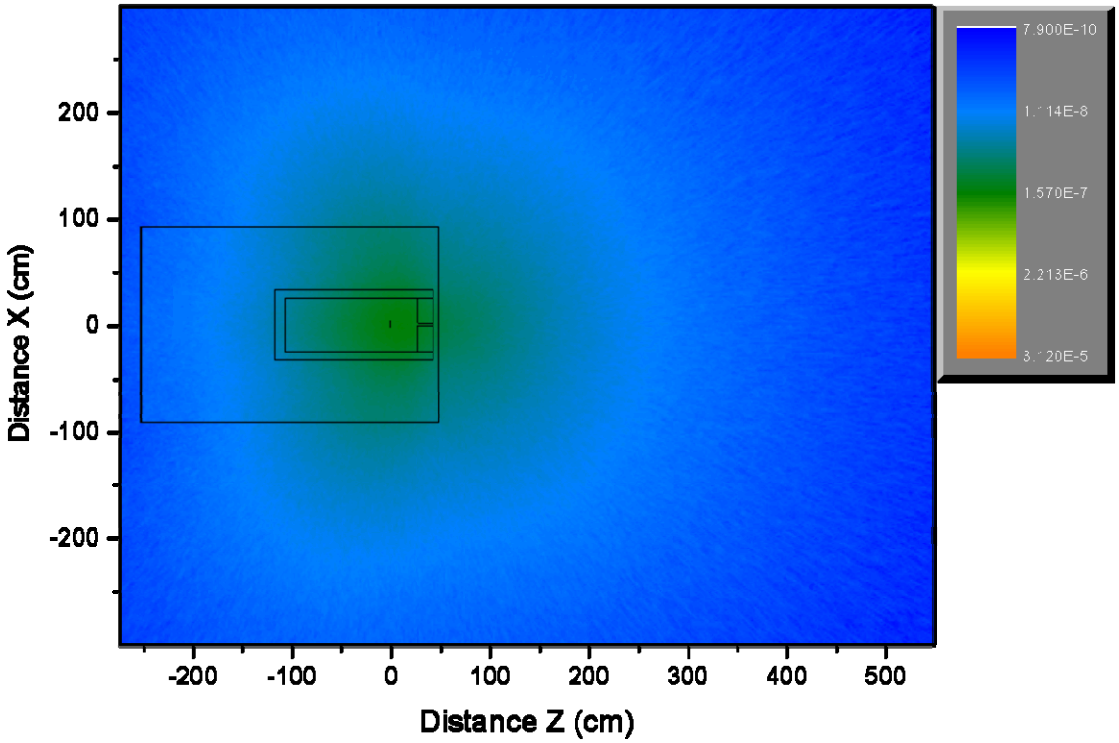

Figure 25. Neutron fluence per source electron (cm^{-2}) over horizontal planes at an elevation of -62 cm.

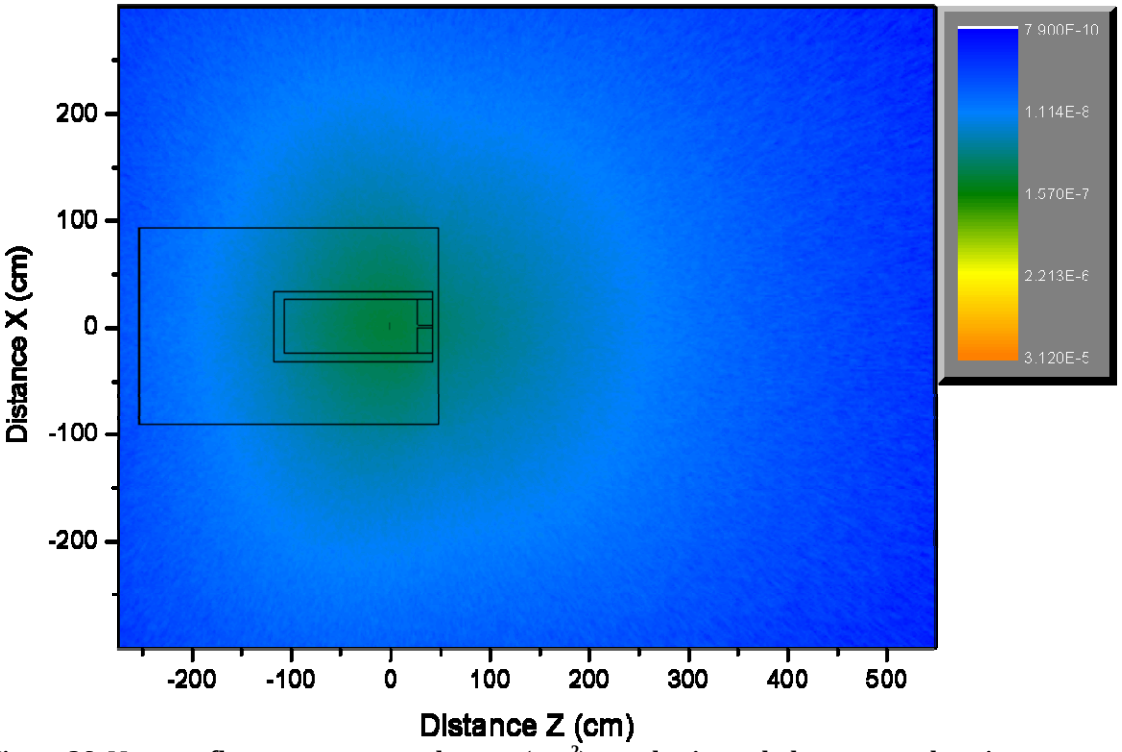

Figure 26. Neutron fluence per source electron (cm^{-2}) over horizontal planes at an elevation of -90.44 cm.

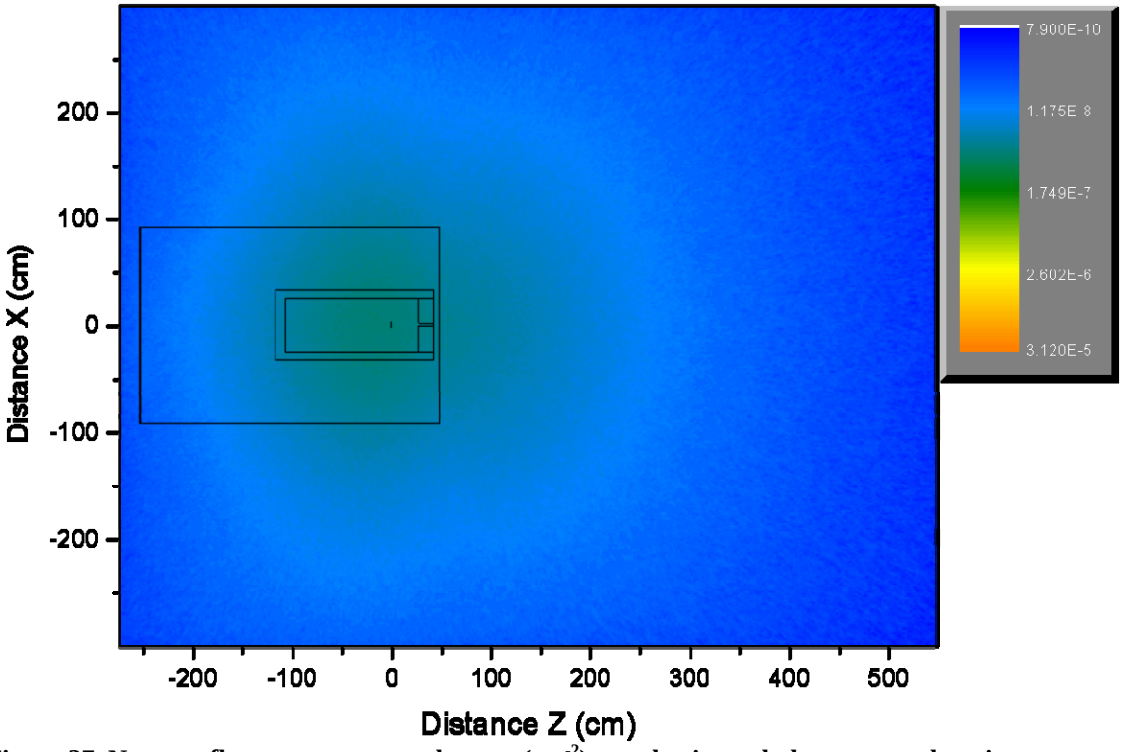

Figure 27. Neutron fluence per source electron (cm^{-2}) over horizontal planes at an elevation of -149 cm.

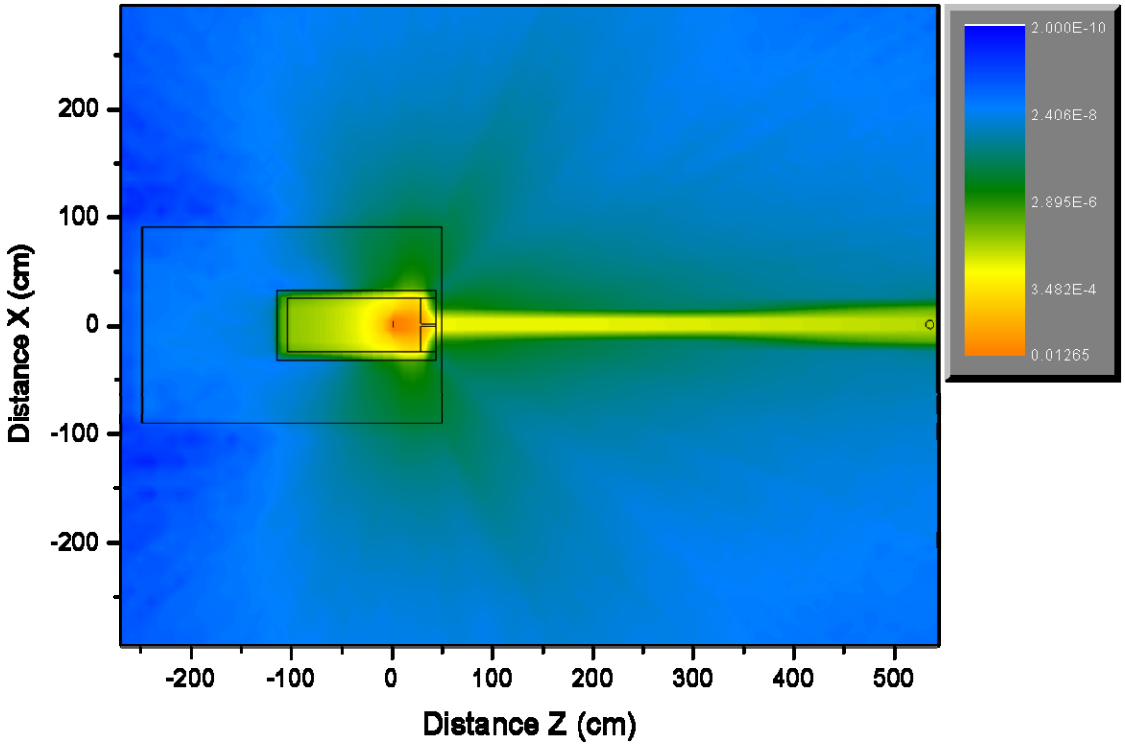

Figure 28. Gamma ray fluence per source electron (cm^{-2}) over horizontal planes at an elevation of 0 cm.

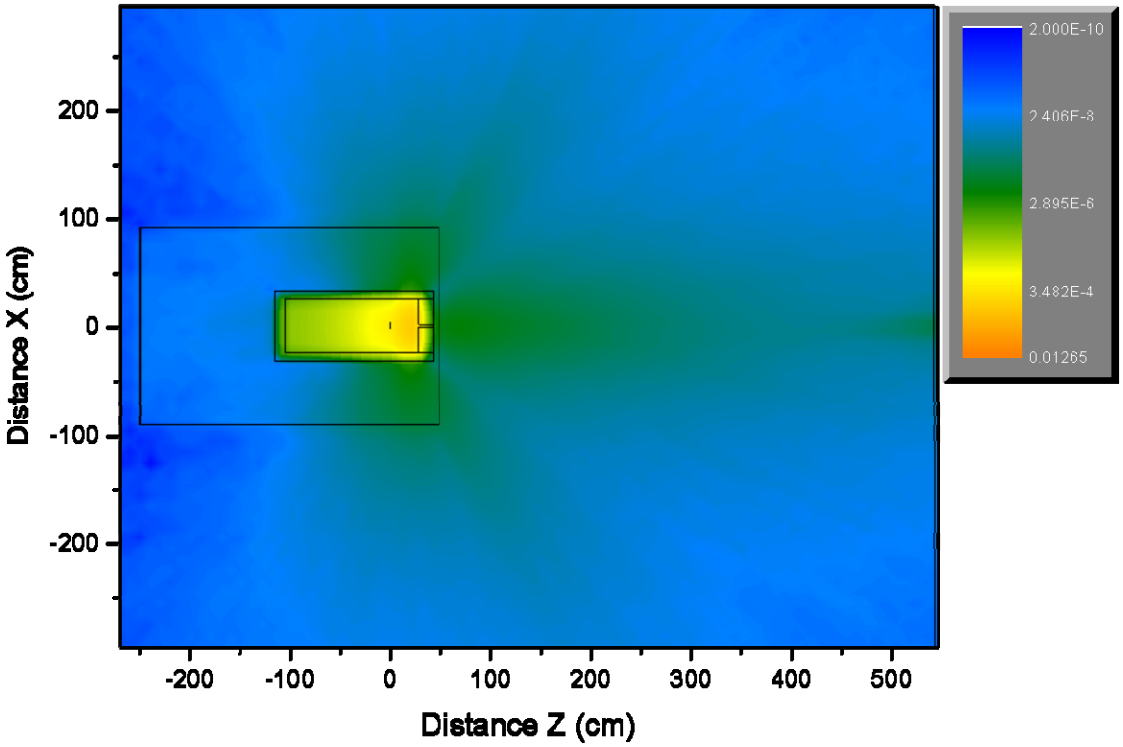

Figure 29. Gamma ray fluence per source electron (cm^{-2}) over horizontal planes at an elevation of -20 cm.

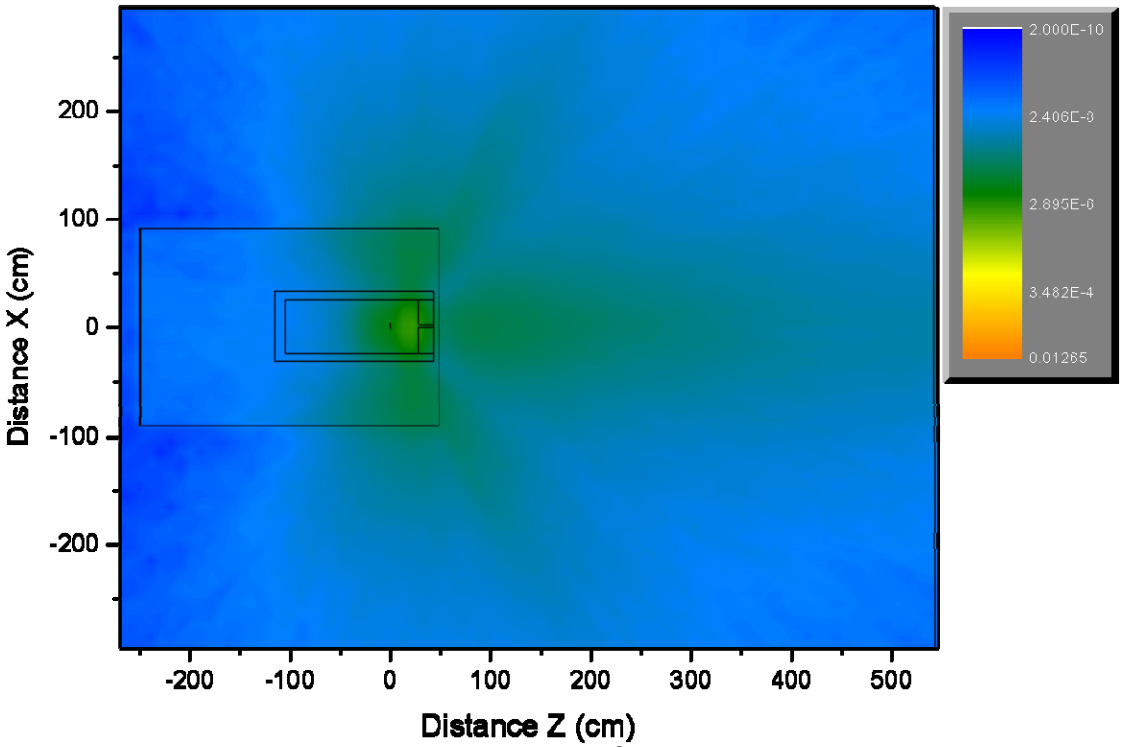

Figure 30. Gamma ray fluence per source electron (cm^{-2}) over horizontal planes at an elevation of -37.62 cm.

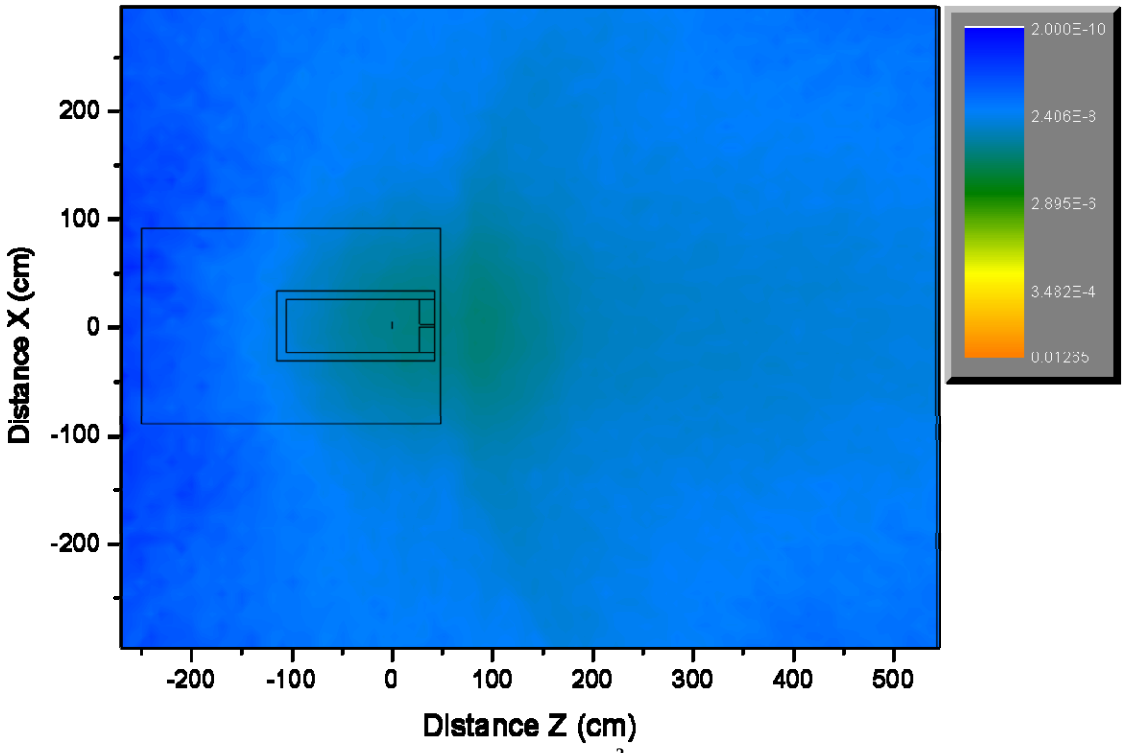

Figure 31. Gamma ray fluence per source electron (cm^{-2}) over horizontal planes at an elevation of -146 cm.

5. TIME AND ENERGY DEPENDENCE OF NEUTRON AND PHOTON FLUX

The MCNPX code ver. 2.5 was used to simulate the number of neutrons that cross the vehicle walls, their energy distribution, as well as their flight time to the vehicle walls. In this section, all results are integrated over the entire surface of the walls. In order to speed up the simulations, appropriate energy cutoffs were again applied. Specifically, an energy cutoff of 4 MeV was used for electrons and gamma rays, while a 10-keV cutoff was applied to the neutrons.

Figure 32 through Figure 34 show the number of neutrons crossing one of the outer walls located vertically along the electron beamline. Only neutrons moving in the outward direction are tallied in these results. The first neutrons created in the converter, the LINAC shielding, or the collimator begin to arrive approximately 20 ns after initial electron start. Prior to this time, a relatively small number of neutrons are observed. These neutrons arrive at small time delays because of their very large energy, or because they were created directly in the wall by high-energy gamma rays. After 20 ns, the number of neutrons that cross the wall gradually increases, while the peaks of the distributions shift to lower energies. This is due to the arrival of the neutrons, which scattered before reaching the wall. Above 75 ns, the distributions consist of multiple peaks due to multiple neutron scatterings before they reach the wall. The number of neutrons (normalized per ns) decreases approximately by a factor of 70 between the time bins 90 and 95 ns and 7 and 8 μs (this bin is not shown).

Similar results are shown in Figure 35 through Figure 37 for the wall located vertically, perpendicular to the beamline in the forward direction. However, this wall is closer to the center of the coordinate system by approximately a factor of two when compared to the side wall discussed earlier. This is reflected in earlier neutron arrival times.

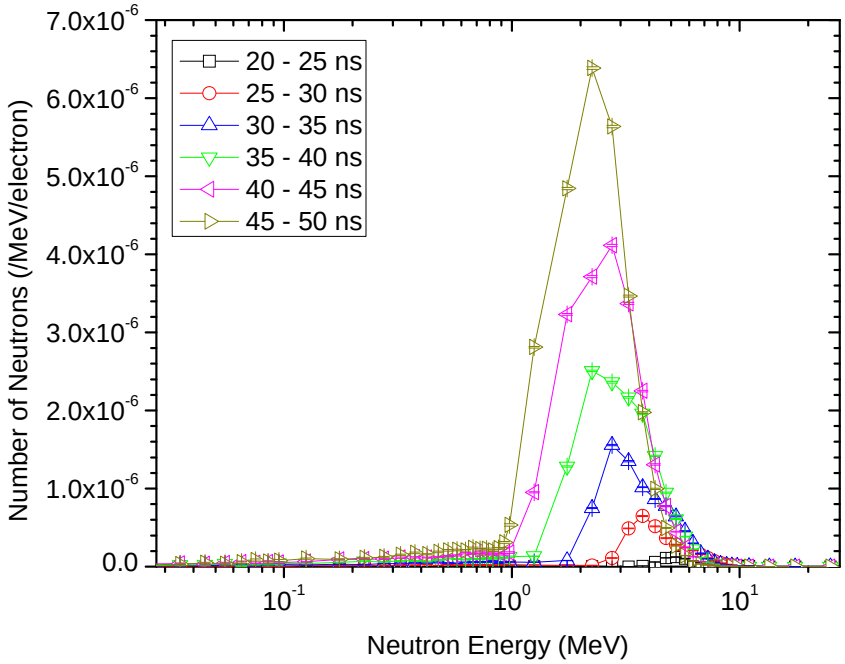

Figure 32. Number of neutrons crossing the vehicle wall located vertically along the beamline for times between 20 and 50 ns.

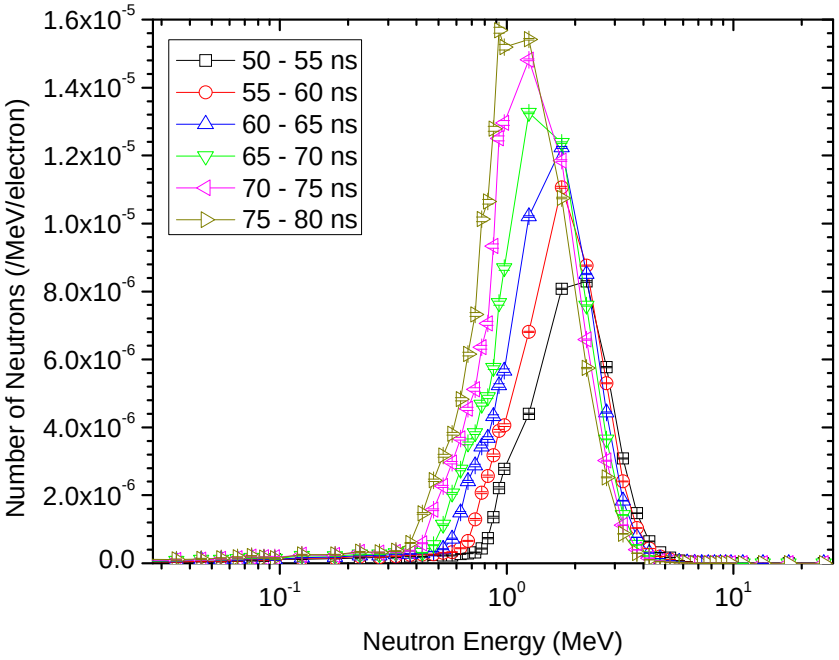

Figure 33. Number of neutrons crossing the vehicle wall located vertically along the beamline between 50 and 80 ns.

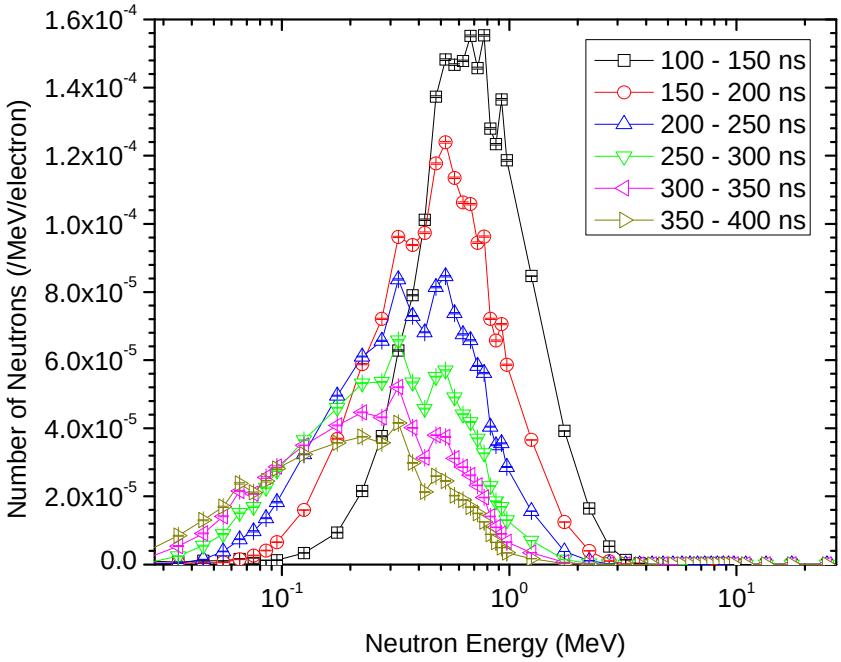

Figure 34. Number of neutrons crossing the vehicle wall located vertically along the beamline between 100 and 400 ns.

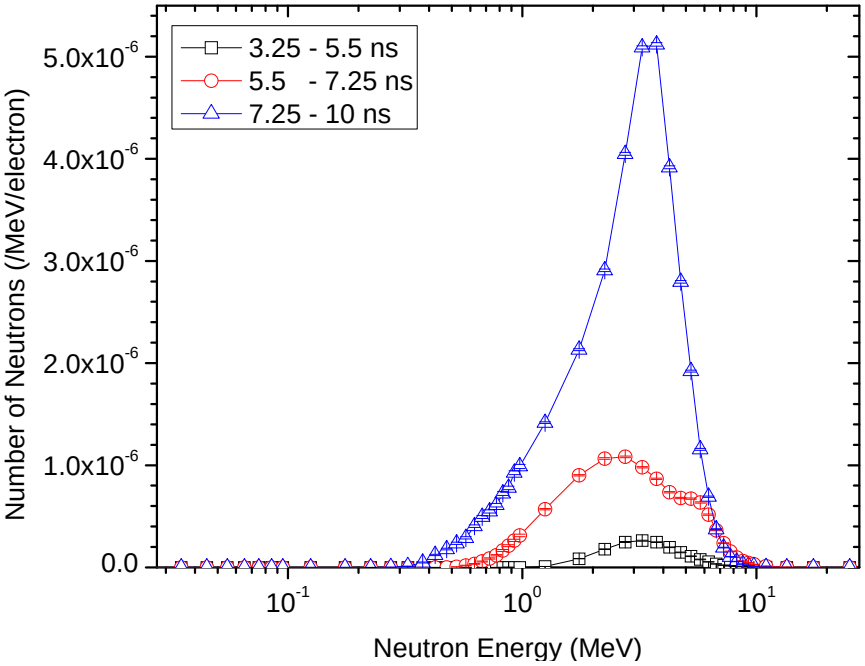

Figure 35. Number of neutrons crossing the vehicle wall located vertically, perpendicular to the beamline in the forward direction, for times between 3.25 and 10 ns.

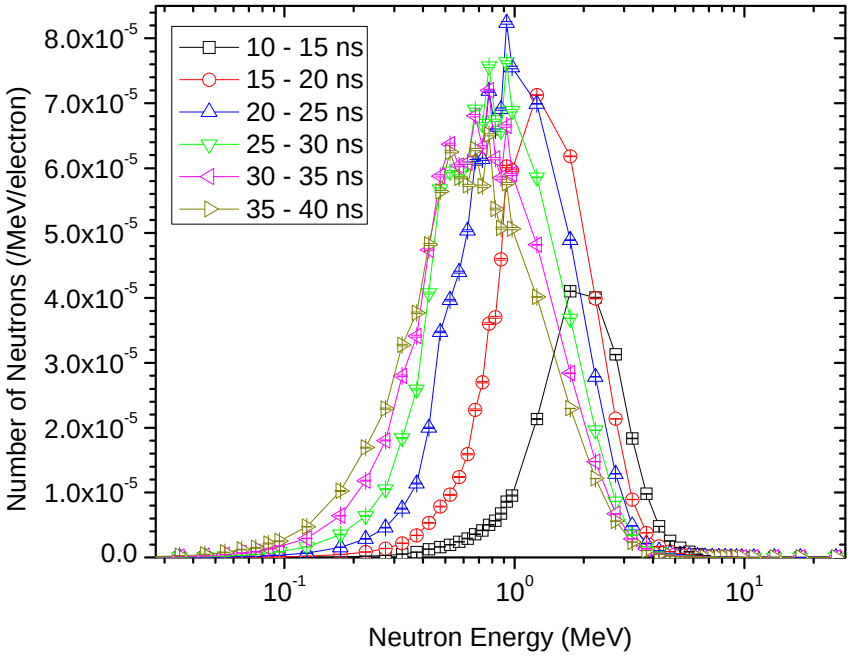

Figure 36. Number of neutrons crossing the vehicle wall located vertically, perpendicular to the beamline in the forward direction, for times between 10 and 40 ns.

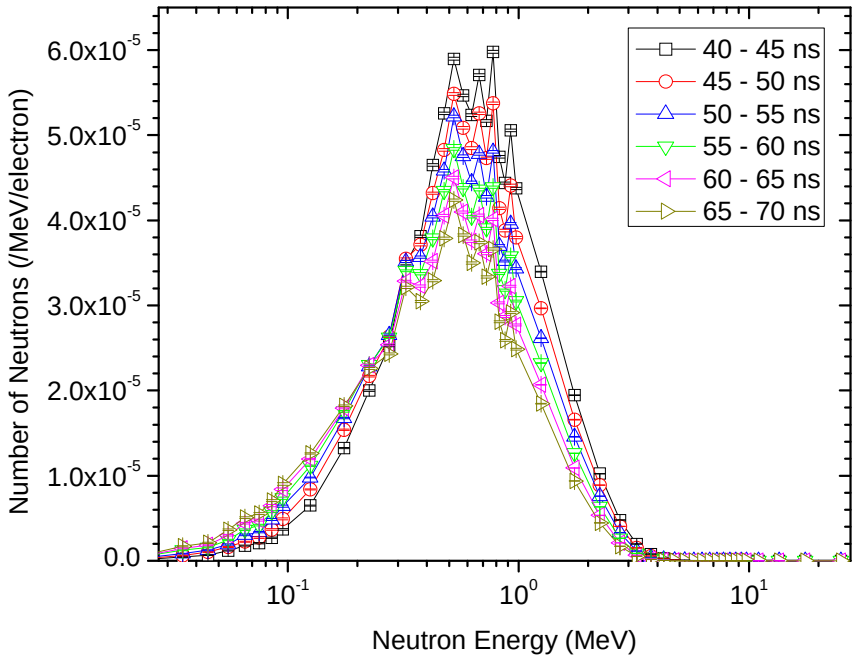

Figure 37. Number of neutrons crossing the vehicle wall located vertically, perpendicular to the beamline in the forward direction, for times between 40 and 70 ns.

Therefore, in order to possibly detect the delayed neutrons, the detectors should be active only after all prompt neutrons have scattered out of the system. These results show this time to be greater than 5 μs after the accelerator pulse.

6. PHOTONUCLEAR SOURCE CHARACTERIZATION

6.1. Photoneutron Production—Prompt Neutrons Only

A two-step method was used to simulate the photonuclear reactions in a given target. First, a modified version of MCNPX was used to calculate the location of photonuclear events and to write a source file to be read by MCNP-PoliMi. In the second step MCNP-PoliMi reads this source file, which contains all the necessary information to start a particle history, and performs the full transport of each photonuclear history. In this work, the MCNPX/MCNP-PoliMi codes were used to model the prompt photoneutron production in two targets located 5 m from the collimator:

1. A 5-kg sphere of depleted uranium (DU): 100% ^{238}U)
2. A 5-kg sphere of highly enriched uranium (HEU): 98% ^{235}U and 2% ^{238}U)

6.2. DU Target

The prompt photoneutron flux was calculated at several different locations, but the results at six planes are included here. The planes are located at 5 m from the collimator, 3 m from the collimator, and at the back of the vehicle in which the accelerator is located (approximately

6.5 cm from the collimator). Three other planes were also plotted that show the prompt photoneutron flux along the side of the vehicle. The first of these planes along the side of the vehicle is located 4 cm in front of the converter plane, the second is 56 cm behind the converter, and the third is 96 cm behind the converter. All of the tallies upstream and downstream of the collimator were perpendicular to the beam axis (shown in Figure 2). The tally at each plane was segmented into several rectangular regions. All of the tally regions are 10 × 10 cm^2 squares. However, the tallies do not extend inside the vehicle, so the tallies directly adjacent to the vehicle have been truncated. The DU prompt photoneutron fluxes at these six locations can be seen in Figure 38 through Figure 43. The relative errors for Figure 38 through Figure 43 are less than 0.05.

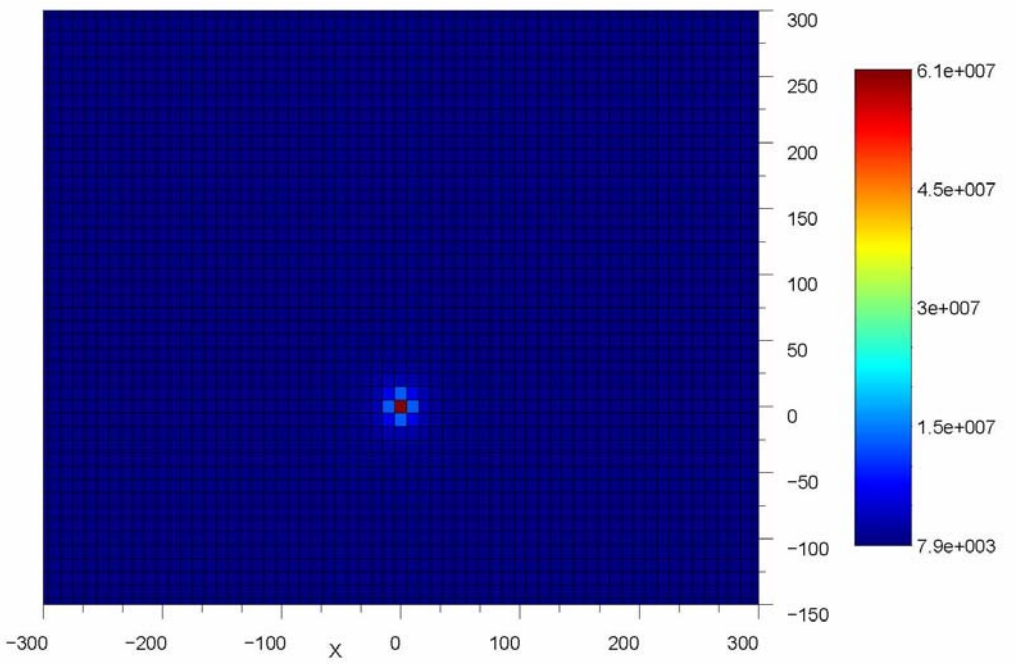

Figure 38. Depleted uranium prompt photoneutron flux ($cm^{-2}sec^{-1}$) 5 m from exit of the collimator (at target).

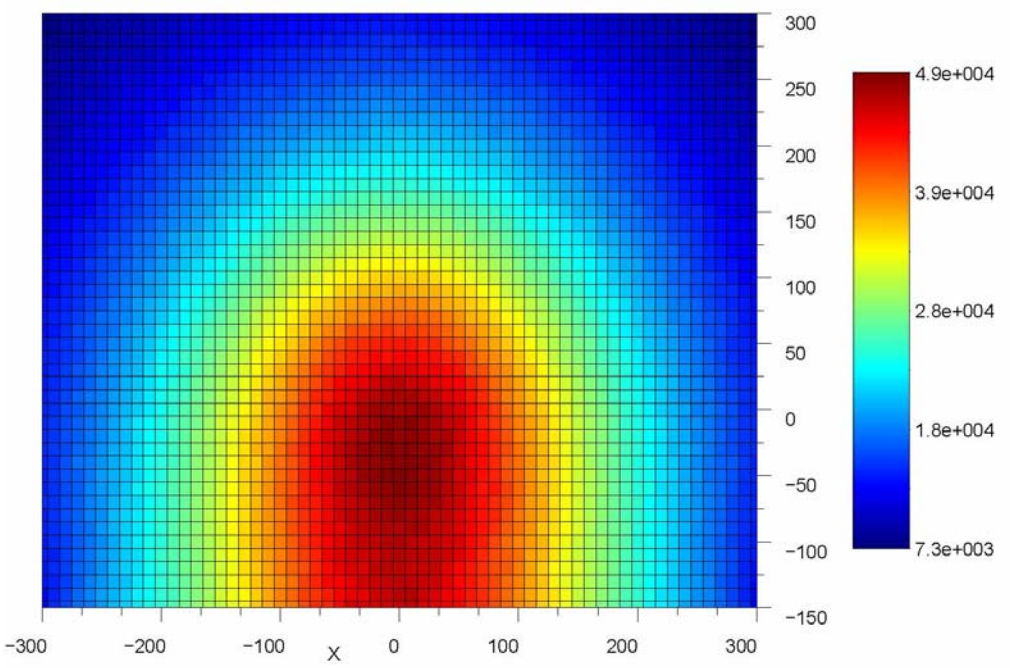

Figure 39. Depleted uranium prompt photoneutron flux ($cm^{-2}sec^{-1}$) 3 m from exit of the collimator.

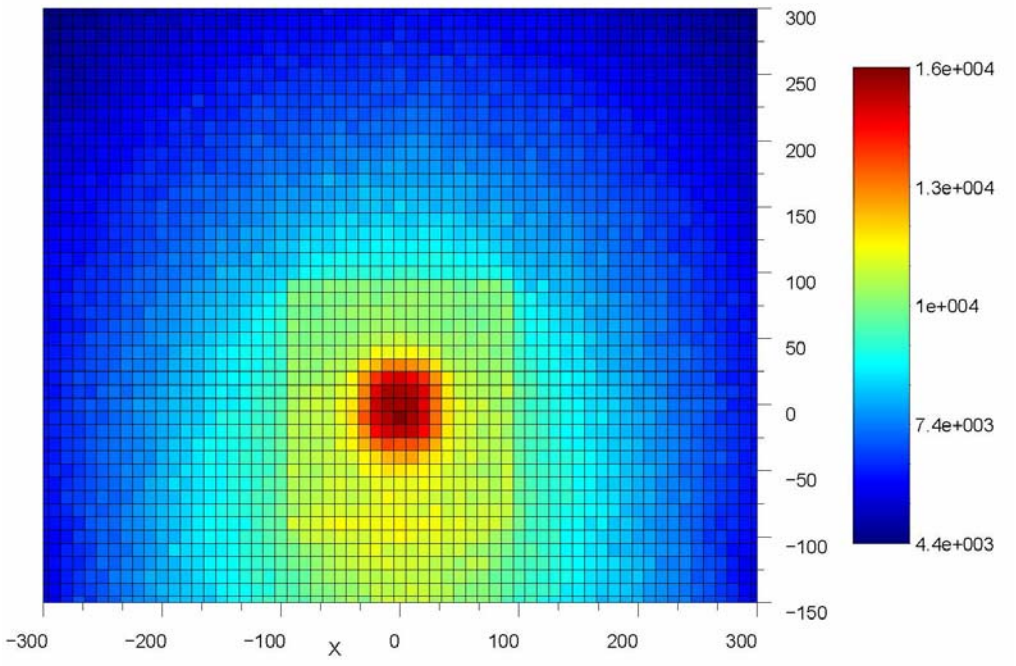

Figure 40. Depleted uranium prompt photoneutron flux ($cm^{-2}sec^{-1}$) 6.5 cm from exit of the collimator.

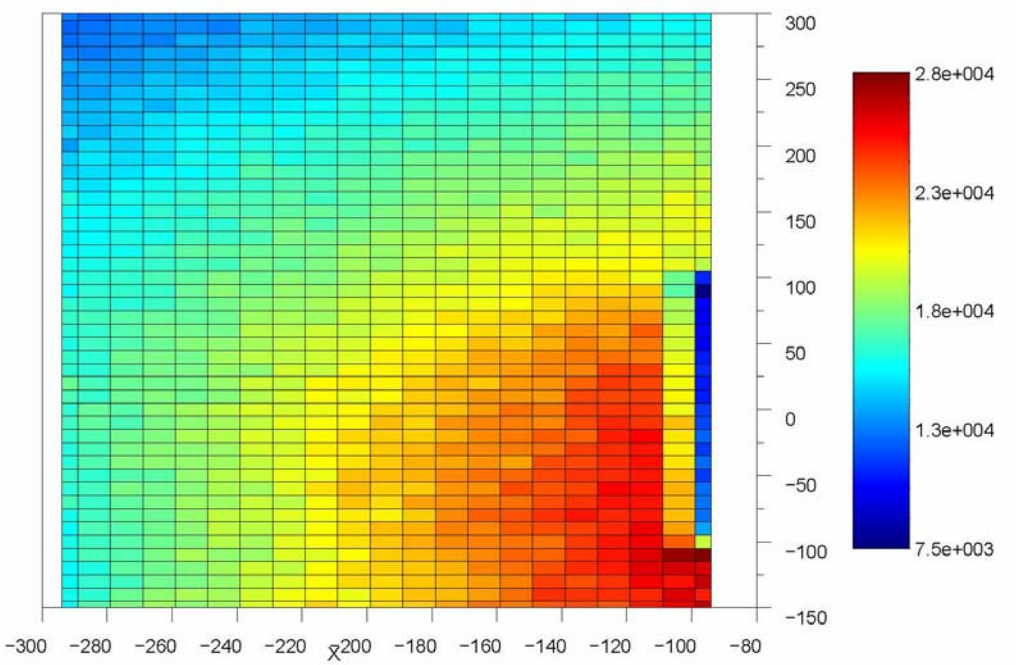

Figure 41. Depleted uranium prompt photoneutron flux ($cm^{-2}sec^{-1}$) on the side of the vehicle 4 cm downstream from the converter. Flux on the other side of the vehicle is symmetric.

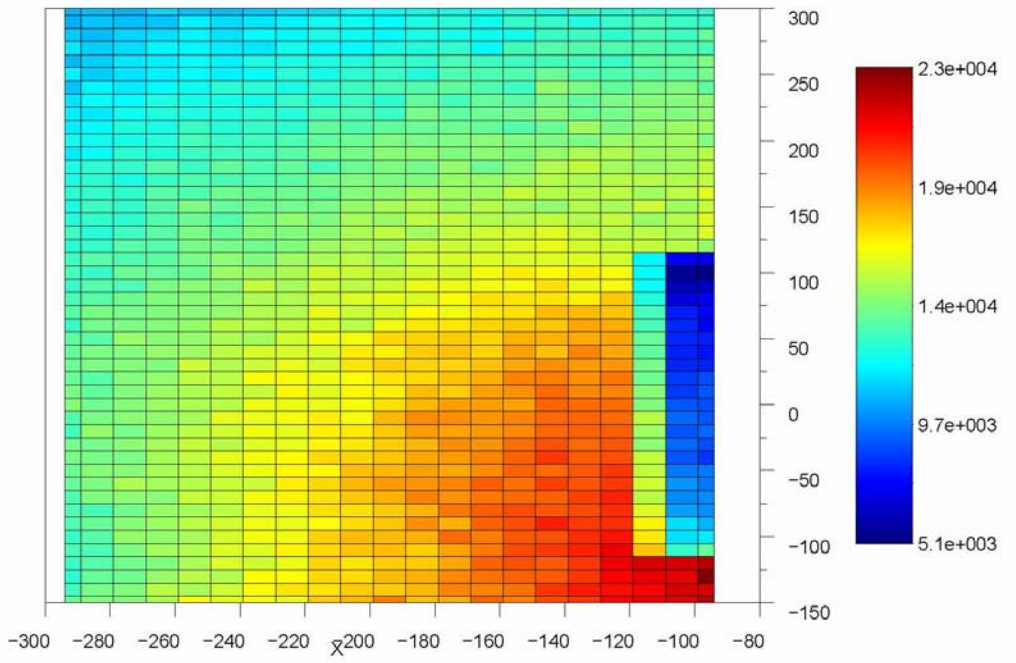

Figure 42. Depleted uranium prompt photoneutron flux ($cm^{-2}sec^{-1}$) on the side of the vehicle 56 cm upstream from the converter. Flux on the other side of the vehicle is symmetric.

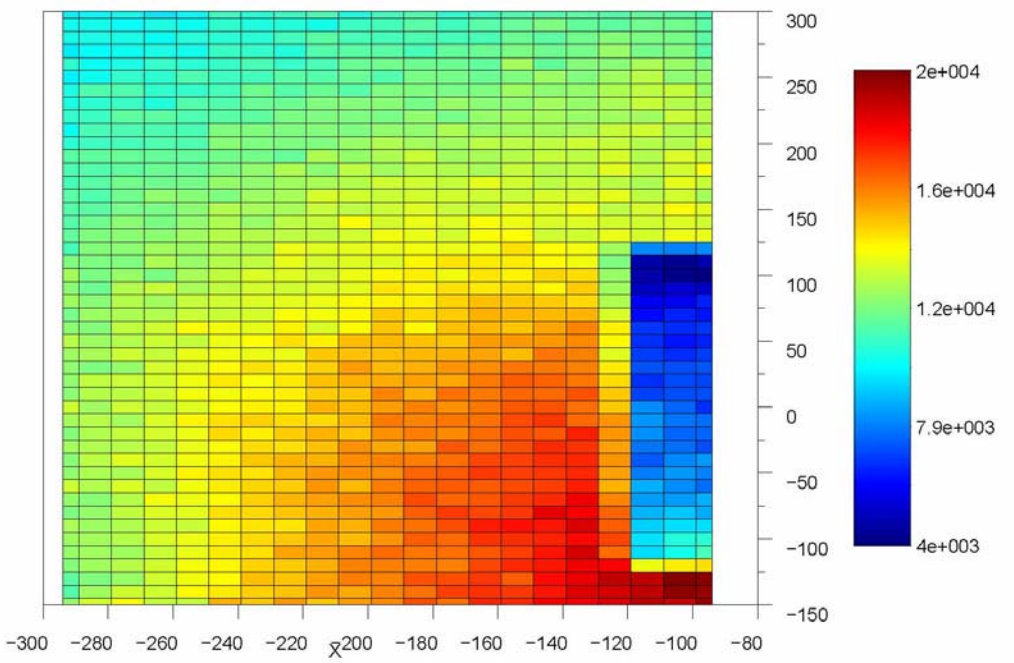

Figure 43. Depleted uranium prompt photoneutron flux ($cm^{-2}sec^{-1}$) on the side of the vehicle 96 cm upstream from the converter. Flux on the other side of the vehicle is symmetric.

One interesting observation in Figure 41 through Figure 43 is that the side of the vehicle causes a "shadow." The side of the vehicle is located at about -95 cm on the *x*-axis and extends from about -125 cm up to 125 cm along the *y*-axis. As one moves from the back of the vehicle toward the front of the vehicle (Figure 41 through Figure 43) the shadow becomes larger as more cells have their line of sight to the target cutoff. In Figure 38 through Figure 43, the effect of the ground reflecting neutrons is apparent.

6.3. HEU Target

The highly enriched uranium prompt photoneutron fluxes at the same six locations can be seen below in Figure 44 through Figure 49. The relative errors for Figure 44 through Figure 49 are again all less than 0.05.

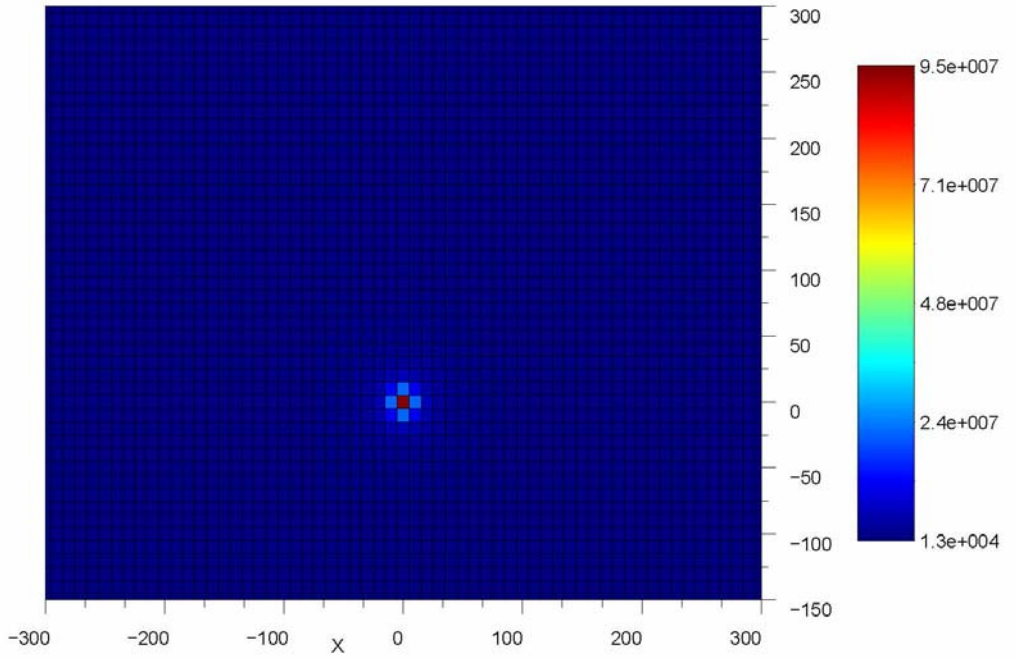

Figure 44. Highly enriched uranium prompt photoneutron flux ($cm^{-2}sec^{-1}$) 5 m from exit of the collimator (at target).

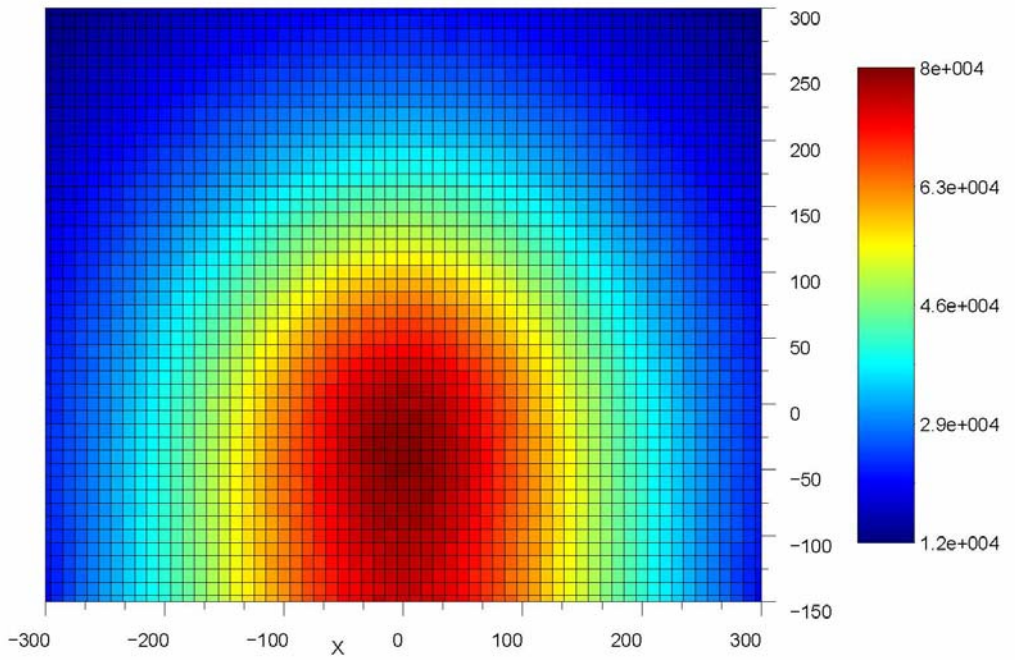

Figure 45. Highly enriched uranium prompt photoneutron flux ($cm^{-2}sec^{-1}$) 3 m from exit of the collimator.

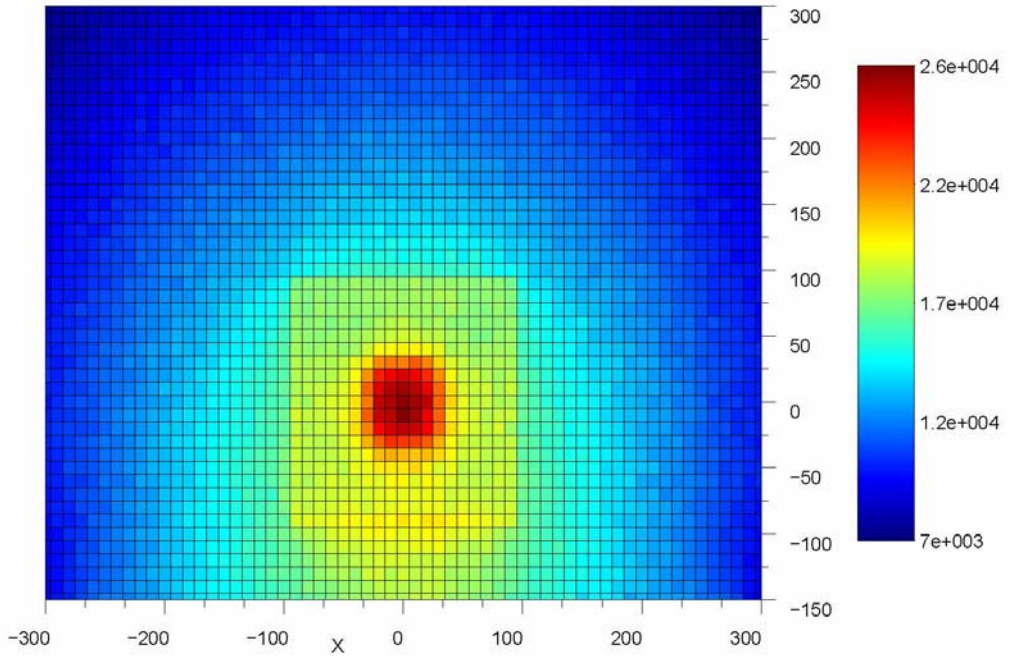

Figure 46. Highly enriched uranium prompt photoneutron flux ($cm^{-2}sec^{-1}$) 6.5 cm from exit of the collimator.

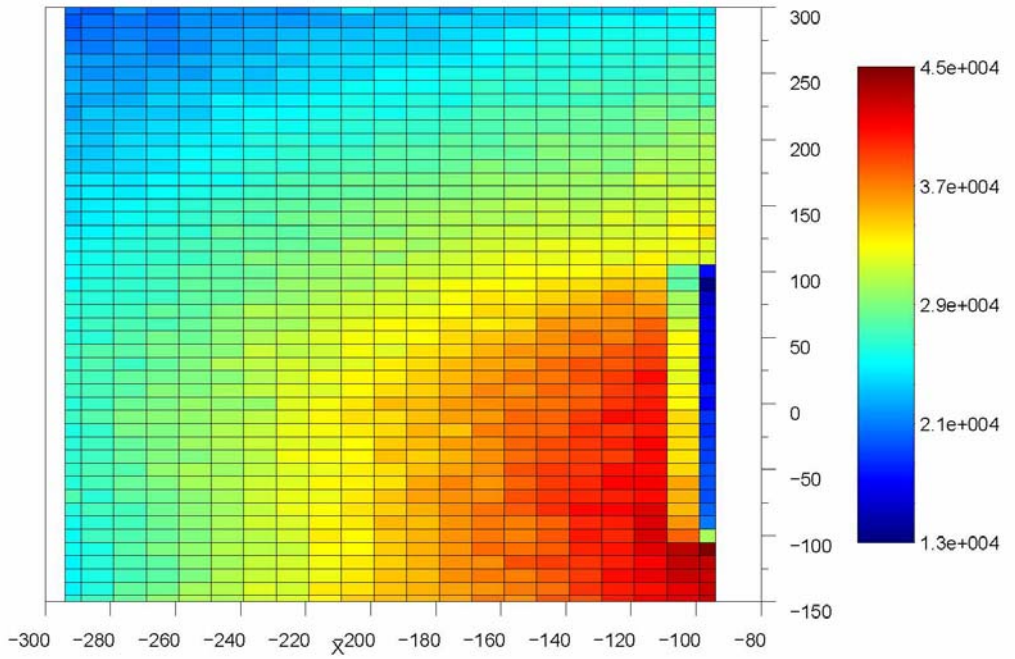

Figure 47. Highly enriched uranium prompt photoneutron flux ($cm^{-2}sec^{-1}$) along the side of the vehicle 4 cm downstream from the converter. Flux on the other side of the vehicle is symmetric.

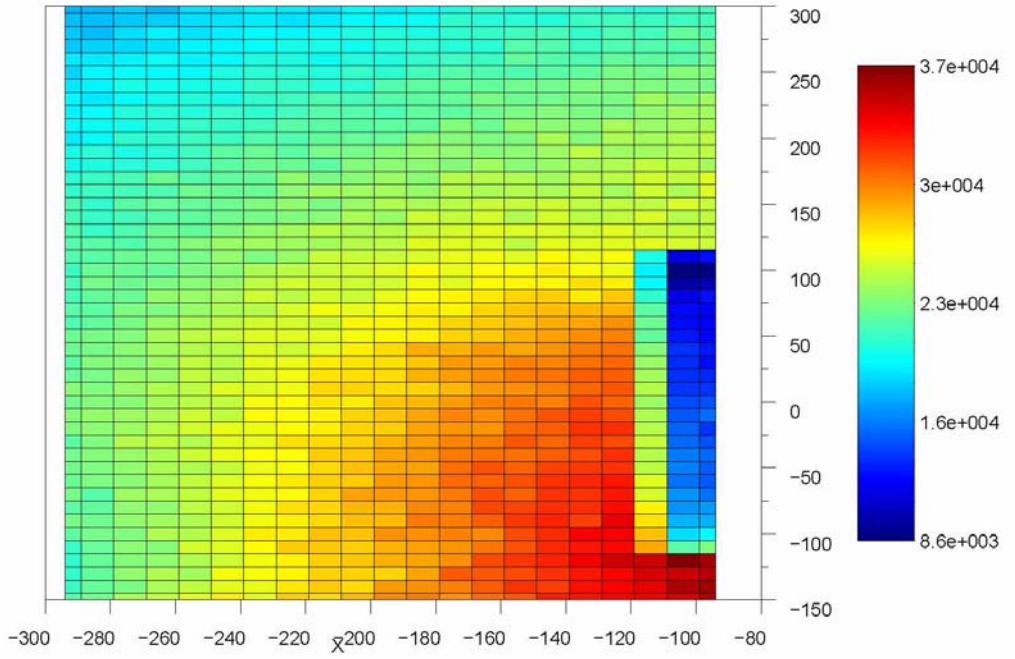

Figure 48. Highly enriched uranium prompt photoneutron flux ($cm^{-2}sec^{-1}$) along the side of the vehicle 56 cm upstream from the converter. Flux on the other side of the vehicle is symmetric.

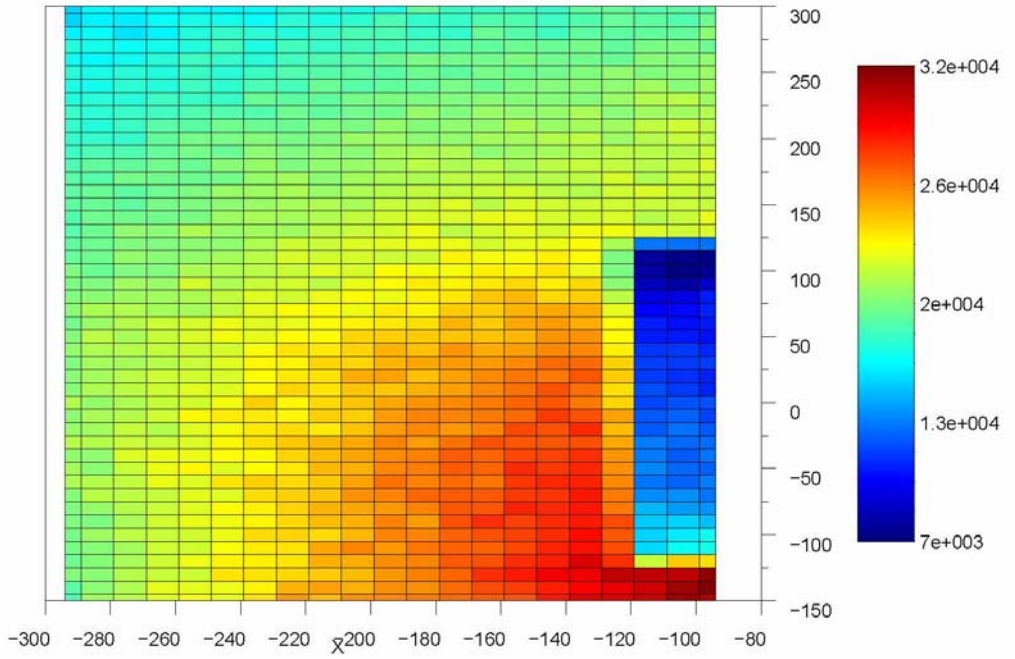

Figure 49. Highly enriched uranium prompt photoneutron flux ($cm^{-2}sec^{-1}$) along the side of the vehicle 96 cm upstream from the converter. Flux on the other side of the vehicle is symmetric.

The primary difference between the response from the HEU target and that of the DU target is the number of neutrons emitted; the flux map is otherwise similar. In fact, the response from the HEU is visually 50 percent greater throughout these results. These flux maps indicate that the detectors should be placed approximately 40 cm away from the vehicle and 150 cm above the ground (shown in Figure 48).

7. DELAYED NEUTRON MODELING

To approximate the relative contribution of delayed neutrons to the total neutron field, a simple delayed neutron source spectrum model was implemented in the MCNPX model (given in Appendix G). A 400-keV Maxwellian energy spectrum was generated homogeneously within the depleted uranium target and the resulting neutron fluence was tallied in the *x*-*z* plane at various *y*-values (elevations) throughout the entire geometry. The spectrum, shown in Figure 50, is expressed in units of delayed neutrons per square-centimeter per MeV for each source-delayed neutron.

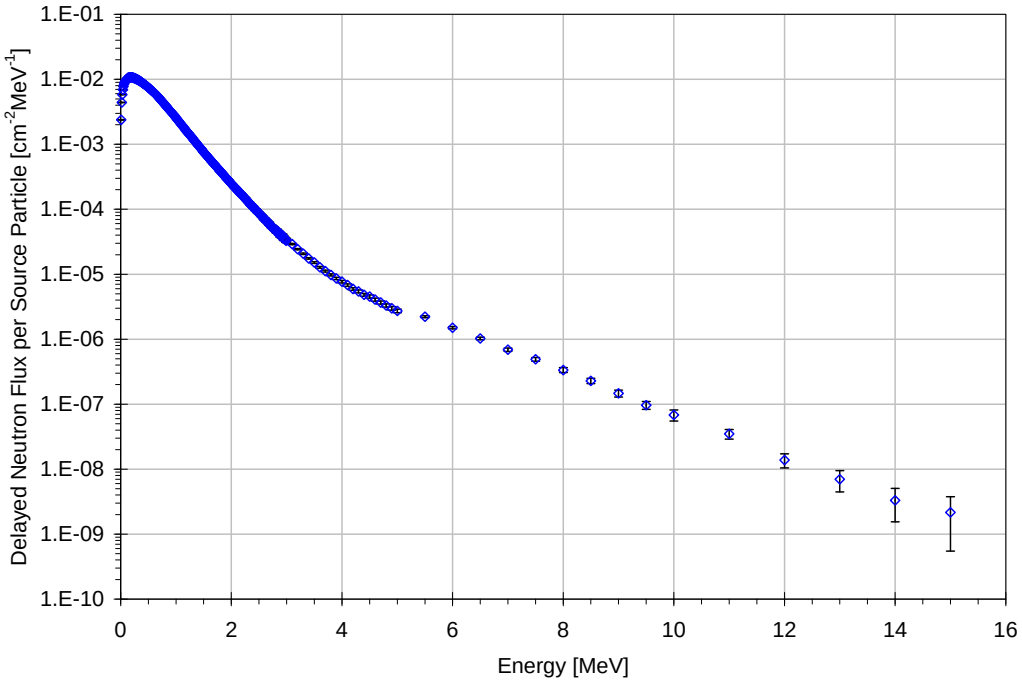

Figure 50. Maxwellian energy spectrum (400 keV) used to approximate the delayed neutron source. The flux is tallied on the surface of the target per source delayed neutron; three-sigma error bars are shown.

Figure 51 shows the results within the *x*-*z* plane at the geometric midplane ($y = 0$) of the system. The isotropic nature of the source is clearly shown. Also, there is a prominent shadowing effect on the neutron fluence due to the vehicle walls and the LINAC shielding. Since the remainder of the geometry is filled with air, there is a negligible attenuation of the neutrons. Instead, the flux is simply reduced in the typical $1/r^2$ manner.

Figure 52 and Figure 53 show the neutron field just inside the LINAC shielding above and below the beamline; the color scale is held constant in order to make a direct comparison to all other figures. As expected, these two neutron fields are fully symmetric about the geometric midplane. Figure 54 shows the fluence just below the LINAC shielding; however, the plotting plane is still close enough to the shielding to observe the shadow. Figure 55 and Figure 56 show the neutron fluence at two locations between LINAC shielding and the vehicle wall. The shadowing effect from the LINAC shielding is no longer visible. Figure 57 shows the results between the vehicle and the soil. The shadowing effect from the vehicle walls is no longer visible.

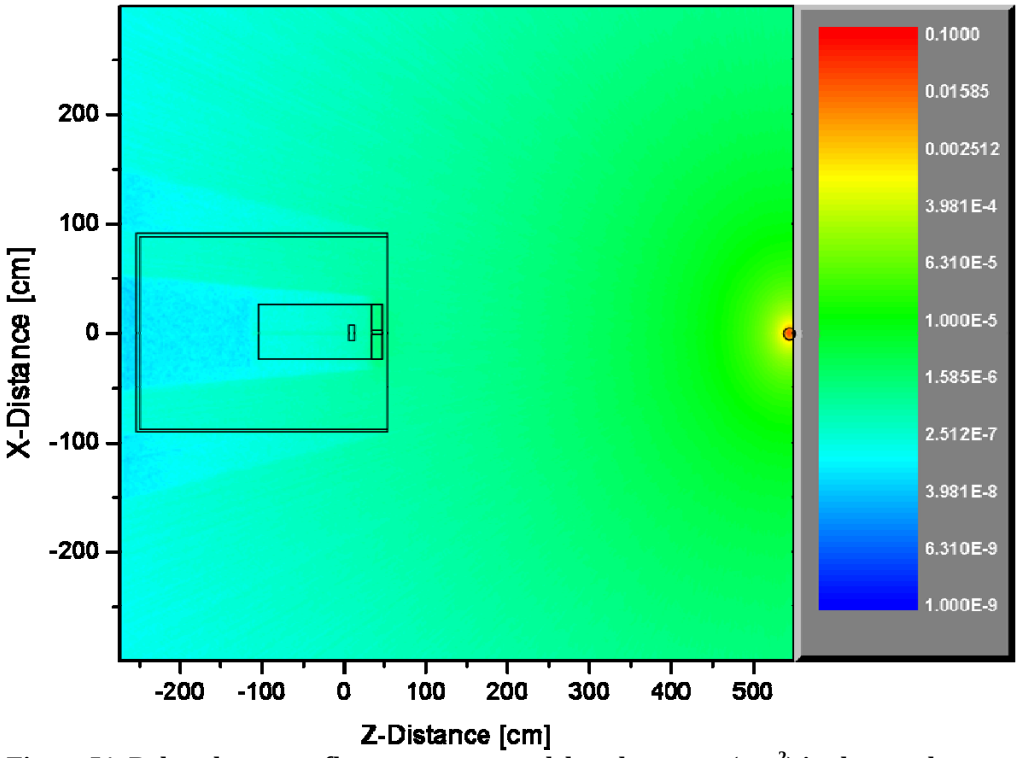

Figure 51. Delayed neutron fluence per source delayed neutron (cm^{-2}) in the *x*-*z* plane centered about y = 0 cm. This is the center-plane of the geometry.

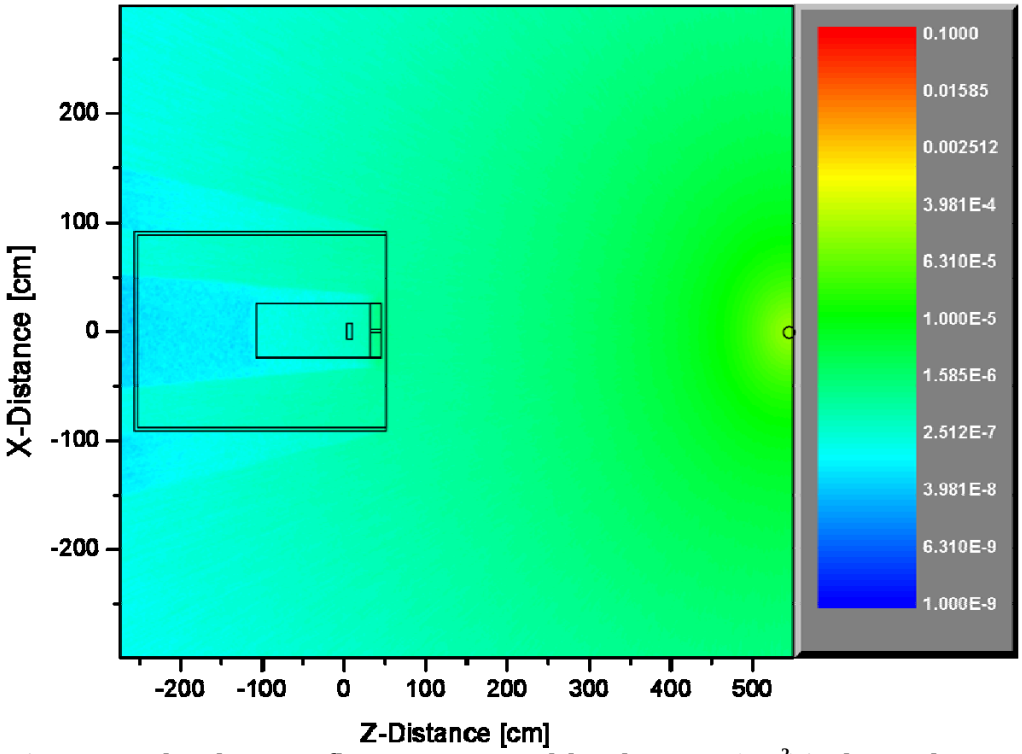

Figure 52. Delayed neutron fluence per source delayed neutron (cm^{-2}) in the *x-z* plane centered about y = 24 cm.

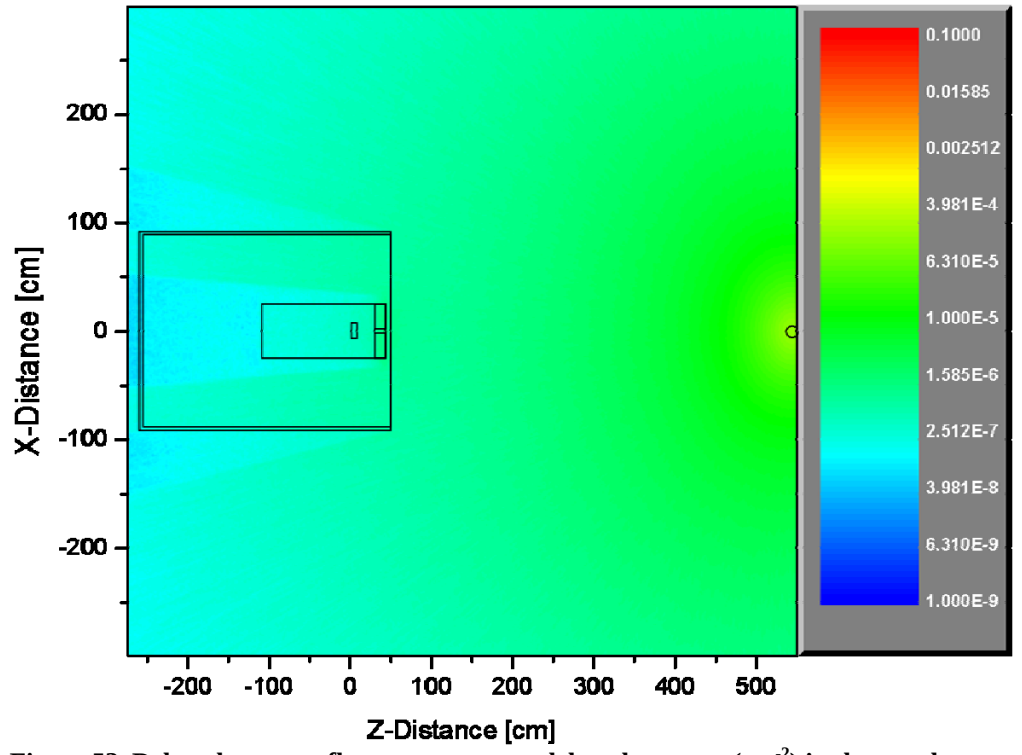

Figure 53. Delayed neutron fluence per source delayed neutron (cm^{-2}) in the *x-z* plane centered about y = -24 cm.

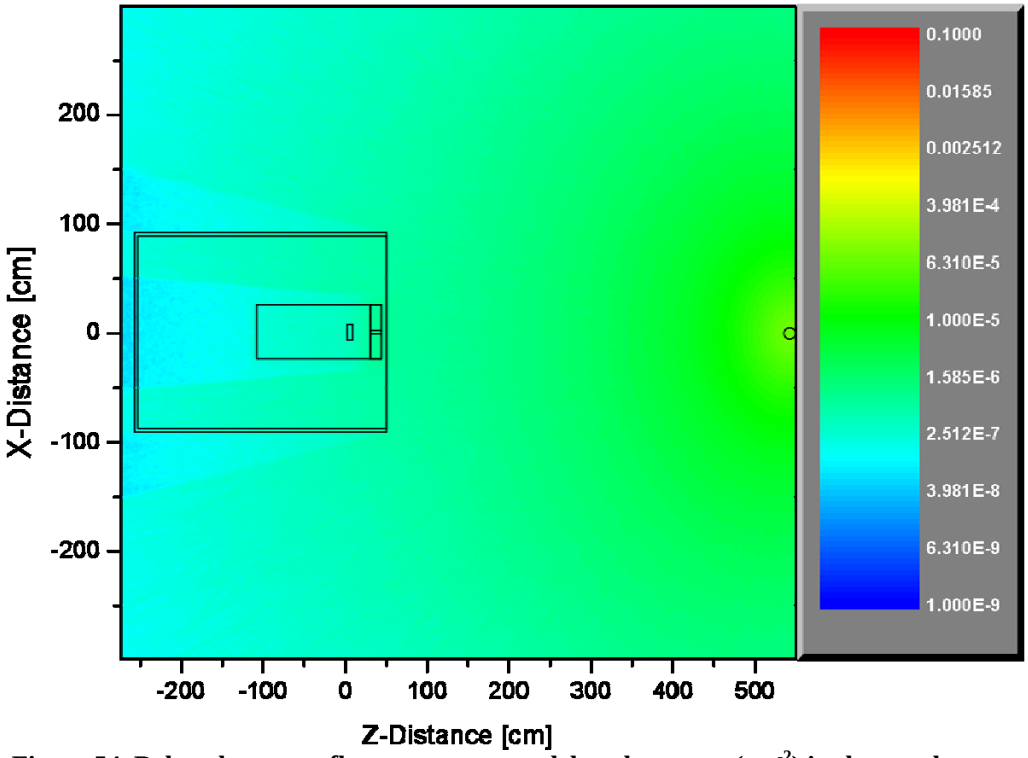

Figure 54. Delayed neutron fluence per source delayed neutron (cm^{-2}) in the *x-z* plane centered about y = -33.62 cm.

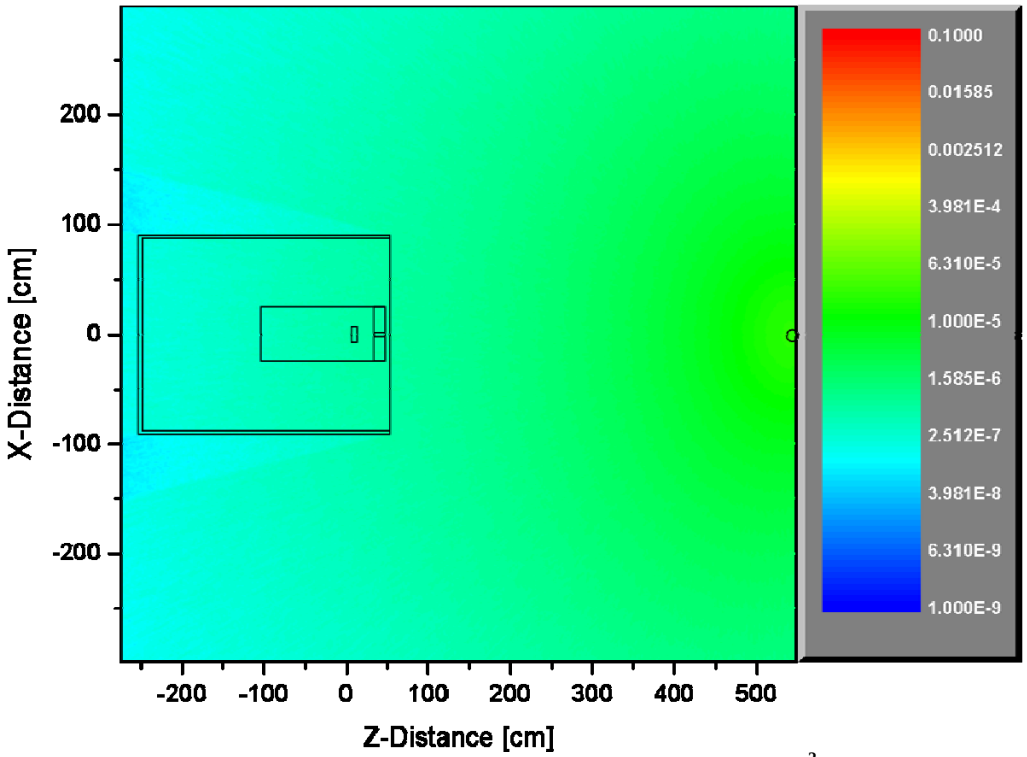

Figure 55. Delayed neutron fluence per source delayed neutron (cm^{-2}) in the *x-z* plane centered about y = -62 cm.

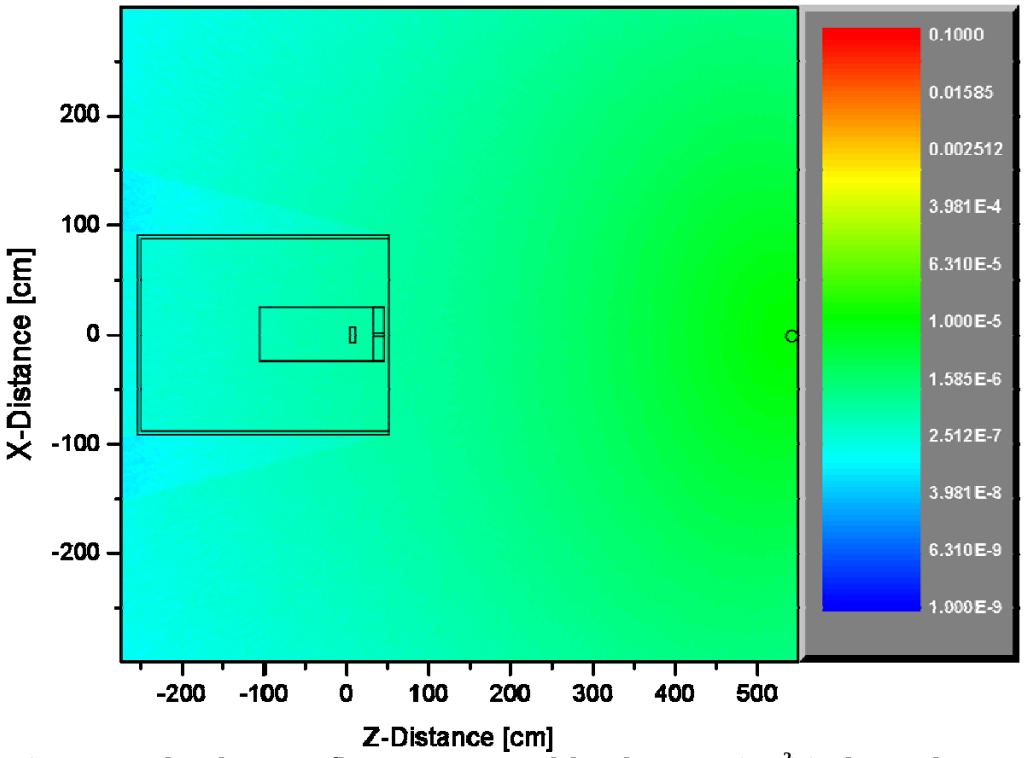

Figure 56. Delayed neutron fluence per source delayed neutron (cm^{-2}) in the *x-z* plane centered about y = -90.44 cm.

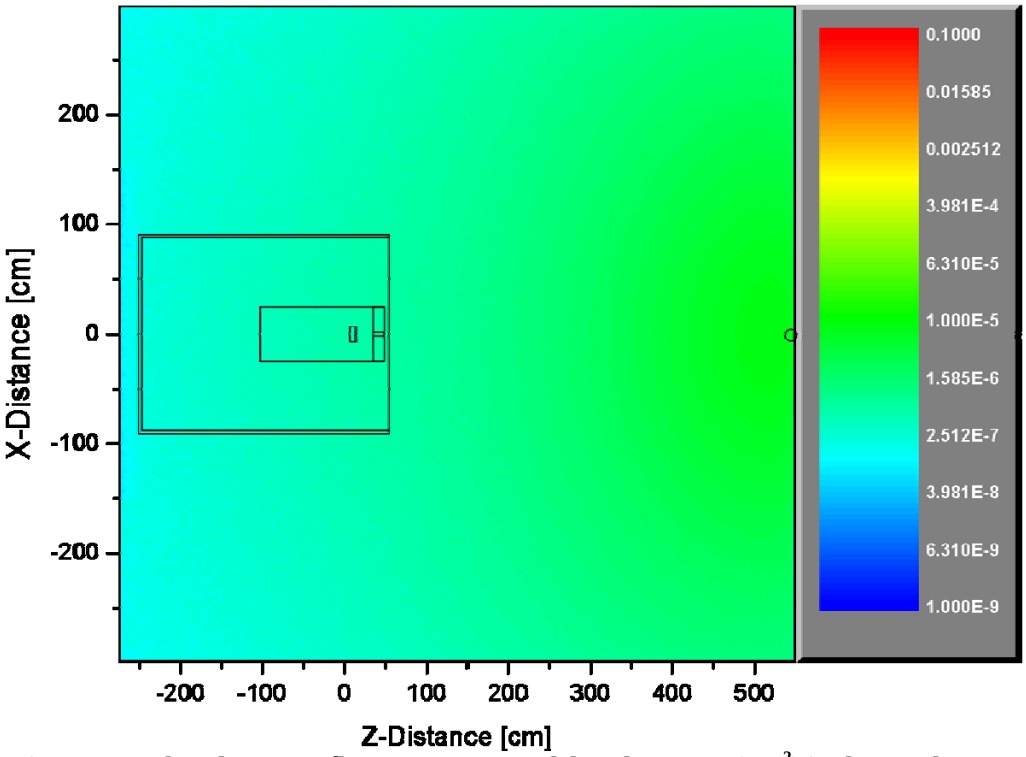

Figure 57. Delayed neutron fluence per source delayed neutron (cm^{-2}) in the *x-z* plane centered about y = -149 cm.

These results are not directly comparable to the prompt neutron results shown in Section 4 because the units are inconsistent—the prompt results are per *source electron,* whereas the delayed results are per *source delayed neutron*. Two primary conversion factors are needed to carry out a reasonable, albeit approximate, comparison of these results:

1. The number of fissions occurring in the target per source electron
2. The number of delayed neutrons released per fission ($\nu\beta$) of ^{238}U

The second of these factors is readily available for neutron-induced fission [3]: $\nu = 2.60$ and $\beta = 0.0157$. As a first approximation, it will be applied here to photon-induced fission. The first factor may be estimated from the MCNPX results to be 4.5e-6 reactions per electron. The delayed neutron fluence is multiplied by the product of these two factors to make a comparison to the prompt results. Figure 58 shows these results for the geometric mid-plane. A visual comparison reveals that the ratio between the delayed neutron field and the prompt neutron field, shown in Figure 22, is approximately 10^{-7}.

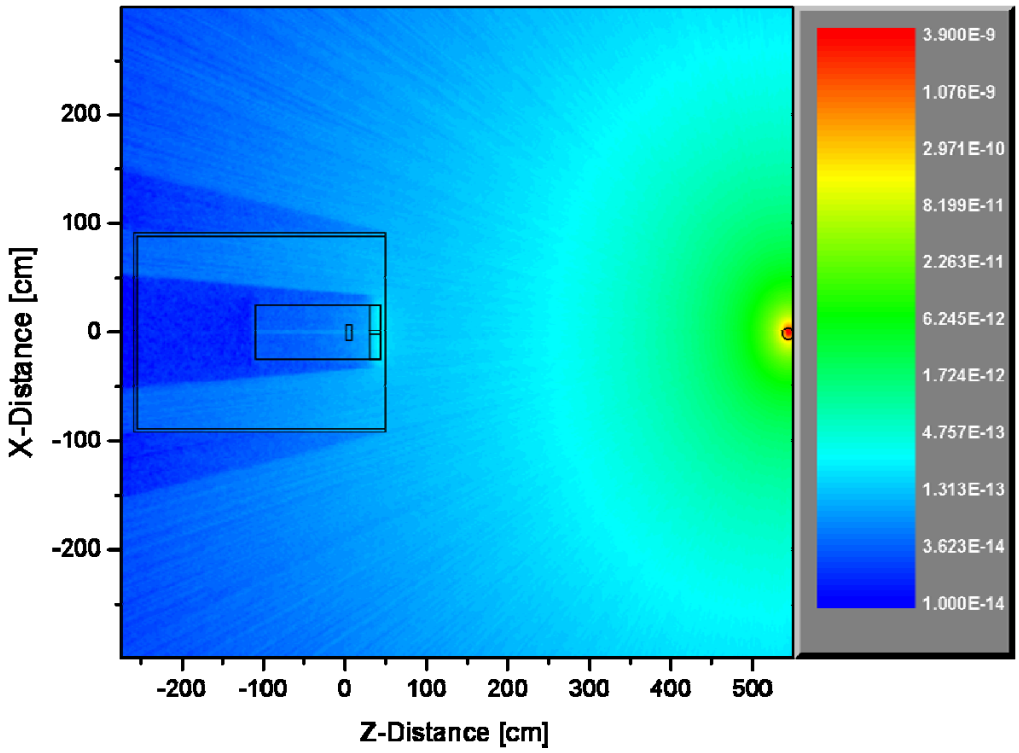

Figure 58. Delayed neutron fluence in the *x-z* plane centered about y = 0-cm scaled to reflect production per source electron.

8. CONCLUSIONS

Monte Carlo models of an active interrogation system, including the accelerator structure, transport vehicle walls, and the surrounding environment (air and soil) have been simulated using specialized versions of MCNPX and MCNP-PoliMi. Both prompt and delayed emissions from

the system, including the accelerator converter and shielding and a depleted uranium target, have been mapped in three dimensions. The time-dependence of the prompt neutrons in the system has also been characterized

Both the prompt and delayed neutrons and gamma rays from the bare target were characterized. The number of delayed neutrons emitted from the target is approximately seven orders of magnitude less than the total number of prompt neutrons emitted from the system. Therefore, in order to possibly detect the delayed neutrons, the detectors should be active only after all prompt neutrons have scattered out of the system. Preliminary results have shown this time to be greater than 5 μs after the accelerator pulse.

These models have also been analyzed to determine the most likely location of the detectors. The flux maps generated with the Monte Carlo model indicate that the detectors should be placed approximately 50 cm behind the exit of the accelerator, 40 cm away from the vehicle, and 150 cm above the ground. This position minimizes the number of neutrons coming from the accelerator structure, which must scatter backward and also receives the maximum flux of prompt neutrons coming from the source. The lead shielding around the accelerator minimizes the gamma ray background from the accelerator in this area.

This type of system is illustrative of a host of real-world scenarios of interest to nonproliferation and homeland security, including active interrogation at a standoff. Due to the multistep procedure of the MCNPX/MCNP-PoliMi code system, the analysis of somewhat modular—meaning that changing details such as the detector type, position, or surroundings does not require a recalculation of the source-target interactions. This feature allows for efficient parametric analysis of numerous system parameters without re-computing the constant source-target behavior. Such efficient analysis mechanisms could prove invaluable in the design and future deployment of an active interrogation detection system. In the future a complete analysis of detector performance and source classification is planned. The results will also be validated through comparison with experimental data.

9. ACKNOWLEDGMENT

Oak Ridge National Laboratory is managed and operated for the Department of Energy by UT-Battelle, LLC, under contract DE-AC05-00OR22725. This work was supported in part by the Defense Threat Reduction Agency (DTRA) and was performed under a Work-for-Others contract with NucSafe, Inc. of Oak Ridge, Tennessee.

10. REFERENCES

1. X-5 Monte Carlo Team, *MCNP—A General Monte Carlo N-Particle Transport Code,* Version 5, vols. 1–3. Los Alamos National Laboratory. LA-UR-03-1987, LA-CP-03-0245, and LA-CP-03-0284 (2003).
2. S. A. Pozzi, E. Padovani, and M. Marseguerra, "MCNP-PoliMi: A Monte Carlo Code for Correlation Measurements," *Nuclear Instruments and Methods,* **A513**: 550–558 (2003).
3. Karl O. Ott and Robert J. Neuhold, *Introductory Nuclear Reactor Dynamics.* American Nuclear Society, La Grange Park, IL (1985).

APPENDIXES

APPENDIX A

MCNPX INPUT FILE FOR SOURCE CHARACTERIZATION

Appendix A. MCNPX Input File for Source Chracterization

Electron Source:

```
25 MeV e-,25 nC per pulse,120 Hz, DU target
c CELL CARDS
c converter
1    1  -19.25      -1 2 -3
c
c pre-collimator
40    3  -11.344      4 -5 6 -7 8  -81 10
41    3  -11.344      4 -5 6 -7 81 -82 10
42    3  -11.344      4 -5 6 -7 82 -83 10
43    3  -11.344      4 -5 6 -7 83 -84 10
44    3  -11.344      4 -5 6 -7 84 -85 10
45    3  -11.344      4 -5 6 -7 85 -86 10
46    3  -11.344      4 -5 6 -7 86 -87 10
47    3  -11.344      4 -5 6 -7 87 -9  10
50    2  -1.205e-3    8  -81 -10
51    2  -1.205e-3    81 -82 -10
52    2  -1.205e-3    82 -83 -10
53    2  -1.205e-3    83 -84 -10
54    2  -1.205e-3    84 -85 -10
55    2  -1.205e-3    85 -86 -10
56    2  -1.205e-3    86 -87 -10
57    2  -1.205e-3    87 -9  -10
c
c soil
8    5  -1.6        11 -12 13 -14 16 -9
c
c target
9    7  -18.95     -18
c
c linac space
120  2  -1.205e-3  -120 -8 #1
c
c linac shielding
121  3  -11.344    -121 120 -8
c
c vehicle walls
100  8  -7.92      -100 101 -9
c air inside vehicle
101  4  -1.205e-3  -101 121 -9 (-4:5:-6:7:-8:9)
c
c air outside vehicle
900  4  -1.205e-3   11 -12 14 -15 16 -9 100
c
c outside world
12 0             -11:12:-13:15:-16:9
c END CELL CARDS-BLANK LINE FOLLOWS

c SURFACE CARDS
c converter
1  CZ   3.81
2  PZ   0.0
3  PZ   0.2286
c
c pre-collimator
c 4  PX -25
c 5  PX  25
c 6  PY -25
```

```
c 7  PY  25
4  PX -32.62
5  PX  32.62
6  PY -32.62
7  PY  32.62
8  PZ  28.1686
81 PZ  30.1686
82 PZ  32.1686
83 PZ  34.1686
84 PZ  36.1686
85 PZ  38.1686
86 PZ  40.1686
87 PZ  42.1686
9  PZ  43.4086
10 KZ 89.1286 4.340277778e-4 -1
c
c boundary planes
11 PX -300
12 PX  300
15 PY  300
16 PZ -275
17 PZ 550
c
c ground
13 PY -250      $ ground 1m thick
14 PY -150      $ beam center-line 1.5m above ground
c
c target
c 18 SZ 543.4086 3.978848
18 SZ 543.4086 5.0
c
c vehicle
100 101 RPP  -93.98 93.98  -93.98 93.98  -152.4  152.4
101 101 RPP  -93.345 93.345  -93.345 93.345  -151.765 152.4
120 102 RPP  -25    25     -25    25     -75     75
121 102 RPP  -32.62 32.62  -32.62 32.62  -85.62  75
c 120 102 RPP  -25    25     -25    25     -75     59.76
c 121 102 RPP  -32.62 32.62  -32.62 32.62  -85.62  59.76
c surfaces for tally segments - exiting precollimator
199 cz 0.15875
200 cz 0.3175
201 cz 0.47625
202 cz 0.635
203 cz 0.79375
204 cz 0.9525
205 cz 1.11125
206 cz 1.27
207 cz 1.77
208 cz 2.27
209 cz 2.77
210 cz 3.27
211 cz 3.77
212 cz 4.27
213 cz 4.77
214 cz 5.27
215 cz 5.77
216 cz 6.27
217 cz 6.77
218 cz 7.27
219 cz 8.27
220 cz 9.27
221 cz 10.27
222 cz 11.27
```

```
223 cz 12.27
224 cz 13.27
225 cz 14.27
226 cz 16.27
227 cz 18.27
228 cz 20.27
229 cz 22.27
230 cz 24.27
231 cz 26.27
232 cz 28.27
233 cz 30.27
234 cz 32.27
235 cz 34.27
236 cz 36.27
237 cz 38.27
238 cz 40.27
239 cz 42.27
240 cz 44.27
241 cz 46.27
242 cz 48.27
243 cz 50
c END SURFACE CARDS-BLANK LINE FOLLOWS

c DATA CARDS
mode n p e
c
c GEOMETRY TRANSLATIONS
TR101   0     0   -102.9914
TR102   0     0    -31.5914
c
c variance reduction
#     ext:p  fcl:p    imp:n    imp:p    imp:e
1     0.5z     0        1        1        1         $ converter
40    0.5z     0        1        2        4         $ pre-collimator
41    0.5z     0        1        4        4
42    0.5z     0        1        8        4
43    0.5z     0        1        16       8
44    0.5z     0        1        32       8
45    0.5z     0        1        64       8
46    0.5z     0        1       128       16
47    0.5z     0        1       256       16
50    0        1        1        2        2         $ pre-coll hole
51    0      .286       1        4        2
52    0      .286       1        8        2
53    0      .286       1        16       2
54    0      .286       1        32       4
55    0      .286       1        64       4
56    0      .286       1       128       4
57    0      .286       1       256       4
8     0.5y     0     .00390625 .0625   .00390625    $ soil
9     0        0        0        0        0         $ target
120   0        1        1        2        1         $ linac space
121   0.5z     0        1        1        1         $ linac shielding
100   0.5z     0     0.0625    0.25    0.0625       $ vehicle walls
101   0       0.25    0.25      0.5     0.25        $ air inside vehicle
900   0        0     0.015625  .125    0.015625     $ air outside vehicle
12    0        0        0        0        0         $ outside world
bbrem 1 1 46i 15 1 2 3 4 5 6 7 8
c
c source
sdef sur=2 erg=d1 dir=d2 vec=0 0 1 nrm=1 pos=0 0 0 rad=d3 axs=0 0 1
     par=e
si1 h 23.75 26.25
```

```
sp1 d 0 1
si2 h -1 0.999847695 1
sp2 d  0 0 1
si3 a 0 0.25
sp3   0 0.25
c
c tallies
c neutron
f1:n 9
fm1 1.872453e13
fs1 -199 -200 -201 -202 -203 -204 -205 -206 -207 -208 -209 -210 -211 -212 -213
     -214 -215 -216 -217 -218 -219 -220 -221 -222 -223 -224 -225 -226 -227 -228
     -229 -230 -231 -232 -233 -234 -235 -236 -237 -238 -239 -240 -241 -242 -243
     t
e1 .2 7i 1 11i 4 4.25 102i 30
c photon
f11:p 9
fm11 1.872453e13
fs11 -199 -200 -201 -202 -203 -204 -205 -206 -207 -208 -209 -210 -211 -212 -213
     -214 -215 -216 -217 -218 -219 -220 -221 -222 -223 -224 -225 -226 -227 -228
     -229 -230 -231 -232 -233 -234 -235 -236 -237 -238 -239 -240 -241 -242 -243
     t
c electron
f21:e 9
fm21 1.872453e13
fs21 -199 -200 -201 -202 -203 -204 -205 -206 -207 -208 -209 -210 -211 -212 -213
     -214 -215 -216 -217 -218 -219 -220 -221 -222 -223 -224 -225 -226 -227 -228
     -229 -230 -231 -232 -233 -234 -235 -236 -237 -238 -239 -240 -241 -242 -243
     t
c all tally parameters
e0 4.25 102i 30
c *c0 90 80 70 60 50 40 35 30 25 20 15 10 7.5 5 2.5 2.4 2.3 2.2 2.1 2 1.9 1.8
c      1.7 1.6 1.5 1.4 1.3 1.2 1.1 1 0.9 0.8 0.7 0.6 0.5 0.4 0.3 0.2 0.1 0
c0 0 1.73648178E-1 3.42020143E-1 5.00000000E-1 6.42787610E-1 7.66044443E-1
     8.19152044E-1 8.66025404E-1 9.06307787E-1 9.39692621E-1 9.65925826E-1
     9.84807753E-1               9.85109326E-1 9.85407898E-1 9.85703469E-1
     9.85996037E-1 9.86285602E-1 9.86572162E-1 9.86855716E-1 9.87136265E-1
     9.87413807E-1 9.87688341E-1 9.87959866E-1 9.88228381E-1 9.88493887E-1
     9.88756381E-1 9.89015863E-1 9.89272333E-1 9.89525789E-1 9.89776231E-1
     9.90023658E-1 9.90268069E-1 9.90509463E-1 9.90747840E-1 9.90983200E-1
     9.91215540E-1 9.91444861E-1 9.91671162E-1 9.91894443E-1 9.92114701E-1
     9.92331938E-1 9.92546152E-1 9.92757342E-1 9.92965508E-1 9.93170650E-1
     9.93372766E-1 9.93571856E-1 9.93767919E-1 9.93960955E-1 9.94150964E-1
     9.94337944E-1 9.94521895E-1 9.94702817E-1 9.94880709E-1 9.95055570E-1
     9.95227400E-1 9.95396198E-1 9.95561965E-1 9.95724698E-1 9.95884399E-1
     9.96041065E-1 9.96194698E-1 9.96345296E-1 9.96492859E-1 9.96637387E-1
     9.96778878E-1 9.96917334E-1 9.97052752E-1 9.97185134E-1 9.97314477E-1
     9.97440783E-1 9.97564050E-1 9.97684279E-1 9.97801468E-1 9.97915618E-1
     9.98026728E-1 9.98134798E-1 9.98239828E-1 9.98341817E-1 9.98440764E-1
     9.98536670E-1 9.98629535E-1 9.98719357E-1 9.98806137E-1 9.98889875E-1
     9.98970570E-1 9.99048222E-1 9.99122830E-1 9.99194395E-1 9.99262916E-1
     9.99328394E-1 9.99390827E-1 9.99450216E-1 9.99506560E-1 9.99559860E-1
     9.99610115E-1 9.99657325E-1 9.99701490E-1 9.99742609E-1 9.99780683E-1
     9.99815712E-1 9.99847695E-1 9.99876632E-1 9.99902524E-1 9.99925370E-1
     9.99945169E-1 9.99961923E-1 9.99975631E-1 9.99986292E-1 9.99993908E-1
     9.99998477E-1 1 t
c
c materials
m1 nlib=66c plib=04p elib=03e pnlib=26u gas=0 estep=4 $ tungsten
     74182 0.2642 74183 0.1428 74184.24u 0.307 74186 0.286
m2 nlib=66c plib=04p elib=03e pnlib=25u gas=1 estep=210 $ air between W & Pb
45% humidity
     1001 1.169196E-02 1002.24u 1.344730E-06
```

```
     7014 7.681679E-01 7015 2.837299E-03
     8016.24u 2.121736E-01 8017 5.168377E-04
     18000.59c 4.611104E-03
c mx2:p 0 5j 18040
mpn2 0 1002 7014 7015 8016 8017 18040
m3 nlib=66c plib=04p elib=03e pnlib=24u gas=0 estep=4 $ lead
     82206 0.255 82207 0.221 82208 0.524
m4 nlib=66c plib=04p elib=03e pnlib=25u gas=1 estep=12 $ air everywhere else
45% humidity
     1001 1.169196E-02 1002.24u 1.344730E-06
     7014 7.681679E-01 7015 2.837299E-03
     8016.24u 2.121736E-01 8017 5.168377E-04
     18000.59c 4.611104E-03
c mx4:p 0 5j 18040
mpn4 0 1002 7014 7015 8016 8017 18040
m5 nlib=66c plib=04p elib=03e pnlib=25u gas=0 estep=3 $ LANL soil + 20% water
     1001 4.832564E-02 1002.24u 5.558087E-06
     8016.24u 6.950058E-01 8017 1.692978E-03
     11023 3.155206E-03
     13027 3.045777E-02
     14028 1.934418E-01 14029 9.822504E-03 14030 6.475067E-03
     19000 4.523070E-03
     26054 4.146826E-04 26056 6.509629E-03 26057 1.503357E-04
     26058 2.000693E-05
c mx5:p 0 8j 19039 4j
mpn5 0 1002 8016 8017 11023 13027 14028 14029 14030 19039
     26054 26056 26057 26058
m6 nlib=66c plib=04p elib=03e pnlib=27u gas=0 estep=4 $ heu rho=18.75
     92235 0.98 92238 0.02
m7 nlib=66c plib=04p elib=03e pnlib=27u gas=0 estep=4 $ du rho=18.95
     92238 1
c stainless steel
M8 NLIB=66c PLIB=04p elib=03e pnlib=25u gas=0 estep=5
     26054 3.470e-3
     26056 5.447e-2
     26057 1.258e-3
     24050 7.573e-4
     24052 1.450e-2
     24053 1.656e-3
     24054 4.122e-4
     28058 5.288e-3
     28060 2.024e-3
     28064 7.148e-4
     25055 1.740e-3
c
TOTNU
c energy and thermal treatment
phys:n 30
phys:p 30 2j -1 0
phys:e 30
c cut off
cut:n j 0.1
cut:p j 4.0
cut:e j 4.0
nps 5e3
c ctme 7200
c peripheral
prdmp j 1e8 j 2 1e8
print
c dbcn 7j 1 4j j
rand gen=2 stride=611671
c end of file
```

APPENDIX B

MCNPX INPUT FILE FOR LINAC BEAM CHARACTERIZATION

Appendix B. MCNPX Input Files for LINAC Beam Characterization

No Soil:

```
25 MeV e-,25 nC per pulse,120 Hz,W converter and Pb pre-collimator only,wwg e
c cell cards
1  1 -19.35     -1 2 -3                    imp:n,p,e=1
2  2 -1.205e-3  4 -5 6 -7 3 -8             imp:n,p,e=1
3  2 -1.205e-3  -11 -9                     imp:n,p,e=2
4  2 -1.205e-3  -11 9                      imp:n,p,e=8
5  3 -11.344    4 -5 6 -7 8 -9 11          imp:n,p,e=2
6  3 -11.344    4 -5 6 -7 9 -10 11         imp:n,p,e=8
7  4 -1.205e-3  (12 -13 14 -15 2 -10) (-4:5:-6:7:-3:10) (1:-2:3)
                                           imp:n,p,e=1
8  4 -1.205e-3  12 -13 14 -15 10 -16       imp:n,p,e=16
9  4 -1.205e-3  12 -13 14 -15 16 -17       imp:n,p,e=32
10 4 -1.205e-3  12 -13 14 -15 17 -18       imp:n,p,e=64
11 4 -1.205e-3  12 -13 14 -15 18 -19       imp:n,p,e=128
12 4 -1.205e-3  12 -13 14 -15 19 -20       imp:n,p,e=256
13 4 -1.205e-3  12 -13 14 -15 20 -21       imp:n,p,e=512
14 0            -12:13:-14:15:-2:21        imp:n,p,e=0

c surface cards
1 cz 3.81
2 pz 0
3 pz 0.2286
4 px -22.86
5 px 22.86
6 py -22.86
7 py 22.86
8 pz 28.1686
9 pz 35.7886
10 pz 43.4086
11 trc 0 0 43.4086 0 0 -15.24 0.9525 1.27
12 px -300
13 px 300
14 py -300
15 py 300
16 pz 543.4084
17 pz 1043.4086
18 pz 1543.4086
19 pz 2043.4086
20 pz 2543.4086
21 pz 3043.4086
c surfaces for tally segments - exiting precollimator
100 cz 1.27
101 cz 5.27
102 cz 9.27
103 cz 13.27
104 cz 17.27
105 cz 21.27
106 cz 25.27
107 cz 29.27
108 cz 33.27
109 cz 37.27
110 cz 41.27
111 cz 45.27
c surfaces for tally segments - air up to 30m
112 cz 10
113 cz 20
114 cz 30
```

```
115 cz 40
116 cz 50
117 cz 60
118 cz 70
119 cz 80
120 cz 90
121 cz 100
122 cz 120
123 cz 140
124 cz 160
125 cz 180
126 cz 200
127 cz 220
128 cz 240
129 cz 260
130 cz 280
131 cz 300

c data cards
mode n p e
c variance reduction
ext:p 0.2z 0 0 0 0.5z 0.5z 0 0 0 0 0 0 0 0
ext:n 0 0 0 0 0.25z 0.3z 0 0 0 0 0 0 0 0
fcl:p 0 1 1 1 0 0 0 0.5 0.5 0.5 0.5 0.5 0.5 0
fcl:n 0 1 1 1 0 0 0 0.5 0.5 0.5 0.5 0.5 0.5 0
wwg 161 0 0 j 0
wwge:n 1 30
wwge:p 1 11 30
wwge:e 1 21 30
mesh geom=xyz ref=0 0 0.1 origin=-300.01 -300.01 -1e-4
     imesh=300.01
     jmesh=300.01
     kmesh=0.2286 28.1686 43.4086 543.4084 1043.4086 1543.4086
           2043.4086 2543.4086 3044
     kints=1 1 15 1 1 1 1 1 1
c source
sdef sur=2 erg=d1 dir=d2 vec=0 0 1 nrm=1 pos=0 0 0 rad=d3 axs=0 0 1
     par=e
si1 h 23.75 26.25
sp1 d 0 1
si2 h -1 0.999847695 1
sp2 d  0 0 1
si3 a 0 0.25
sp3   0 0.25
c tallies
c tallies exiting precollimator
f1:n 10
fm1 1.872453e13
fs1 -100 -101 -102 -103 -104 -105 -106 -107 -108 -109 -110 -111 t
c
f11:p 10
fm11 1.872453e13
fs11 -100 -101 -102 -103 -104 -105 -106 -107 -108 -109 -110 -111 t
c
f21:e 10
fm21 1.872453e13
fs21 -100 -101 -102 -103 -104 -105 -106 -107 -108 -109 -110 -111 t
c e0 1e-6 1e-5 1e-4 1e-3 1e-2 1e-1
e0 2e-1 3e-1 4e-1 5e-1 6e-1 7e-1 8e-1 9e-1
     1 2 3 4 5 6 7 8 9
     11 12 13 14 15 16 17 18 19
     20 21 22 23 24 25 26 27 28 29 30 t
*c0 90 80 70 60 50 40 35 30 25 20 15 10 7.5 5 2.5 0 t
```

```
c diagnotic tallies
f31:e 3
c31 1
fm31 1.872453e13
c
f41:e 8
c41 1
fm41 1.872453e13
fs41 -11.1 t
c tallies up 30m after precollimator
f51:n 16
fm51 1.872453e13
fs51 -112 -113 -114 -115 -116 -117 -118 -119 -120 -121 -122 -123 -124
     -125 -126 -127 -128 -129 -130 -131 t
c
f61:n 17
fm61 1.872453e13
fs61 -112 -113 -114 -115 -116 -117 -118 -119 -120 -121 -122 -123 -124
     -125 -126 -127 -128 -129 -130 -131 t
c
f71:n 18
fm71 1.872453e13
fs71 -112 -113 -114 -115 -116 -117 -118 -119 -120 -121 -122 -123 -124
     -125 -126 -127 -128 -129 -130 -131 t
c
f81:n 19
fm81 1.872453e13
fs81 -112 -113 -114 -115 -116 -117 -118 -119 -120 -121 -122 -123 -124
     -125 -126 -127 -128 -129 -130 -131 t
c
f91:n 20
fm91 1.872453e13
fs91 -112 -113 -114 -115 -116 -117 -118 -119 -120 -121 -122 -123 -124
     -125 -126 -127 -128 -129 -130 -131 t
c
f101:n 21
fm101 1.872453e13
fs101 -112 -113 -114 -115 -116 -117 -118 -119 -120 -121 -122 -123 -124
     -125 -126 -127 -128 -129 -130 -131 t
c
f111:p 16
fm111 1.872453e13
fs111 -112 -113 -114 -115 -116 -117 -118 -119 -120 -121 -122 -123 -124
     -125 -126 -127 -128 -129 -130 -131 t
c
f121:p 17
fm121 1.872453e13
fs121 -112 -113 -114 -115 -116 -117 -118 -119 -120 -121 -122 -123 -124
     -125 -126 -127 -128 -129 -130 -131 t
c
f131:p 18
fm131 1.872453e13
fs131 -112 -113 -114 -115 -116 -117 -118 -119 -120 -121 -122 -123 -124
     -125 -126 -127 -128 -129 -130 -131 t
c
f141:p 19
fm141 1.872453e13
fs141 -112 -113 -114 -115 -116 -117 -118 -119 -120 -121 -122 -123 -124
     -125 -126 -127 -128 -129 -130 -131 t
c
f151:p 20
fm151 1.872453e13
fs151 -112 -113 -114 -115 -116 -117 -118 -119 -120 -121 -122 -123 -124
```

```
     -125 -126 -127 -128 -129 -130 -131 t
c
f161:p 21
fm161 1.872453e13
fs161 -112 -113 -114 -115 -116 -117 -118 -119 -120 -121 -122 -123 -124
     -125 -126 -127 -128 -129 -130 -131 t
c
f171:e 16
fm171 1.872453e13
fs171 -112 -113 -114 -115 -116 -117 -118 -119 -120 -121 -122 -123 -124
     -125 -126 -127 -128 -129 -130 -131 t
c
f181:e 17
fm181 1.872453e13
fs181 -112 -113 -114 -115 -116 -117 -118 -119 -120 -121 -122 -123 -124
     -125 -126 -127 -128 -129 -130 -131 t
c
f191:e 18
fm191 1.872453e13
fs191 -112 -113 -114 -115 -116 -117 -118 -119 -120 -121 -122 -123 -124
     -125 -126 -127 -128 -129 -130 -131 t
c
f201:e 19
fm201 1.872453e13
fs201 -112 -113 -114 -115 -116 -117 -118 -119 -120 -121 -122 -123 -124
     -125 -126 -127 -128 -129 -130 -131 t
c
f211:e 20
fm211 1.872453e13
fs211 -112 -113 -114 -115 -116 -117 -118 -119 -120 -121 -122 -123 -124
     -125 -126 -127 -128 -129 -130 -131 t
c
f221:e 21
fm221 1.872453e13
fs221 -112 -113 -114 -115 -116 -117 -118 -119 -120 -121 -122 -123 -124
     -125 -126 -127 -128 -129 -130 -131 t
c materials
m1 nlib=66c plib=04p elib=03e pnlib=26u gas=0 estep=4 $ tungsten
     74182 0.2642 74183 0.1428 74184.24u 0.307 74186 0.286
m2 nlib=66c plib=04p elib=03e pnlib=25u gas=1 estep=210 $ air between W & Pb
     7014 -7.524886e-1 7015 -2.779386e-3
     8016.24u -2.312178e-1 8017 -5.632278e-4
     18000.59c -1.2827e-2
     6000 -1.24e-4
mx2:p 4j 18040 6012
m3 nlib=66c plib=04p elib=03e pnlib=24u gas=0 estep=4 $ lead
     82206 0.255 82207 0.221 82208 0.524
m4 nlib=66c plib=04p elib=03e pnlib=25u gas=1 estep=12 $ air everywhere else
     7014 -7.524886e-1 7015 -2.779386e-3
     8016.24u -2.312178e-1 8017 -5.632278e-4
     18000.59c -1.2827e-2
     6000 -1.24e-4
mx4:p 4j 18040 6012
c energy and thermal treatment
phys:n 30
phys:p 30 2j -1 0
phys:e 30
c cut off
cut:n j 0.1
cut:p j 0.1
cut:e j 0.1
nps 1e6
c peripheral
```

```
prdmp 3j 2
print
dbcn 7j j 4j 458751
c end of file
```

With Soil:

```
25 MeV e-,25 nC per pulse,120 Hz,W converter Pb pre-collimator & soil
c cell cards
1  1 -19.35     -1 2 -3                     imp:n,p,e=1
2  2 -1.205e-3  4 -5 6 -7 3 -8              imp:n,p,e=4
3  2 -1.205e-3  -11 -9                      imp:n,p,e=16
4  2 -1.205e-3  -11 9                       imp:n,p,e=64
5  3 -11.344    4 -5 6 -7 8 -9 11           imp:n,p,e=16
6  3 -11.344    4 -5 6 -7 9 -10 11          imp:n,p,e=64
7  4 -1.205e-3  (12 -13 14 -15 2 -10) (-4:5:-6:7:-3:10) (1:-2:3)
                                            imp:n,p,e=0
8  4 -1.205e-3  12 -13 14 -15 10 -16        imp:n,p,e=128
9  4 -1.205e-3  12 -13 14 -15 16 -17        imp:n,p,e=128
10 4 -1.205e-3  12 -13 14 -15 17 -18        imp:n,p,e=512
11 4 -1.205e-3  12 -13 14 -15 18 -19        imp:n,p,e=512
12 4 -1.205e-3  12 -13 14 -15 19 -20        imp:n,p,e=1024
13 4 -1.205e-3  12 -13 14 -15 20 -21        imp:n,p,e=1024
14 5 -1.6       12 -13 -14 22 2 -10         imp:n,p,e=0
15 5 -1.6       12 -13 -14 22 10 -16        imp:n,p,e=128
16 5 -1.6       12 -13 -14 22 16 -17        imp:n,p,e=128
17 5 -1.6       12 -13 -14 22 17 -18        imp:n,p,e=512
18 5 -1.6       12 -13 -14 22 18 -19        imp:n,p,e=512
19 5 -1.6       12 -13 -14 22 19 -20        imp:n,p,e=1024
20 5 -1.6       12 -13 -14 22 20 -21        imp:n,p,e=1024
21 0            -12:13:-22:15:-2:21         imp:n,p,e=0

c surface cards
1 cz 3.81
2 pz 0
3 pz 0.2286
4 px -22.86
5 px 22.86
6 py -22.86
7 py 22.86
8 pz 28.1686
9 pz 35.7886
10 pz 43.4086
11 trc 0 0 43.4086 0 0 -15.24 0.9525 1.27
12 px -300
13 px 300
14 py -150      $ beam center line 1.5m above ground
15 py 300
16 pz 543.4086
17 pz 1043.4086
18 pz 1543.4086
19 pz 2043.4086
20 pz 2543.4086
21 pz 3043.4086
22 py -250      $ ground 1m thick

c data cards
mode n p e
c variance reduction
ext:p 0.2z 0 0 0 0.5z 0.5z 0 0 0 0 0 0 0 0 0 0 0 0 0 0 0
ext:n 0 0 0 0 0 0.25z 0.3z 0 0 0 0 0 0 0 0 0 0 0 0 0 0 0
fcl:p 0 1 1 1 0 0 0 0.5 0.5 0.5 0.5 0.5 0.5 0 0 0 0 0 0 0 0
```

```
fcl:n 0 1 1 1 0 0 0 0.5 0.5 0.5 0.5 0.5 0.5 0 0 0 0 0 0 0 0
c wwe:n 1 30
c wwe:p 4 11 30
c wwe:e 4 21 30
c wwp:n 2 j 1000 0 -1 0
c wwp:p 2 j 1000 0 -1 0
c wwp:e 2 j 1000 0 -1 0
wwg 101 0 0 j 0
wwge:n 1 30
wwge:p 4 11 30
wwge:e 4 21 30
mesh geom=xyz ref=0 0 0.1 origin=-300.01 -250.01 -1e-4
     imesh=-22.86 22.86 300.01
     jmesh=-170 -165 -150 -22.86 22.86 300.01
     jints=8 1 5 1 1 1
     kmesh=0.2286 28.1686 43.4086 543.4086 1043.4086 1543.4086
           2043.4086 2543.4086 3044
     kints=1 1 15 1 1 1 1 1 1
bbrem 1 1 46i 10 1 2 3 4 5
c source
sdef sur=2 erg=d1 dir=d2 vec=0 0 1 nrm=1 pos=0 0 0 rad=d3 axs=0 0 1
     par=e
si1 h 23.75 26.25
sp1 d 0 1
si2 h -1 0.999847695 1
sp2 d  0 0 1
si3 a 0 0.25
sp3   0 0.25
c tallies
f101:p 21
fm101 1.872453e13
fs 14 t
tf101 3j 1
e0 2e-1 3e-1 4e-1 5e-1 6e-1 7e-1 8e-1 9e-1
     1 115i 30
*c0 90 80 70 60 50 40 35 30 25 20 15 10 7.5 5 2.5 0 t
c tallies up 30m after precollimator
tmesh
  rmesh1:p flux
  cora1 -300 9i -100 19i 100 9i 300
  corb1 -150 4i -100 19i 100 9i 300
  corc1 543.4086 543.408601
  rmesh11:p flux
  cora11 -300 9i -100 19i 100 9i 300
  corb11 -150 4i -100 19i 100 9i 300
  corc11 1043.4086 1043.408601
  rmesh21:p flux
  cora21 -300 9i -100 19i 100 9i 300
  corb21 -150 4i -100 19i 100 9i 300
  corc21 1543.4086 1543.408601
  rmesh31:p flux
  cora31 -300 9i -100 19i 100 9i 300
  corb31 -150 4i -100 19i 100 9i 300
  corc31 2043.4086 2043.408601
  rmesh41:p flux
  cora41 -300 9i -100 19i 100 9i 300
  corb41 -150 4i -100 19i 100 9i 300
  corc41 2543.4086 2543.408601
  rmesh51:p flux
  cora51 -300 9i -100 19i 100 9i 300
  corb51 -150 4i -100 19i 100 9i 300
  corc51 3043.408599 3043.4086
endmd
```

```
fm1 1.872453e13
fm11 1.872453e13
fm21 1.872453e13
fm31 1.872453e13
fm41 1.872453e13
fm51 1.872453e13
c materials
m1 nlib=66c plib=04p elib=03e pnlib=26u gas=0 estep=4 $ tungsten
     74182 0.2642 74183 0.1428 74184.24u 0.307 74186 0.286
m2 nlib=66c plib=04p elib=03e pnlib=25u gas=1 estep=210 $ air between W & Pb
     7014 -7.524886e-1 7015 -2.779386e-3
     8016.24u -2.312178e-1 8017 -5.632278e-4
     18000.59c -1.2827e-2
     6000 -1.24e-4
mx2:p 4j 18040 6012
m3 nlib=66c plib=04p elib=03e pnlib=24u gas=0 estep=4 $ lead
     82206 0.255 82207 0.221 82208 0.524
m4 nlib=66c plib=04p elib=03e pnlib=25u gas=1 estep=12 $ air everywhere else
     7014 -7.524886e-1 7015 -2.779386e-3
     8016.24u -2.312178e-1 8017 -5.632278e-4
     18000.59c -1.2827e-2
     6000 -1.24e-4
mx4:p 4j 18040 6012
m5 nlib=66c plib=04p elib=03e pnlib=25u gas=0 estep=3 $ LANL soil
     1001 -1.99977e-3 1002.24u -2.3e-7
     8016.24u -.524722 8017 -.001278
     11023 -.021
     13027 -.061
     14028 -.318192 14029 -.016157 14030 -.010651
     19000 -.029
     26054 -9.352e-4 26056 -1.468064e-2 26057 -3.3904e-4 26058 -4.512e-5
mx5:p 0 8j 19039 4j
c energy and thermal treatment
phys:n 30
phys:p 30 2j -1 0
phys:e 30
c cut off
cut:n j 0.1
cut:p j 4.0
cut:e j 4.0
nps 1e6
c ctme 15
c peripheral
prdmp 3j 2
print
dbcn 7j 1 4j 458751
c end of file
```

APPENDIX C

MCNPX INPUT FILES FOR NEUTRON AND PHOTON FLUX MAPS

Appendix C. MCNPX Input Files for Neutron and Photon Flux Maps

Neutron Field Input File:

```
Coupled electron-gamma-neutron problem, DU target, 2D neutron field
c CELL CARDS
c converter
1    1  -19.25      -1 2 -3                     IMP:N,P,E=1
c
c pre-collimator
4    3  -11.344      4 -5 6 -7 8 -9 10          IMP:N,P,E=1
c
c soil
8    5  -1.6        11 -12 13 -14 16 -17        IMP:N,P,E=1
c
c target
9    7  -18.95     -18                         IMP:N,P,E=1
c
c linac space
120  2  -1.205e-3  -120 #1 #4                   IMP:N,P,E=1
c
c linac shielding
121  3  -11.344    -121 120                    IMP:N,P,E=1
c
c vehicle walls
100  8  -7.92      -100 101                    IMP:N,P,E=1
c air inside vehicle
101  2  -1.205e-3  -101 121                    IMP:N,P,E=1
c
c air outside vehicle
900  2  -1.205e-3   11 -12 14 -15 16 -17 100 18 IMP:N,P,E=1
c
c outside world
12 0             -11:12:-13:15:-16:17          IMP:N,P,E=0
c END CELL CARDS-BLANK LINE FOLLOWS

c SURFACE CARDS
c converter
1  CZ   3.81
2  PZ   0.0
3  PZ   0.2286
c
c pre-collimator
4  PX -25
5  PX  25
6  PY -25
7  PY  25
8  PZ  28.1686
9  PZ  43.4086
10 KZ  89.1286 4.340277778e-4 -1
c
c boundary planes
11 PX -300
12 PX  300
15 PY  300
16 PZ -275
17 PZ  550
c
c ground
13 PY -250      $ ground 1m thick
14 PY -150      $ beam center-line 1.5m above ground
```

```
c
c target
18 SZ 543.4086 3.978848
c
c vehicle
100 101 RPP  -92.075  92.075 -92.075  92.075 -150.495  152.4
101 101 RPP  -91.44   91.44  -91.44   91.44  -149.86   152.4
120 102 RPP  -25      25     -25      25     -75       75
121 102 RPP  -32.62   32.62  -32.62   32.62  -85.62    75
c
c END SURFACE CARDS-BLANK LINE FOLLOWS

c DATA CARDS
c
c GEOMETRY TRANSLATIONS
TR101   0     0   -102.9914
TR102   0     0    -31.5914
c
c MATERIAL DEFINITIONS
c tungsten
M1   NLIB=66c  PLIB=04p  ELIB=03e  PNLIB=24u
     74182     0.2642
     74183     0.1428
     74184     0.307
     74186     0.286
c
c air at 45% humidity
M2   NLIB=66c  PLIB=04p  ELIB=03e  PNLIB=24u
     1001      1.169196E-02
     1002      1.344730E-06
     7014      7.681679E-01
     7015      2.837299E-03
     8016      2.121736E-01
     8017      5.168377E-04
     18000.59c 4.611104E-03
c
c natural lead
M3   NLIB=66c  PLIB=04p  ELIB=03e  PNLIB=24u
     82206     0.255
     82207     0.221
     82208     0.524
c
c LANL soil with 20% of water
M5   NLIB=66c  PLIB=04p  ELIB=03e  PNLIB=24u
     1001      4.832564E-02
     1002      5.558087E-06
     8016      6.950058E-01
     8017      1.692978E-03
     11023     3.155206E-03
     13027     3.045777E-02
     14028     1.934420e-1
     14029     9.822516e-3
     14030     6.475075e-3
     19000     4.523070E-03
     26054     4.146826E-04
     26056     6.509629E-03
     26057     1.503357E-04
     26058     2.000693E-05
c
c depleted uranium
M7   NLIB=66c  PLIB=04p  ELIB=03e  PNLIB=27u
     92238     1.0
c
```

```
c stainless steel
M8   NLIB=66c  PLIB=04p  ELIB=03e  PNLIB=24u
     26054     3.470e-3
     26056     5.447e-2
     26057     1.258e-3
     24050     7.573e-4
     24052     1.450e-2
     24053     1.656e-3
     24054     4.122e-4
     28058     5.288e-3
     28060     2.024e-3
     28064     7.148e-4
     25055     1.740e-3
c
c SOURCE DEFINITION
MODE E  P  N
SDEF PAR=E SUR=2 ERG=D1 DIR=D2 VEC=0 0 1 NRM=1 POS=0 0 0 RAD=D3 AXS=0 0 1
SI1  H  23.75 26.25
SP1  D  0  1
SI2  H -1  0.999847695  1
SP2  D  0  0  1
SI3  A  0  0.25
SP3  0  0.25
c END OF SOURCE DEFINITION
c
PHYS:E  30
PHYS:P  3J  1
PHYS:N  30
c energy cutoff 4 MeV for electrons and gammas
CUT:E   J   4
CUT:P   J   4
CUT:N   2J -0.001
TOTNU
NPS     1.5E8
PRINT   10 40 50 110 126 140
PRDMP   J  -200  J  1
c
c MESH TALLIES
tmesh
c ZX plane 1
rmesh1:n flux
cora1    -300 299i 300
corb1      23       25
corc1    -275 410i 550
c ZX plane 2
rmesh21:n flux
cora21   -300 299i 300
corb21     -1        1
corc21   -275 410i 550
c ZX plane 3
rmesh31:n flux
cora31   -300 299i 300
corb31    -25      -23
corc31   -275 410i 550
c ZX plane 4
rmesh41:n flux
cora41  -300 299i 300
corb41   -34.62   -32.62
corc41  -275 410i 550
c ZX plane 5
rmesh51:n flux
cora51  -300 299i 300
corb51   -63      -61
```

```
corc51  -275 410i 550
c ZX plane 6
rmesh61:n flux
cora61  -300 299i 300
corb61   -91.44   -89.44
corc61  -275 410i 550
c ZX plane 7
rmesh71:n flux
cora71  -300 299i 300
corb71  -150     -148
corc71  -275 410i 550
endmd
c END OF FILE
```

Gamma Ray Field Input File:

```
Coupled electron-gamma-neutron problem, DU target, 2D gamma field
c CELL CARDS
c converter
1    1  -19.25      -1 2 -3                  IMP:N,P,E=1
c
c pre-collimator
4    3  -11.344      4 -5 6 -7 8 -9 10       IMP:N,P,E=1
c
c soil
8    5  -1.6        11 -12 13 -14 16 -17     IMP:N,P,E=1
c
c target
9    7  -18.95     -18                       IMP:N,P,E=1
c
c linac space
120  2  -1.205e-3  -120 #1 #4                IMP:N,P,E=1
c
c linac shielding
121  3  -11.344    -121 120                  IMP:N,P,E=1
c
c vehicle walls
100  8  -7.92      -100 101                  IMP:N,P,E=1
c air inside vehicle
101  2  -1.205e-3  -101 121                  IMP:N,P,E=1
c
c air outside vehicle
900  2  -1.205e-3   11 -12 14 -15 16 -17 100 18 IMP:N,P,E=1
c
c outside world
12 0             -11:12:-13:15:-16:17        IMP:N,P,E=0
c END CELL CARDS-BLANK LINE FOLLOWS

c SURFACE CARDS
c converter
1  CZ   3.81
2  PZ   0.0
3  PZ   0.2286
c
c pre-collimator
4  PX -25
5  PX  25
6  PY -25
7  PY  25
8  PZ  28.1686
9  PZ  43.4086
10 KZ  89.1286 4.340277778e-4 -1
```

```
c
c boundary planes
11 PX -300
12 PX  300
15 PY  300
16 PZ -275
17 PZ  550
c
c ground
13 PY -250      $ ground 1m thick
14 PY -150      $ beam center-line 1.5m above ground
c
c target
18 SZ 543.4086 3.978848
c
c vehicle
100 101 RPP  -93.98 93.98  -93.98 93.98  -152.4  152.4
101 101 RPP  -91.44 91.44  -91.44 91.44  -149.86 152.4
120 102 RPP  -25    25     -25    25     -75     75
121 102 RPP  -32.62 32.62  -32.62 32.62  -85.62  75
c
c END SURFACE CARDS-BLANK LINE FOLLOWS

c DATA CARDS
c
c GEOMETRY TRANSLATIONS
TR101   0     0   -102.9914
TR102   0     0    -31.5914
c
c MATERIAL DEFINITIONS
c tungsten
M1   NLIB=66c  PLIB=04p  ELIB=03e  PNLIB=24u
     74182     0.2642
     74183     0.1428
     74184     0.307
     74186     0.286
c
c air at 45% humidity
M2   NLIB=66c  PLIB=04p  ELIB=03e  PNLIB=24u
     1001      1.169196E-02
     1002      1.344730E-06
     7014      7.681679E-01
     7015      2.837299E-03
     8016      2.121736E-01
     8017      5.168377E-04
     18000.59c 4.611104E-03
c
c natural lead
M3   NLIB=66c  PLIB=04p  ELIB=03e  PNLIB=24u
     82206     0.255
     82207     0.221
     82208     0.524
c
c LANL soil with 20% of water
M5   NLIB=66c  PLIB=04p  ELIB=03e  PNLIB=24u
     1001      4.832564E-02
     1002      5.558087E-06
     8016      6.950058E-01
     8017      1.692978E-03
     11023     3.155206E-03
     13027     3.045777E-02
     14028     1.934420e-1
     14029     9.822516e-3
```

```
     14030     6.475075e-3
     19000     4.523070E-03
     26054     4.146826E-04
     26056     6.509629E-03
     26057     1.503357E-04
     26058     2.000693E-05
c
c depleted uranium
M7   NLIB=66c  PLIB=04p  ELIB=03e  PNLIB=27u
     92238     1.0
c
c stainless steel
M8   NLIB=66c  PLIB=04p  ELIB=03e  PNLIB=24u
     26054     3.470e-3
     26056     5.447e-2
     26057     1.258e-3
     24050     7.573e-4
     24052     1.450e-2
     24053     1.656e-3
     24054     4.122e-4
     28058     5.288e-3
     28060     2.024e-3
     28064     7.148e-4
     25055     1.740e-3
c
c SOURCE DEFINITION
MODE E  P  N
SDEF PAR=E SUR=2 ERG=D1 DIR=D2 VEC=0 0 1 NRM=1 POS=0 0 0 RAD=D3 AXS=0 0 1
SI1  H  23.75 26.25
SP1  D  0  1
SI2  H -1  0.999847695  1
SP2  D  0  0  1
SI3  A  0  0.25
SP3  0  0.25
c END OF SOURCE DEFINITION
c
PHYS:E  30
PHYS:P  3J 1
PHYS:N  30
c energy cutoff 100 keV for electrons and gammas
CUT:E   J  0.1
CUT:P   J  0.1
c bremsstrahlung biasing
c BBREM   1  1  46i  5  1
TOTNU
NPS     5E8
PRINT   10 40 50 110 126 140
PRDMP   J  -60  J  2
c
c MESH TALLIES
tmesh
c ZX planes 1-5
rmesh1:p flux
cora1  -300 59i 300
corb1   -25  4i  25
corc1  -275 81i 550
c ZX plane 6
rmesh61:p flux
cora61 -300 59i 300
corb61  -42.62  -32.62
corc61 -275 81i 550
c ZX plane 7
rmesh71:p flux
```

```
cora71 -300 59i 300
corb71  -67     -57
corc71 -275 81i 550
c ZX plane 8
rmesh81:p flux
cora81 -300 59i 300
corb81  -91.44  -81.44
corc81 -275 81i 550
c ZX planes 9-14
rmesh91:p flux
cora91 -300 59i 300
corb91 -150  5i -93.98
corc91 -275 81i 550
endmd
c END OF FILE
```

APPENDIX D

NEUTRON AND PHOTON FLUENCE MAP ERRORS

Appendix D. Neutron and Photon Fluence Map Errors

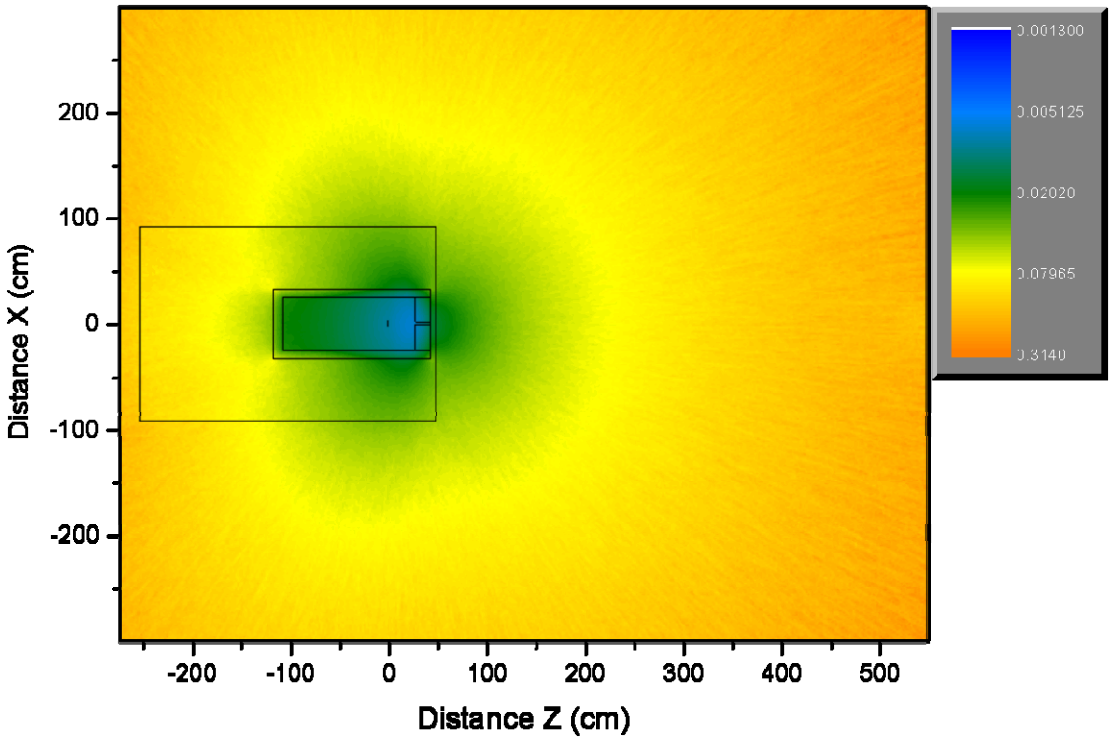

Figure D-1. Relative errors for the neutron fluence map shown in Figure 21.

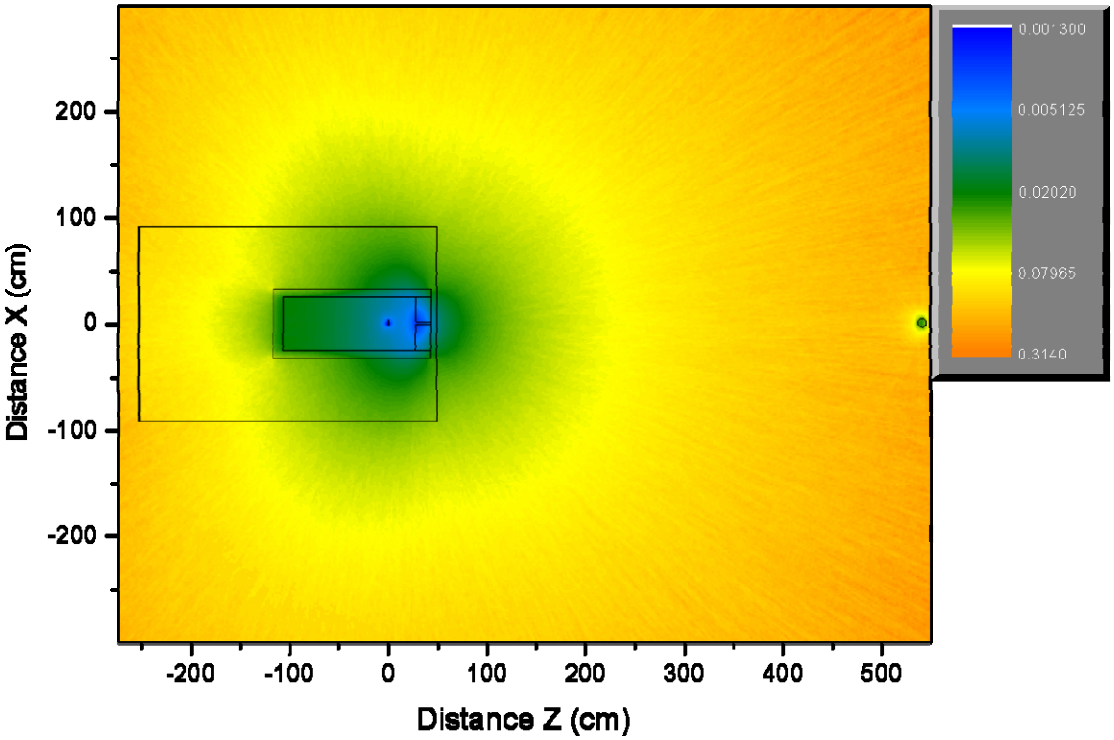

Figure D-2. Relative errors for the neutron fluence map shown in Figure 22.

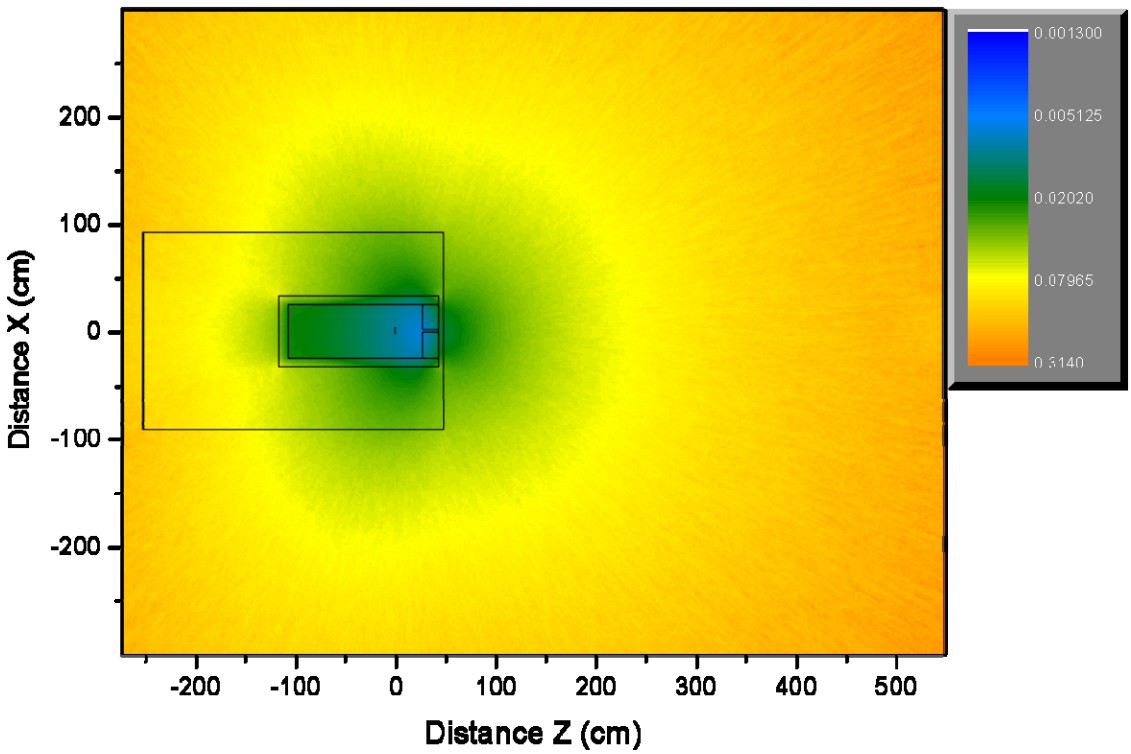

Figure D-3. Relative errors for the neutron fluence map shown in Figure 23.

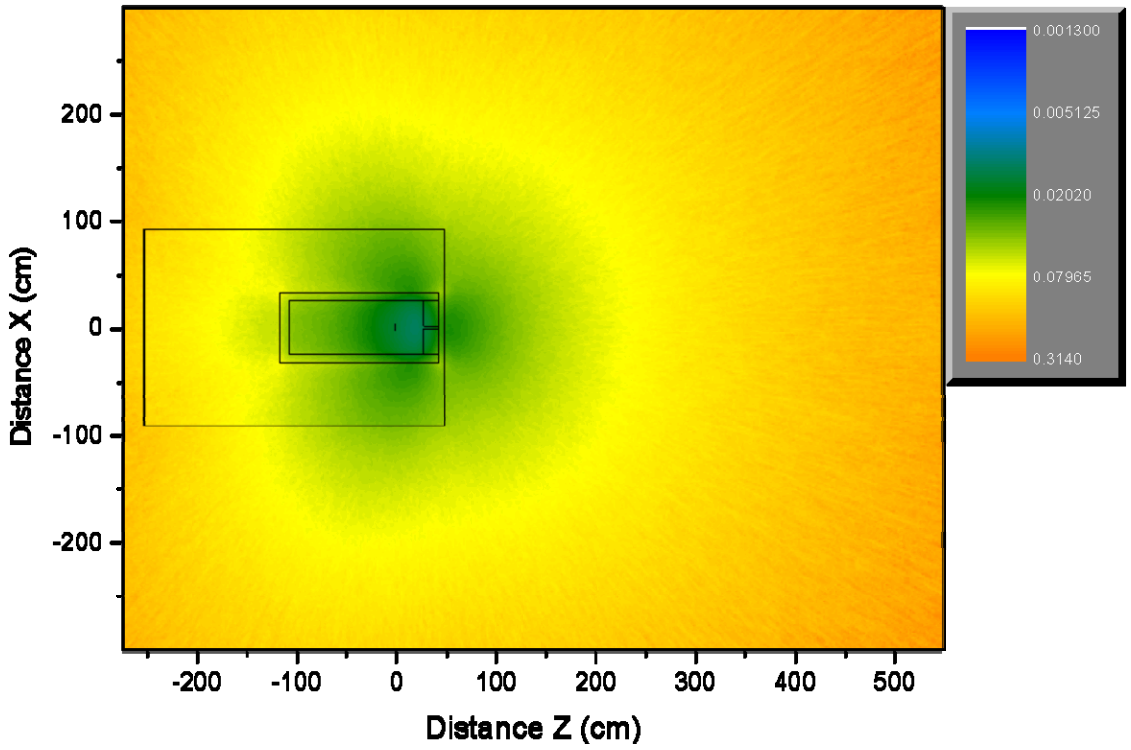

Figure D-4. Relative errors for the neutron fluence map shown in Figure 24.

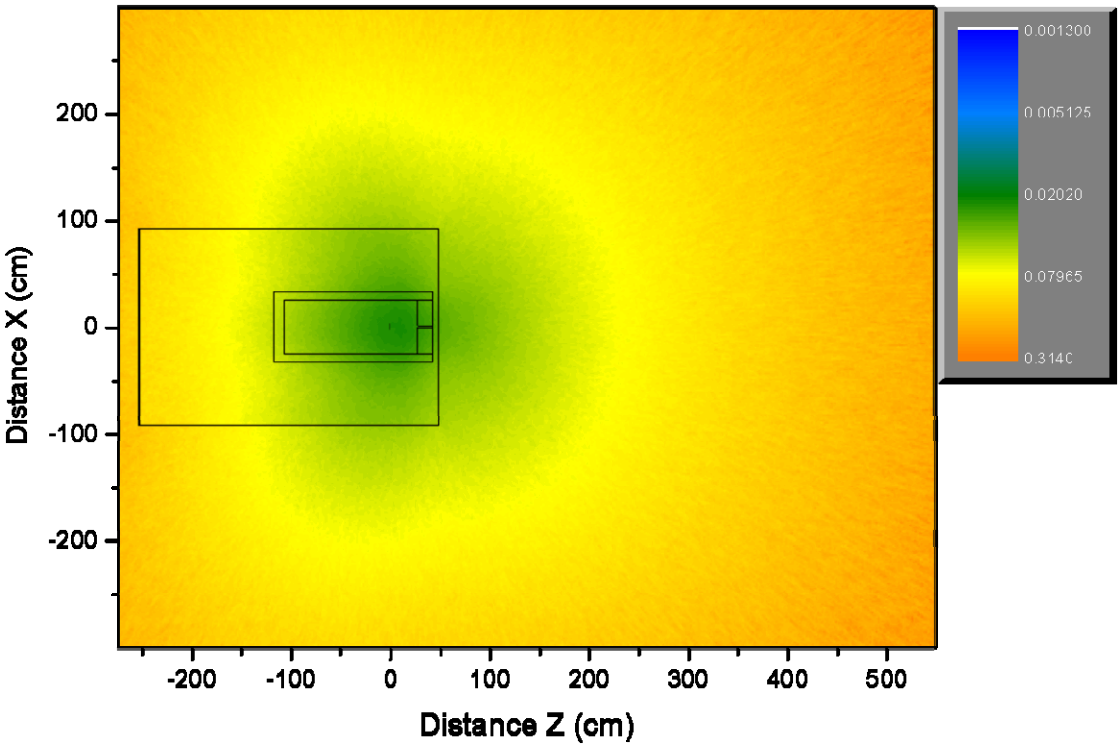

Figure D-5. Relative errors for the neutron fluence map shown in Figure 25.

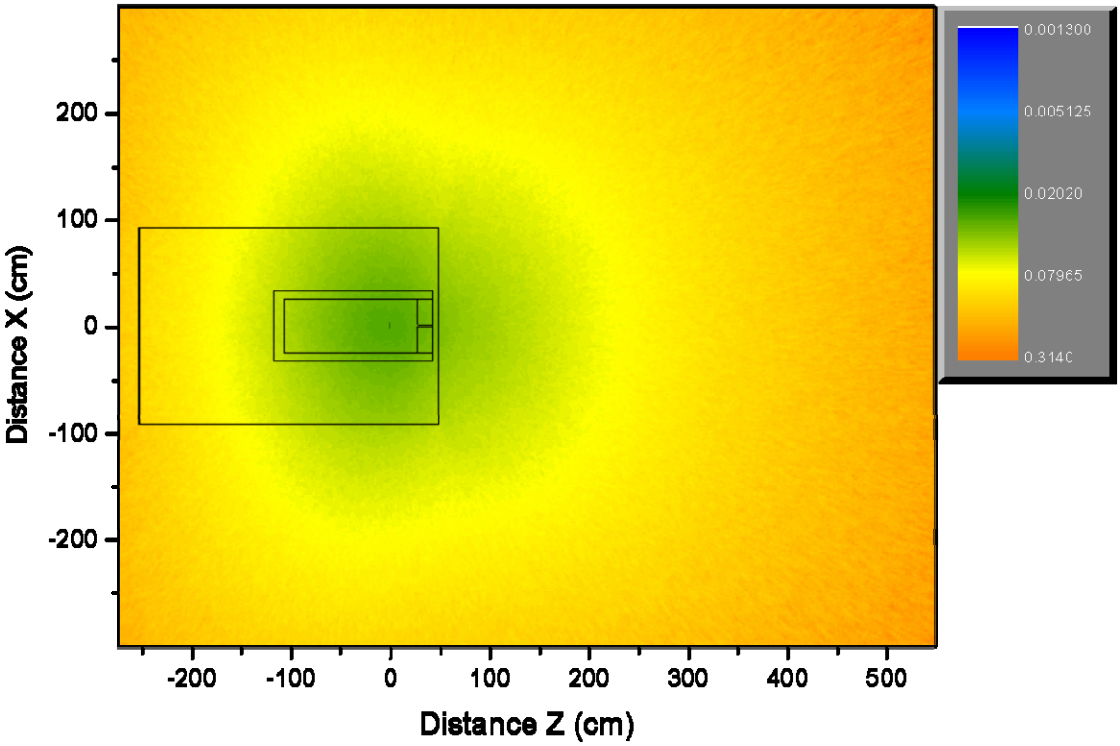

Figure D-6. Relative errors for the neutron fluence map shown in Figure 26.

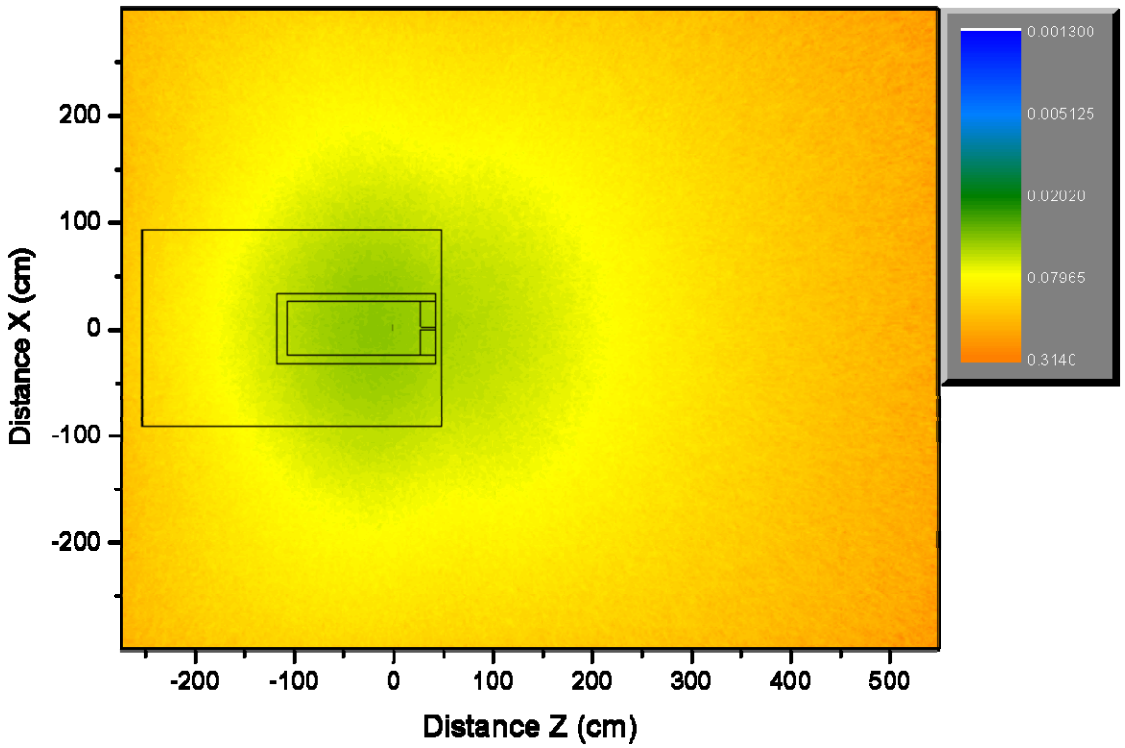

Figure D-7. Relative errors for the neutron fluence map shown in Figure 27.

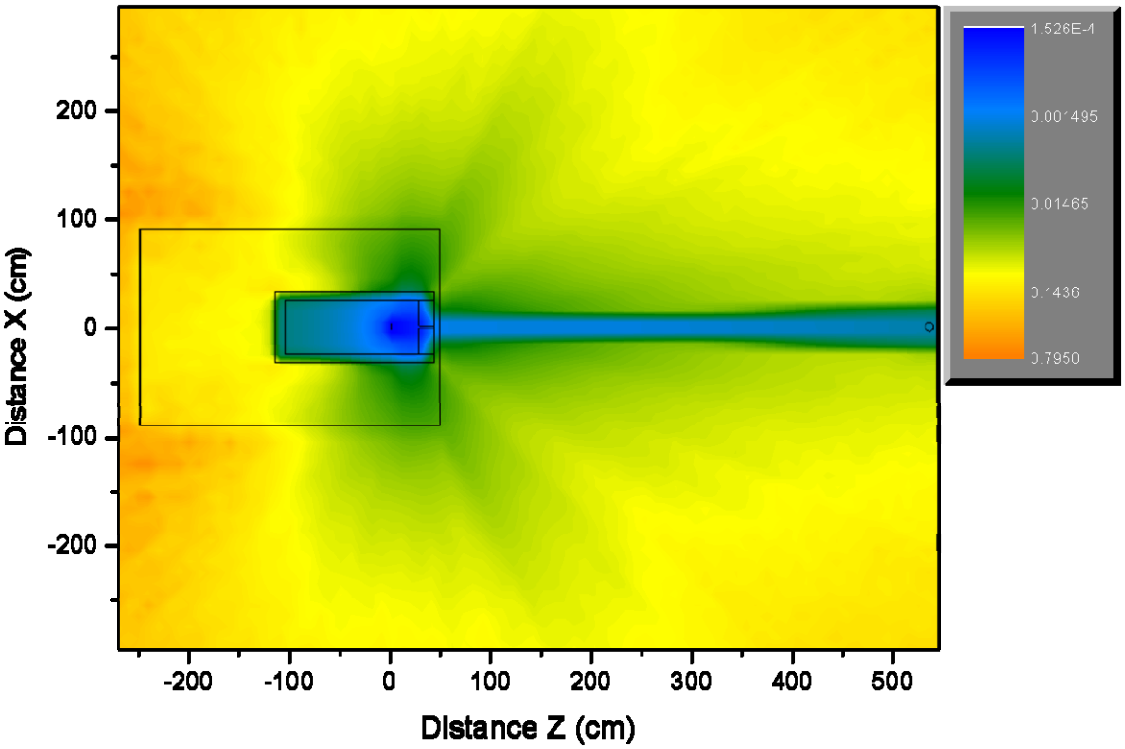

Figure D-8. Relative errors for the gamma ray fluence map shown in Figure 28.

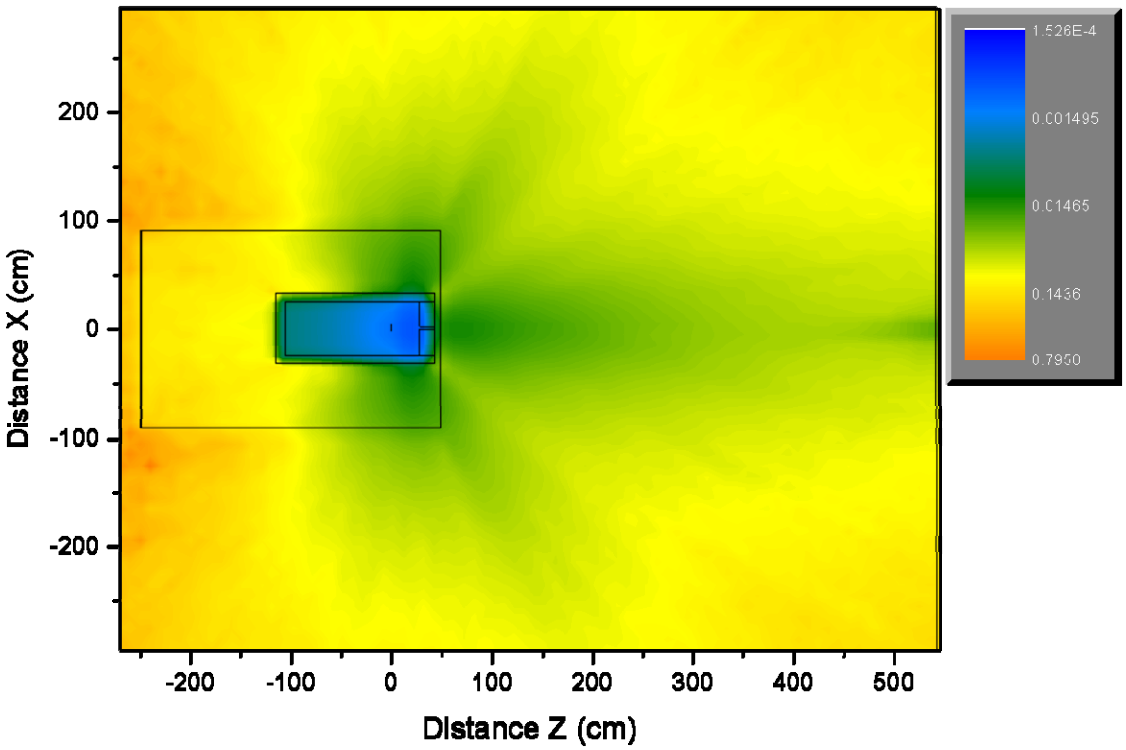

Figure D-9. Relative errors for the gamma ray fluence map shown in Figure 29.

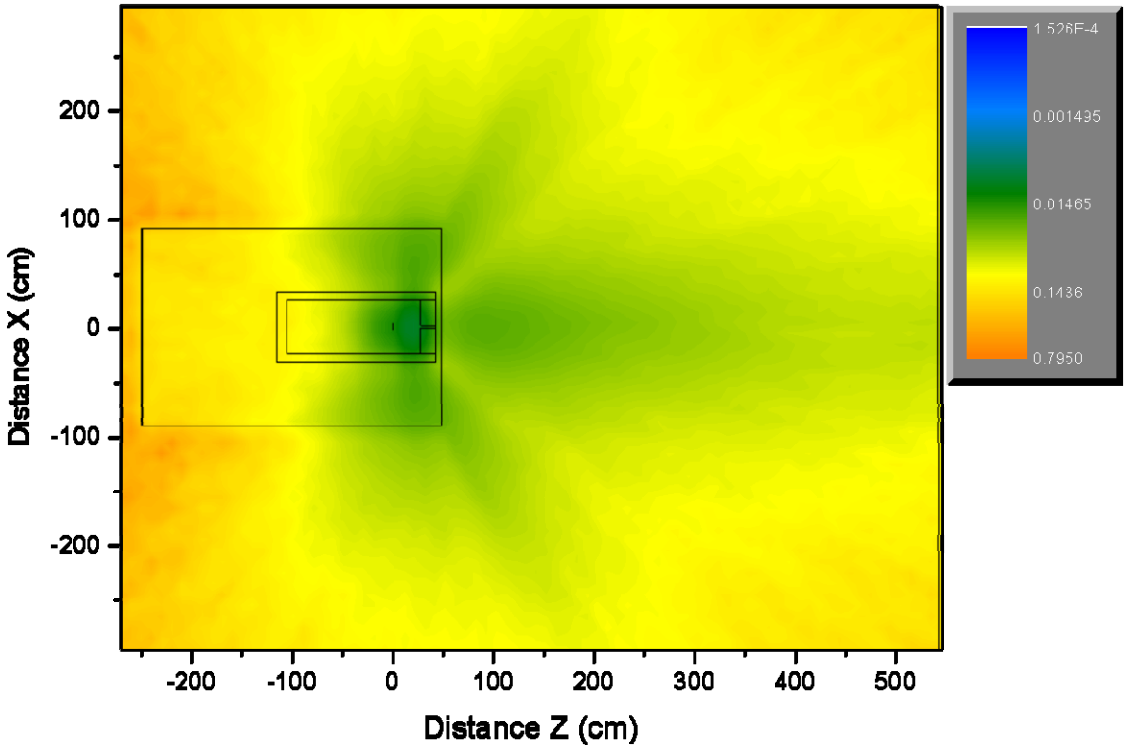

Figure D-10. Relative errors for the gamma ray fluence map shown in Figure 30.

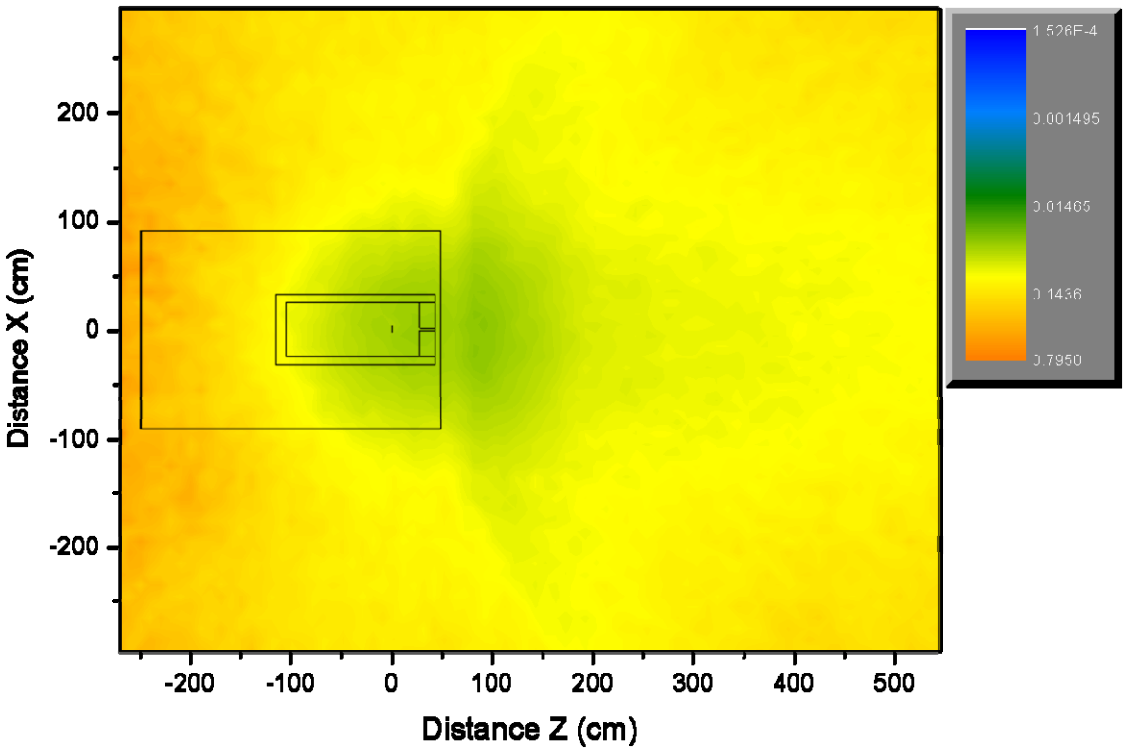

Figure D-11. Relative errors for the gamma ray fluence map shown in Figure 31.

APPENDIX E

MCNPX INPUT FILE FOR TIME-ENERGY DEPENDENCE

Appendix E. MCNPX Input File for Time-Energy Dependence

```
Coupled electron-gamma-neutron problem, DU target
c neutrons through the vehicle walls, the target surface flagged
c CELL CARDS
c converter
1    1  -19.25      -1 2 -3                  IMP:N,P,E=1
c
c pre-collimator
4    3  -11.344      4 -5 6 -7 8 -9 10       IMP:N,P,E=1
c
c soil
8    5  -1.6        11 -12 13 -14 16 -17     IMP:N,P,E=1
c
c target
9    7  -18.95     -18                       IMP:N,P,E=1
c
c linac space
120  2  -1.205e-3  -120 #1 #4                IMP:N,P,E=1
c
c linac shielding
121  3  -11.344    -121 120                  IMP:N,P,E=1
c
c vehicle walls
100  8  -7.92      -100 101                  IMP:N,P,E=1
c air inside vehicle
101  2  -1.205e-3  -101 121                  IMP:N,P,E=1
c
c air outside vehicle
900  2  -1.205e-3   11 -12 14 -15 16 -17 100 18 IMP:N,P,E=1
c
c outside world
12 0             -11:12:-13:15:-16:17        IMP:N,P,E=0
c END CELL CARDS-BLANK LINE FOLLOWS

c SURFACE CARDS
c converter
1  CZ   3.81
2  PZ   0.0
3  PZ   0.2286
c
c pre-collimator
4  PX -25
5  PX  25
6  PY -25
7  PY  25
8  PZ  28.1686
9  PZ  43.4086
10 KZ  89.1286 4.340277778e-4 -1
c
c boundary planes
11 PX -300
12 PX  300
15 PY  300
16 PZ -275
17 PZ  550
c
c ground
13 PY -250      $ ground 1m thick
14 PY -150      $ beam center-line 1.5m above ground
c
```

```
c target
18 SZ 543.4086 3.978848
c
c vehicle
100 101 RPP  -92.075 92.075 -92.075 92.075 -150.495 152.4
101 101 RPP  -91.44  91.44  -91.44  91.44  -149.86  152.4
120 102 RPP  -25     25     -25     25     -75      75
121 102 RPP  -32.62  32.62  -32.62  32.62  -85.62   75
c
c END SURFACE CARDS-BLANK LINE FOLLOWS

c DATA CARDS
c
c GEOMETRY TRANSLATIONS
TR101   0     0   -102.9914
TR102   0     0    -31.5914
c
c MATERIAL DEFINITIONS
c tungsten
M1   NLIB=66c  PLIB=04p  ELIB=03e  PNLIB=24u
     74182     0.2642
     74183     0.1428
     74184     0.307
     74186     0.286
c
c air at 45% humidity
M2   NLIB=66c  PLIB=04p  ELIB=03e  PNLIB=24u
     1001      1.169196E-02
     1002      1.344730E-06
     7014      7.681679E-01
     7015      2.837299E-03
     8016      2.121736E-01
     8017      5.168377E-04
     18000.59c 4.611104E-03
c
c natural lead
M3   NLIB=66c  PLIB=04p  ELIB=03e  PNLIB=24u
     82206     0.255
     82207     0.221
     82208     0.524
c
c LANL soil with 20% of water
M5   NLIB=66c  PLIB=04p  ELIB=03e  PNLIB=24u
     1001      4.832564E-02
     1002      5.558087E-06
     8016      6.950058E-01
     8017      1.692978E-03
     11023     3.155206E-03
     13027     3.045777E-02
     14028     1.934420e-1
     14029     9.822516e-3
     14030     6.475075e-3
     19000     4.523070E-03
     26054     4.146826E-04
     26056     6.509629E-03
     26057     1.503357E-04
     26058     2.000693E-05
c
c depleted uranium
M7   NLIB=66c  PLIB=04p  ELIB=03e  PNLIB=27u
     92238     1.0
c
c stainless steel
```

```
M8   NLIB=66c  PLIB=04p  ELIB=03e  PNLIB=24u
     26054     3.470e-3
     26056     5.447e-2
     26057     1.258e-3
     24050     7.573e-4
     24052     1.450e-2
     24053     1.656e-3
     24054     4.122e-4
     28058     5.288e-3
     28060     2.024e-3
     28064     7.148e-4
     25055     1.740e-3
c
c SOURCE DEFINITION
MODE E  P  N
SDEF PAR=E SUR=2 ERG=D1 DIR=D2 VEC=0 0 1 NRM=1 POS=0 0 0 RAD=D3 AXS=0 0 1
SI1  H  23.75 26.25
SP1  D  0  1
SI2  H -1  0.999847695  1
SP2  D  0  0  1
SI3  A  0  0.25
SP3  0  0.25
c END OF SOURCE DEFINITION
c
PHYS:E  30
PHYS:P  0.001 2J  1
PHYS:N  30
c energy cutoff 4 MeV for electrons
CUT:E   J   4
CUT:P   2J
CUT:N   2J -0.01
TOTNU
NPS     8e8
PRINT   10 40 50 70 86 110 126 130 140
PRDMP   J  -60  J  2
c
c TALLIES
T0    0.01 3i 0.1 3i 1 17i 10 17i 100 8i 1e3 8i 1e4 3i 1e5 3i 1e6 5e6 1e7
E0    0.001 8i 0.01 8i 0.1 17i 1 17i 10 12 15 20 30
F1:N  100.1 100.2 100.3 100.4 100.5 100.6 T
C1    0  1  T
SF1   18
FQ1   T E C
c END OF FILE
```

APPENDIX F

MCNP-POLIMI INPUT FILES FOR PHOTONUCLEAR SOURCES

Appendix F. MCNP-PoliMi Input Files for Photonuclear Sources

DU Target:

```
25 MeV e-,25 nC per pulse,120 Hz, DU target without delayed neutrons
c CELL CARDS
c converter
1    1  -19.25      -1 2 -3                  IMP:N,P=1
c
c pre-collimator
4    3  -11.344      4 -5 6 -7 8 -9 10       IMP:N,P=1
c
c soil
8    5  -1.6        11 -12 13 -14 16 -17     IMP:N,P=1
c
c target
9    7  -18.95     -18                       IMP:N,P=1
c
c linac space
120  2  -1.205e-3  -120 #1 #4                IMP:N,P=1
c
c linac shielding
121  3  -11.344    -121 120                  IMP:N,P=1
c
c vehicle walls
100  8  -7.92      -100 101                  IMP:N,P=1
c air inside vehicle
101  2  -1.205e-3  -101 121                  IMP:N,P=1
c
c air outside vehicle
900  2  -1.205e-3   11 -12 14 -15 16 -17 100 18
                    20 23 25 31 32 33 34 35
                    36 37 38 39 40 41 42 43
                    44 45 46 47 48 49 50 51   IMP:N,P=1
c
c tally voxels
201 2 -1.205e-3  -201   U=1        LAT=1      IMP:N,P=1
231 2 -1.205e-3  -231   U=2        LAT=1      IMP:N,P=1
251 2 -1.205e-3  -251   U=3        LAT=1      IMP:N,P=1
311 2 -1.205e-3  -311   U=4        LAT=1      IMP:N,P=1
321 2 -1.205e-3  -321   U=5        LAT=1      IMP:N,P=1
331 2 -1.205e-3  -331   U=6        LAT=1      IMP:N,P=1
341 2 -1.205e-3  -341   U=7        LAT=1      IMP:N,P=1
351 2 -1.205e-3  -351   U=8        LAT=1      IMP:N,P=1
361 2 -1.205e-3  -361   U=9        LAT=1      IMP:N,P=1
371 2 -1.205e-3  -371   U=10       LAT=1      IMP:N,P=1
381 2 -1.205e-3  -381   U=11       LAT=1      IMP:N,P=1
391 2 -1.205e-3  -391   U=12       LAT=1      IMP:N,P=1
401 2 -1.205e-3  -401   U=13       LAT=1      IMP:N,P=1
411 2 -1.205e-3  -411   U=14       LAT=1      IMP:N,P=1
421 2 -1.205e-3  -421   U=15       LAT=1      IMP:N,P=1
431 2 -1.205e-3  -431   U=16       LAT=1      IMP:N,P=1
441 2 -1.205e-3  -441   U=17       LAT=1      IMP:N,P=1
451 2 -1.205e-3  -451   U=18       LAT=1      IMP:N,P=1
461 2 -1.205e-3  -461   U=19       LAT=1      IMP:N,P=1
471 2 -1.205e-3  -471   U=20       LAT=1      IMP:N,P=1
481 2 -1.205e-3  -481   U=21       LAT=1      IMP:N,P=1
491 2 -1.205e-3  -491   U=22       LAT=1      IMP:N,P=1
501 2 -1.205e-3  -501   U=23       LAT=1      IMP:N,P=1
511 2 -1.205e-3  -511   U=24       LAT=1      IMP:N,P=1
c
```

```
c tally planes
20 0             -20    FILL=1                IMP:N,P=1
23 0             -23    FILL=2                IMP:N,P=1
25 0             -25    FILL=3                IMP:N,P=1
31 0             -31    FILL=4                IMP:N,P=1
32 0             -32    FILL=5                IMP:N,P=1
33 0             -33    FILL=6                IMP:N,P=1
34 0             -34    FILL=7                IMP:N,P=1
35 0             -35    FILL=8                IMP:N,P=1
36 0             -36    FILL=9                IMP:N,P=1
37 0             -37    FILL=10               IMP:N,P=1
38 0             -38    FILL=11               IMP:N,P=1
39 0             -39    FILL=12               IMP:N,P=1
40 0             -40    FILL=13               IMP:N,P=1
41 0             -41    FILL=14               IMP:N,P=1
42 0             -42    FILL=15               IMP:N,P=1
43 0             -43    FILL=16               IMP:N,P=1
44 0             -44    FILL=17               IMP:N,P=1
45 0             -45    FILL=18               IMP:N,P=1
46 0             -46    FILL=19               IMP:N,P=1
47 0             -47    FILL=20               IMP:N,P=1
48 0             -48    FILL=21               IMP:N,P=1
49 0             -49    FILL=22               IMP:N,P=1
50 0             -50    FILL=23               IMP:N,P=1
51 0             -51    FILL=24               IMP:N,P=1
c
c outside world
12 0             -11:12:-13:15:-16:17         IMP:N,P=0
c END CELL CARDS-BLANK LINE FOLLOWS

c SURFACE CARDS
c converter
1  CZ   3.81
2  PZ   0.0
3  PZ   0.2286
c
c pre-collimator
4  PX -25
5  PX  25
6  PY -25
7  PY  25
8  PZ  28.1686
9  PZ  43.4086
10 KZ 89.1286 4.340277778e-4 -1
c
c boundary planes
11 PX -300
12 PX  300
15 PY  300
16 PZ -275
17 PZ 550
c
c ground
13 PY -250      $ ground 1m thick
14 PY -150      $ beam center-line 1.5m above ground
c
c du target
18 SZ 543.4086 3.978848
c
c vehicle
100 101 RPP  -93.98 93.98  -93.98 93.98  -152.4  152.4
101 101 RPP  -91.44 91.44  -91.44 91.44  -149.86 152.4
120 102 RPP  -25    25     -25    25     -75     75
```

```
121 102 RPP  -32.62 32.62  -32.62 32.62  -85.62  75
c
c tally voxels
201  1   RPP  -5 5  -5 5  -0.5 0.5
231  4   RPP  -5 5  -5 5  -0.5 0.5
251  6   RPP  -5 5  -5 5  -0.5 0.5
311  12  RPP  -5 5  -5 5  -0.5 0.5
321  13  RPP  -5 5  -5 5  -0.5 0.5
331  14  RPP  -5 5  -5 5  -0.5 0.5
341  15  RPP  -5 5  -5 5  -0.5 0.5
351  16  RPP  -5 5  -5 5  -0.5 0.5
361  17  RPP  -5 5  -5 5  -0.5 0.5
371  18  RPP  -5 5  -5 5  -0.5 0.5
381  19  RPP  -5 5  -5 5  -0.5 0.5
391  20  RPP  -5 5  -5 5  -0.5 0.5
401  21  RPP  -5 5  -5 5  -0.5 0.5
411  22  RPP  -5 5  -5 5  -0.5 0.5
421  23  RPP  -5 5  -5 5  -0.5 0.5
431  24  RPP  -5 5  -5 5  -0.5 0.5
441  25  RPP  -5 5  -5 5  -0.5 0.5
451  26  RPP  -5 5  -5 5  -0.5 0.5
461  27  RPP  -5 5  -5 5  -0.5 0.5
471  28  RPP  -5 5  -5 5  -0.5 0.5
481  29  RPP  -5 5  -5 5  -0.5 0.5
491  30  RPP  -5 5  -5 5  -0.5 0.5
501  31  RPP  -5 5  -5 5  -0.5 0.5
511  32  RPP  -5 5  -5 5  -0.5 0.5
c
c tally planes
20    1  RPP  -300   300     -150 300  -0.5 0.5
23    4  RPP  -300   300     -150 300  -0.5 0.5
25    6  RPP  -300   300     -150 300  -0.5 0.5
31   12  RPP  -100   100     -150 300  -0.5 0.5
32   13  RPP  -100   100     -150 300  -0.5 0.5
33   14  RPP  -93.98  93.98     0 200  -0.5 0.5
34   15  RPP  -100   100     -150 300  -0.5 0.5
35   16  RPP  -100   100     -150 300  -0.5 0.5
36   17  RPP  -93.98  93.98     0 200  -0.5 0.5
37   18  RPP  -100    100    -150 300  -0.5 0.5
38   19  RPP  -100    100    -150 300  -0.5 0.5
39   20  RPP  -93.98   93.98    0 200  -0.5 0.5
40   21  RPP  -100    100    -150 300  -0.5 0.5
41   22  RPP  -100    100    -150 300  -0.5 0.5
42   23  RPP  -93.98   93.98    0 200  -0.5 0.5
43   24  RPP  -100    100    -150 300  -0.5 0.5
44   25  RPP  -100    100    -150 300  -0.5 0.5
45   26  RPP  -93.98   93.98    0 200  -0.5 0.5
46   27  RPP  -100    100    -150 300  -0.5 0.5
47   28  RPP  -100    100    -150 300  -0.5 0.5
48   29  RPP  -93.98   93.98    0 200  -0.5 0.5
49   30  RPP  -100    100    -150 300  -0.5 0.5
50   31  RPP  -100    100    -150 300  -0.5 0.5
51   32  RPP  -93.98   93.98    0 200  -0.5 0.5
c END SURFACE CARDS-BLANK LINE FOLLOWS

c DATA CARDS
c
c GEOMETRY TRANSLATIONS
TR1     0     0     50.0
TR4     0     0    343.4086
TR6     0     0    538.4086
TR12 -193.98  0     24.0
TR13  193.98  0     24.0
```

```
TR14    0    93.98  24.0
TR15 -193.98  0      4.0
TR16  193.98  0      4.0
TR17    0    93.98   4.0
TR18 -193.98  0    -16.0
TR19  193.98  0    -16.0
TR20    0    93.98 -16.0
TR21 -193.98  0    -36.0
TR22  193.98  0    -36.0
TR23    0    93.98 -36.0
TR24 -193.98  0    -56.0
TR25  193.98  0    -56.0
TR26    0    93.98 -56.0
TR27 -193.98  0    -76.0
TR28  193.98  0    -76.0
TR29    0    93.98 -76.0
TR30 -193.98  0    -96.0
TR31  193.98  0    -96.0
TR32    0    93.98 -96.0
TR101   0     0   -102.9914
TR102   0     0    -31.5914
c
c SDEF CARD - MANDITORY
SDEF
c
c MATERIAL DEFINITIONS
c tungsten
M1 NLIB=60c PLIB=02p
     74182 0.2642
     74183 0.1428
     74184 0.307
     74186 0.286
c
c air at 45% humidity
M2 NLIB=60c PLIB=02p
     1001      1.169196E-02
     1002      1.344730E-06
     7014      7.681679E-01
     7015      2.837299E-03
     8016      2.121736E-01
     8017      5.168377E-04
     18000.59c 4.611104E-03
c
c natural lead
M3 NLIB=60c PLIB=02p
     82206 0.255
     82207 0.221
     82208 0.524
c
c lanl soil with 20% water
M5 NLIB=60c PLIB=02p
     1001  4.832564E-02
     1002  5.558087E-06
     8016  6.950058E-01
     8017  1.692978E-03
     11023 3.155206E-03
     13027 3.045777E-02
     14000 2.097394E-01
     19000 4.523070E-03
     26054 4.146826E-04
     26056 6.509629E-03
     26057 1.503357E-04
     26058 2.000693E-05
```

```
c
c depleted uranium
M7 NLIB=60c PLIB=02p
     92238 1.0
c
c stainless steel
M8 NLIB=60c PLIB=02p
     26054 3.470e-3
     26056 5.447e-2
     26057 1.258e-3
     24050 7.573e-4
     24052 1.450e-2
     24053 1.656e-3
     24054 4.122e-4
     28058 5.288e-3
     28060 2.024e-3
     28064 7.148e-4
     25055 1.740e-3
c
TOTNU
MODE   N  P
PHYS:N 30 30
PHYS:P 3J
CUT:P  2J 0
NPS    1
PRINT  10 40 50 110 126 128 140
IDUM   55 1 2 1 1
RDUM   0.001 0.001 $ J J J 1000 9E4
FILES 21 du5p0.d J F 6J 55 du5mt.xo
dbcn 7j        1
c
c tallies
F14:N (20<201[-30:30 -15:30 0:0])
FM14 1.872453e13
F24:N (23<231[-30:30 -15:30 0:0])
FM24 1.872453e13
F34:N (25<251[-30:30 -15:30 0:0])
FM34 1.872453e13
c
F44:N (31<311[-10:10 -15:30 0:0])
FM44 1.872453e13
F54:N (32<321[-10:10 -15:30 0:0])
FM54 1.872453e13
F64:N (33<331[-10:10 -10:10 0:0])
FM64 1.872453e13
c
F74:N (34<341[-10:10 -15:30 0:0])
FM74 1.872453e13
F84:N (35<351[-10:10 -15:30 0:0])
FM84 1.872453e13
F94:N (36<361[-10:10 -10:10 0:0])
FM94 1.872453e13
c
F104:N (37<371[-10:10 -15:30 0:0])
FM104 1.872453e13
F114:N (38<381[-10:10 -15:30 0:0])
FM114 1.872453e13
F124:N (39<391[-10:10  -10:10 0:0])
FM124 1.872453e13
c
F134:N (40<401[-10:10 -15:30 0:0])
FM134 1.872453e13
F144:N (41<411[-10:10 -15:30 0:0])
```

```
FM144 1.872453e13
F154:N (42<421[-10:10 -10:10 0:0])
FM154 1.872453e13
c
F164:N (43<431[-10:10 -15:30 0:0])
FM164 1.872453e13
F174:N (44<441[-10:10 -15:30 0:0])
FM174 1.872453e13
F184:N (45<451[-10:10 -10:10 0:0])
FM184 1.872453e13
c
F194:N (46<461[-10:10 -15:30 0:0])
FM194 1.872453e13
F204:N (47<471[-10:10 -15:30 0:0])
FM204 1.872453e13
F214:N (48<481[-10:10 -10:10 0:0])
FM214 1.872453e13
c
F224:N (49<491[-10:10 -15:30 0:0])
FM224 1.872453e13
F234:N (50<501[-10:10 -15:30 0:0])
FM234 1.872453e13
F244:N (51<511[-10:10 -10:10 0:0])
FM244 1.872453e13
c
c
F254:P (20<201[-30:30 -15:30 0:0])
FM254 1.872453e13
F264:P (23<231[-30:30 -15:30 0:0])
FM264 1.872453e13
F274:P (25<251[-30:30 -15:30 0:0])
FM274 1.872453e13
c
F284:P (31<311[-10:10  -15:30 0:0])
FM284 1.872453e13
F294:P (32<321[-10:10  -15:30 0:0])
FM294 1.872453e13
F304:P (33<331[-10:10  -10:10 0:0])
FM304 1.872453e13
c
F314:P (34<341[-10:10 -15:30 0:0])
FM314 1.872453e13
F324:P (35<351[-10:10 -15:30 0:0])
FM324 1.872453e13
F334:P (36<361[-10:10 -10:10 0:0])
FM334 1.872453e13
c
F344:P (37<371[-10:10 -15:30 0:0])
FM344 1.872453e13
F354:P (38<381[-10:10 -15:30 0:0])
FM354 1.872453e13
F364:P (39<391[-10:10 -10:10 0:0])
FM364 1.872453e13
c
F374:P (40<401[-10:10 -15:30 0:0])
FM374 1.872453e13
F384:P (41<411[-10:10 -15:30 0:0])
FM384 1.872453e13
F394:P (42<421[-10:10 -10:10 0:0])
FM394 1.872453e13
c
F404:P (43<431[-10:10 -15:30 0:0])
FM404 1.872453e13
```

```
F414:P (44<441[-10:10 -15:30 0:0])
FM414 1.872453e13
F424:P (45<451[-10:10 -10:10 0:0])
FM424 1.872453e13
c
F434:P (46<461[-10:10 -15:30 0:0])
FM434 1.872453e13
F444:P (47<471[-10:10 -15:30 0:0])
FM444 1.872453e13
F454:P (48<481[-10:10 -10:10 0:0])
FM454 1.872453e13
c
F464:P (49<491[-10:10 -15:30 0:0])
FM464 1.872453e13
F474:P (50<501[-10:10 -15:30 0:0])
FM474 1.872453e13
F484:P (51<511[-10:10 -10:10 0:0])
FM484 1.872453e13
c END OF FILE
```

HEU Target:

```
25 MeV e-,25 nC per pulse,120 Hz, HEU target without delayed neutrons
c CELL CARDS
c converter
1    1  -19.25      -1 2 -3                  IMP:N,P=1
c
c pre-collimator
4    3  -11.344      4 -5 6 -7 8 -9 10       IMP:N,P=1
c
c soil
8    5  -1.6        11 -12 13 -14 16 -17     IMP:N,P=1
c
c target
9    7  -18.75     -18                       IMP:N,P=1
c
c linac space
120  2  -1.205e-3  -120 #1 #4                IMP:N,P=1
c
c linac shielding
121  3  -11.344    -121 120                  IMP:N,P=1
c
c vehicle walls
100  8  -7.92      -100 101                  IMP:N,P=1
c air inside vehicle
101  2  -1.205e-3  -101 121                  IMP:N,P=1
c
c air outside vehicle
900  2  -1.205e-3   11 -12 14 -15 16 -17 100 18
                    20 23 25 31 32 33 34 35
                    36 37 38 39 40 41 42 43
                    44 45 46 47 48 49 50 51   IMP:N,P=1
c
c tally voxels
201 2 -1.205e-3  -201   U=1        LAT=1      IMP:N,P=1
231 2 -1.205e-3  -231   U=2        LAT=1      IMP:N,P=1
251 2 -1.205e-3  -251   U=3        LAT=1      IMP:N,P=1
311 2 -1.205e-3  -311   U=4        LAT=1      IMP:N,P=1
321 2 -1.205e-3  -321   U=5        LAT=1      IMP:N,P=1
331 2 -1.205e-3  -331   U=6        LAT=1      IMP:N,P=1
341 2 -1.205e-3  -341   U=7        LAT=1      IMP:N,P=1
351 2 -1.205e-3  -351   U=8        LAT=1      IMP:N,P=1
```

```
361 2 -1.205e-3  -361   U=9        LAT=1      IMP:N,P=1
371 2 -1.205e-3  -371   U=10       LAT=1      IMP:N,P=1
381 2 -1.205e-3  -381   U=11       LAT=1      IMP:N,P=1
391 2 -1.205e-3  -391   U=12       LAT=1      IMP:N,P=1
401 2 -1.205e-3  -401   U=13       LAT=1      IMP:N,P=1
411 2 -1.205e-3  -411   U=14       LAT=1      IMP:N,P=1
421 2 -1.205e-3  -421   U=15       LAT=1      IMP:N,P=1
431 2 -1.205e-3  -431   U=16       LAT=1      IMP:N,P=1
441 2 -1.205e-3  -441   U=17       LAT=1      IMP:N,P=1
451 2 -1.205e-3  -451   U=18       LAT=1      IMP:N,P=1
461 2 -1.205e-3  -461   U=19       LAT=1      IMP:N,P=1
471 2 -1.205e-3  -471   U=20       LAT=1      IMP:N,P=1
481 2 -1.205e-3  -481   U=21       LAT=1      IMP:N,P=1
491 2 -1.205e-3  -491   U=22       LAT=1      IMP:N,P=1
501 2 -1.205e-3  -501   U=23       LAT=1      IMP:N,P=1
511 2 -1.205e-3  -511   U=24       LAT=1      IMP:N,P=1
c
c tally planes
20 0             -20    FILL=1                IMP:N,P=1
23 0             -23    FILL=2                IMP:N,P=1
25 0             -25    FILL=3                IMP:N,P=1
31 0             -31    FILL=4                IMP:N,P=1
32 0             -32    FILL=5                IMP:N,P=1
33 0             -33    FILL=6                IMP:N,P=1
34 0             -34    FILL=7                IMP:N,P=1
35 0             -35    FILL=8                IMP:N,P=1
36 0             -36    FILL=9                IMP:N,P=1
37 0             -37    FILL=10               IMP:N,P=1
38 0             -38    FILL=11               IMP:N,P=1
39 0             -39    FILL=12               IMP:N,P=1
40 0             -40    FILL=13               IMP:N,P=1
41 0             -41    FILL=14               IMP:N,P=1
42 0             -42    FILL=15               IMP:N,P=1
43 0             -43    FILL=16               IMP:N,P=1
44 0             -44    FILL=17               IMP:N,P=1
45 0             -45    FILL=18               IMP:N,P=1
46 0             -46    FILL=19               IMP:N,P=1
47 0             -47    FILL=20               IMP:N,P=1
48 0             -48    FILL=21               IMP:N,P=1
49 0             -49    FILL=22               IMP:N,P=1
50 0             -50    FILL=23               IMP:N,P=1
51 0             -51    FILL=24               IMP:N,P=1
c
c outside world
12 0             -11:12:-13:15:-16:17         IMP:N,P=0
c END CELL CARDS-BLANK LINE FOLLOWS

c SURFACE CARDS
c converter
1  CZ   3.81
2  PZ   0.0
3  PZ   0.2286
c
c pre-collimator
4  PX -25
5  PX  25
6  PY -25
7  PY  25
8  PZ  28.1686
9  PZ  43.4086
10 KZ 89.1286 4.340277778e-4 -1
c
c boundary planes
```

```
11 PX -300
12 PX  300
15 PY  300
16 PZ -275
17 PZ  550
c
c ground
13 PY -250      $ ground 1m thick
14 PY -150      $ beam center-line 1.5m above ground
c
c heu target
18 SZ 543.4086 3.992945
c
c vehicle
100 101 RPP  -93.98 93.98  -93.98 93.98  -152.4  152.4
101 101 RPP  -91.44 91.44  -91.44 91.44  -149.86 152.4
120 102 RPP  -25    25     -25    25     -75     75
121 102 RPP  -32.62 32.62  -32.62 32.62  -85.62  75
c
c tally voxels
201  1   RPP  -5 5  -5 5  -0.5 0.5
231  4   RPP  -5 5  -5 5  -0.5 0.5
251  6   RPP  -5 5  -5 5  -0.5 0.5
311  12  RPP  -5 5  -5 5  -0.5 0.5
321  13  RPP  -5 5  -5 5  -0.5 0.5
331  14  RPP  -5 5  -5 5  -0.5 0.5
341  15  RPP  -5 5  -5 5  -0.5 0.5
351  16  RPP  -5 5  -5 5  -0.5 0.5
361  17  RPP  -5 5  -5 5  -0.5 0.5
371  18  RPP  -5 5  -5 5  -0.5 0.5
381  19  RPP  -5 5  -5 5  -0.5 0.5
391  20  RPP  -5 5  -5 5  -0.5 0.5
401  21  RPP  -5 5  -5 5  -0.5 0.5
411  22  RPP  -5 5  -5 5  -0.5 0.5
421  23  RPP  -5 5  -5 5  -0.5 0.5
431  24  RPP  -5 5  -5 5  -0.5 0.5
441  25  RPP  -5 5  -5 5  -0.5 0.5
451  26  RPP  -5 5  -5 5  -0.5 0.5
461  27  RPP  -5 5  -5 5  -0.5 0.5
471  28  RPP  -5 5  -5 5  -0.5 0.5
481  29  RPP  -5 5  -5 5  -0.5 0.5
491  30  RPP  -5 5  -5 5  -0.5 0.5
501  31  RPP  -5 5  -5 5  -0.5 0.5
511  32  RPP  -5 5  -5 5  -0.5 0.5
c
c tally planes
20    1  RPP  -300   300     -150 300  -0.5 0.5
23    4  RPP  -300   300     -150 300  -0.5 0.5
25    6  RPP  -300   300     -150 300  -0.5 0.5
31   12  RPP  -100   100     -150 300  -0.5 0.5
32   13  RPP  -100   100     -150 300  -0.5 0.5
33   14  RPP  -93.98  93.98     0 200  -0.5 0.5
34   15  RPP  -100   100     -150 300  -0.5 0.5
35   16  RPP  -100   100     -150 300  -0.5 0.5
36   17  RPP  -93.98  93.98     0 200  -0.5 0.5
37   18  RPP  -100    100    -150 300  -0.5 0.5
38   19  RPP  -100    100    -150 300  -0.5 0.5
39   20  RPP  -93.98   93.98    0 200  -0.5 0.5
40   21  RPP  -100    100    -150 300  -0.5 0.5
41   22  RPP  -100    100    -150 300  -0.5 0.5
42   23  RPP  -93.98   93.98    0 200  -0.5 0.5
43   24  RPP  -100    100    -150 300  -0.5 0.5
44   25  RPP  -100    100    -150 300  -0.5 0.5
```

```
45   26  RPP  -93.98   93.98    0 200  -0.5 0.5
46   27  RPP  -100    100    -150 300  -0.5 0.5
47   28  RPP  -100    100    -150 300  -0.5 0.5
48   29  RPP  -93.98   93.98    0 200  -0.5 0.5
49   30  RPP  -100    100    -150 300  -0.5 0.5
50   31  RPP  -100    100    -150 300  -0.5 0.5
51   32  RPP  -93.98   93.98    0 200  -0.5 0.5
c END SURFACE CARDS-BLANK LINE FOLLOWS

c DATA CARDS
c
c GEOMETRY TRANSLATIONS
TR1     0     0     50.0
TR4     0     0    343.4086
TR6     0     0    538.4086
TR12 -193.98  0     24.0
TR13  193.98  0     24.0
TR14    0    93.98  24.0
TR15 -193.98  0      4.0
TR16  193.98  0      4.0
TR17    0    93.98   4.0
TR18 -193.98  0    -16.0
TR19  193.98  0    -16.0
TR20    0    93.98 -16.0
TR21 -193.98  0    -36.0
TR22  193.98  0    -36.0
TR23    0    93.98 -36.0
TR24 -193.98  0    -56.0
TR25  193.98  0    -56.0
TR26    0    93.98 -56.0
TR27 -193.98  0    -76.0
TR28  193.98  0    -76.0
TR29    0    93.98 -76.0
TR30 -193.98  0    -96.0
TR31  193.98  0    -96.0
TR32    0    93.98 -96.0
TR101   0     0   -102.9914
TR102   0     0    -31.5914
c
c SDEF CARD - MANDITORY
SDEF
c
c MATERIAL DEFINITIONS
c tungsten
M1 NLIB=60c PLIB=02p
     74182 0.2642
     74183 0.1428
     74184 0.307
     74186 0.286
c
c air at 45% humidity
M2 NLIB=60c PLIB=02p
     1001      1.169196E-02
     1002      1.344730E-06
     7014      7.681679E-01
     7015      2.837299E-03
     8016      2.121736E-01
     8017      5.168377E-04
     18000.59c 4.611104E-03
c
c natural lead
M3 NLIB=60c PLIB=02p
     82206 0.255
```

```
     82207 0.221
     82208 0.524
c
c lanl soil with 20% water
M5 NLIB=60c PLIB=02p
     1001  4.832564E-02
     1002  5.558087E-06
     8016  6.950058E-01
     8017  1.692978E-03
     11023 3.155206E-03
     13027 3.045777E-02
     14000 2.097394E-01
     19000 4.523070E-03
     26054 4.146826E-04
     26056 6.509629E-03
     26057 1.503357E-04
     26058 2.000693E-05
c
c highly enriched uranium
M7 NLIB=60c PLIB=02p
     92238 0.02
     92235 0.98
c
c stainless steel
M8 NLIB=60c PLIB=02p
     26054 3.470e-3
     26056 5.447e-2
     26057 1.258e-3
     24050 7.573e-4
     24052 1.450e-2
     24053 1.656e-3
     24054 4.122e-4
     28058 5.288e-3
     28060 2.024e-3
     28064 7.148e-4
     25055 1.740e-3
c
TOTNU
MODE   N  P
PHYS:N 30 30
PHYS:P 3J
CUT:P  2J 0
NPS    1
PRINT  10 40 50 110 126 128 140
IDUM   55 1 2 1 1
RDUM   0.001 0.001 $ J J J 1000 9E4
FILES 21 heu5p0.d J F 6J 55 heu5mt.xo
dbcn 7j        1
c
c tallies
F14:N (20<201[-30:30 -15:30 0:0])
FM14 1.872453e13
F24:N (23<231[-30:30 -15:30 0:0])
FM24 1.872453e13
F34:N (25<251[-30:30 -15:30 0:0])
FM34 1.872453e13
c
F44:N (31<311[-10:10 -15:30 0:0])
FM44 1.872453e13
F54:N (32<321[-10:10 -15:30 0:0])
FM54 1.872453e13
F64:N (33<331[-10:10 -10:10 0:0])
FM64 1.872453e13
```

```
c
F74:N (34<341[-10:10 -15:30 0:0])
FM74 1.872453e13
F84:N (35<351[-10:10 -15:30 0:0])
FM84 1.872453e13
F94:N (36<361[-10:10 -10:10 0:0])
FM94 1.872453e13
c
F104:N (37<371[-10:10 -15:30 0:0])
FM104 1.872453e13
F114:N (38<381[-10:10 -15:30 0:0])
FM114 1.872453e13
F124:N (39<391[-10:10  -10:10 0:0])
FM124 1.872453e13
c
F134:N (40<401[-10:10 -15:30 0:0])
FM134 1.872453e13
F144:N (41<411[-10:10 -15:30 0:0])
FM144 1.872453e13
F154:N (42<421[-10:10 -10:10 0:0])
FM154 1.872453e13
c
F164:N (43<431[-10:10 -15:30 0:0])
FM164 1.872453e13
F174:N (44<441[-10:10 -15:30 0:0])
FM174 1.872453e13
F184:N (45<451[-10:10 -10:10 0:0])
FM184 1.872453e13
c
F194:N (46<461[-10:10 -15:30 0:0])
FM194 1.872453e13
F204:N (47<471[-10:10 -15:30 0:0])
FM204 1.872453e13
F214:N (48<481[-10:10 -10:10 0:0])
FM214 1.872453e13
c
F224:N (49<491[-10:10 -15:30 0:0])
FM224 1.872453e13
F234:N (50<501[-10:10 -15:30 0:0])
FM234 1.872453e13
F244:N (51<511[-10:10 -10:10 0:0])
FM244 1.872453e13
c
c
F254:P (20<201[-30:30 -15:30 0:0])
FM254 1.872453e13
F264:P (23<231[-30:30 -15:30 0:0])
FM264 1.872453e13
F274:P (25<251[-30:30 -15:30 0:0])
FM274 1.872453e13
c
F284:P (31<311[-10:10  -15:30 0:0])
FM284 1.872453e13
F294:P (32<321[-10:10  -15:30 0:0])
FM294 1.872453e13
F304:P (33<331[-10:10  -10:10 0:0])
FM304 1.872453e13
c
F314:P (34<341[-10:10 -15:30 0:0])
FM314 1.872453e13
F324:P (35<351[-10:10 -15:30 0:0])
FM324 1.872453e13
F334:P (36<361[-10:10 -10:10 0:0])
```

```
FM334 1.872453e13
c
F344:P (37<371[-10:10 -15:30 0:0])
FM344 1.872453e13
F354:P (38<381[-10:10 -15:30 0:0])
FM354 1.872453e13
F364:P (39<391[-10:10 -10:10 0:0])
FM364 1.872453e13
c
F374:P (40<401[-10:10 -15:30 0:0])
FM374 1.872453e13
F384:P (41<411[-10:10 -15:30 0:0])
FM384 1.872453e13
F394:P (42<421[-10:10 -10:10 0:0])
FM394 1.872453e13
c
F404:P (43<431[-10:10 -15:30 0:0])
FM404 1.872453e13
F414:P (44<441[-10:10 -15:30 0:0])
FM414 1.872453e13
F424:P (45<451[-10:10 -10:10 0:0])
FM424 1.872453e13
c
F434:P (46<461[-10:10 -15:30 0:0])
FM434 1.872453e13
F444:P (47<471[-10:10 -15:30 0:0])
FM444 1.872453e13
F454:P (48<481[-10:10 -10:10 0:0])
FM454 1.872453e13
c
F464:P (49<491[-10:10 -15:30 0:0])
FM464 1.872453e13
F474:P (50<501[-10:10 -15:30 0:0])
FM474 1.872453e13
F484:P (51<511[-10:10 -10:10 0:0])
FM484 1.872453e13
c END OF FILE
```

APPENDIX G

MCNPX INPUT FILE FOR THE DELAYED NEUTRON SOURCE

Appendix G. MCNPX Input File for the Delayed Neutron Source

```
Approximate delayed neutron source, DU target, 2D neutron field
c CELL CARDS
c converter
1    1  -19.25      -1 2 -3                  IMP:N,P=1
c
c pre-collimator
4    3  -11.344      4 -5 6 -7 8 -9 10       IMP:N,P=1
c
c soil
8    5  -1.6        11 -12 13 -14 16 -17     IMP:N,P=1
c
c target
9    7  -18.95     -18                       IMP:N,P=1
c
c linac space
120  2  -1.205e-3  -120 #1 #4                IMP:N,P=1
c
c linac shielding
121  3  -11.344    -121 120                  IMP:N,P=1
c
c vehicle walls
100  8  -7.92      -100 101                  IMP:N,P=1
c air inside vehicle
101  2  -1.205e-3  -101 121                  IMP:N,P=1
c
c air outside vehicle
900  2  -1.205e-3   11 -12 14 -15 16 -17 100 18 IMP:N,P=1
c
c outside world
12 0             -11:12:-13:15:-16:17        IMP:N,P=0
c END CELL CARDS-BLANK LINE FOLLOWS

c SURFACE CARDS
c converter
1  CZ   3.81
2  PZ   0.0
3  PZ   0.2286
c
c pre-collimator
4  PX -25
5  PX  25
6  PY -25
7  PY  25
8  PZ  28.1686
9  PZ  43.4086
10 KZ  89.1286 4.340277778e-4 -1
c
c boundary planes
11 PX -300
12 PX  300
15 PY  300
16 PZ -275
17 PZ  550
c
c ground
13 PY -250      $ ground 1m thick
14 PY -150      $ beam center-line 1.5m above ground
c
c target
```

```
18 SZ 543.4086 3.978848
c
c vehicle
100 101 RPP  -92.075 92.075 -92.075 92.075 -150.495 152.4
101 101 RPP  -91.44  91.44  -91.44  91.44  -149.86  152.4
120 102 RPP  -25     25     -25     25     -75      75
121 102 RPP  -32.62  32.62  -32.62  32.62  -85.62   75
c
c END SURFACE CARDS-BLANK LINE FOLLOWS

c DATA CARDS
c
c GEOMETRY TRANSLATIONS
TR101   0     0   -102.9914
TR102   0     0    -31.5914
c
c MATERIAL DEFINITIONS
c tungsten
M1   NLIB=60c  PLIB=02p
     74182     0.2642
     74183     0.1428
     74184     0.307
     74186     0.286
c
c air at 45% humidity
M2   NLIB=60c  PLIB=02p
     1001      1.169196E-02
     1002      1.344730E-06
     7014      7.681679E-01
     7015      2.837299E-03
     8016      2.121736E-01
     8017      5.168377E-04
     18000.59c 4.611104E-03
c
c natural lead
M3   NLIB=60c  PLIB=02p
     82206     0.255
     82207     0.221
     82208     0.524
c
c LANL soil with 20% of water
M5   NLIB=60c  PLIB=02p
     1001      4.832564E-02
     1002      5.558087E-06
     8016      6.950058E-01
     8017      1.692978E-03
     11023     3.155206E-03
     13027     3.045777E-02
     14000     2.097395E-01
c     14028     1.934420e-1
c     14029     9.822516e-3
c     14030     6.475075e-3
     19000     4.523070E-03
     26054     4.146826E-04
     26056     6.509629E-03
     26057     1.503357E-04
     26058     2.000693E-05
c
c depleted uranium
M7   NLIB=60c  PLIB=02p
     92238     1.0
c
c stainless steel
```

```
M8   NLIB=60c  PLIB=02p
     26054     3.470e-3
     26056     5.447e-2
     26057     1.258e-3
     24050     7.573e-4
     24052     1.450e-2
     24053     1.656e-3
     24054     4.122e-4
     28058     5.288e-3
     28060     2.024e-3
     28064     7.148e-4
     25055     1.740e-3
c
c SOURCE DEFINITION
c Delayed neutron source approximated as a 400keV Maxwellian distribution
c sampled uniformly in the spherical depleted uranium target
SDEF PAR=N  ERG=D1  POS=0.0 0.0 543.4086  RAD=D2
SP1  -2  0.40
SI2  3.9978848
c END OF SOURCE DEFINITION
c
MODE P N
c PHYS:P  3J  1
PHYS:N  30
c CUT:P   J   4
CUT:N   2J -0.001
TOTNU
NPS     5E8
PRINT   10 40 50 110 126 140
c PRDMP   J  -60  J  2
c
c TALLY SPECIFICATION
FC2 Neutron energy tally on the surface of the target
F2:N  18
E2 0 299i 3 19i 5 9i 10 11 12 13 14 15
c
c MESH TALLIES
c ZX plane y=0 (y goes from -1 cm to 1 cm)
tmesh
rmesh1:n flux
cora1  -300 299i 300
corb1    -1       1
corc1  -275 411i 550
endmd
c END OF FILE
```

APPENDIX H

RELATIVE ERRORS ON DELAYED NEUTRON FLUENCE MAPS

Appendix H. Relative Errors on Delayed Neutron Fluence Maps

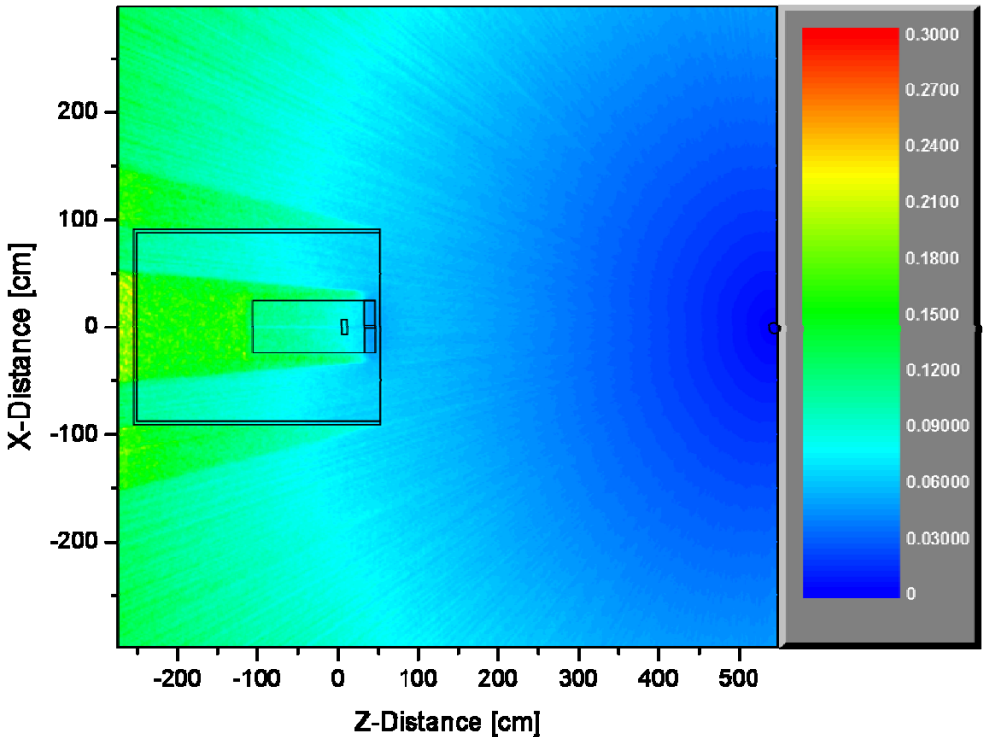

Figure H-1. Relative errors for the delayed neutron fluence map shown in Figure 51.

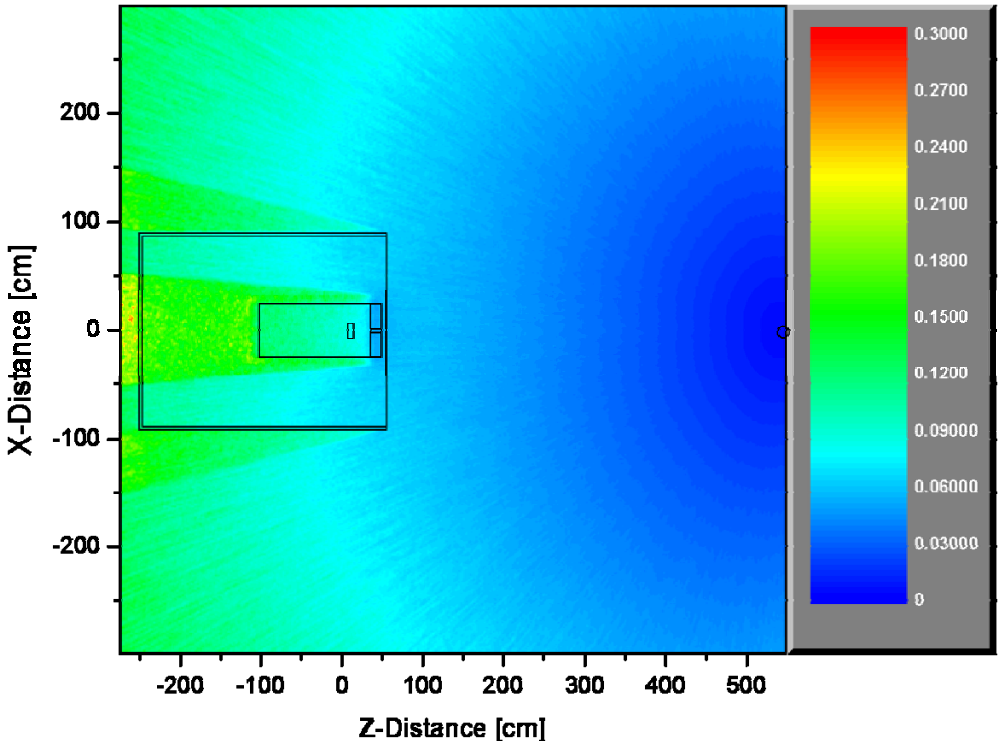

Figure H-2. Relative errors for the delayed neutron fluence map shown in Figure 52.

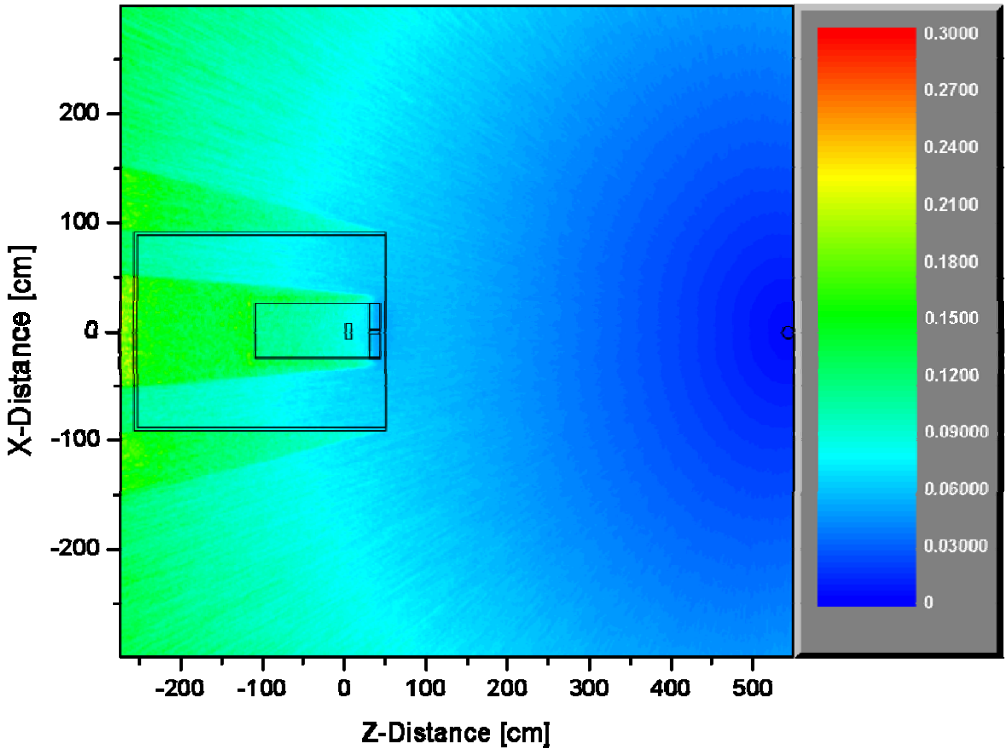

Figure H-3. Relative errors for the delayed neutron fluence map shown in Figure 53.

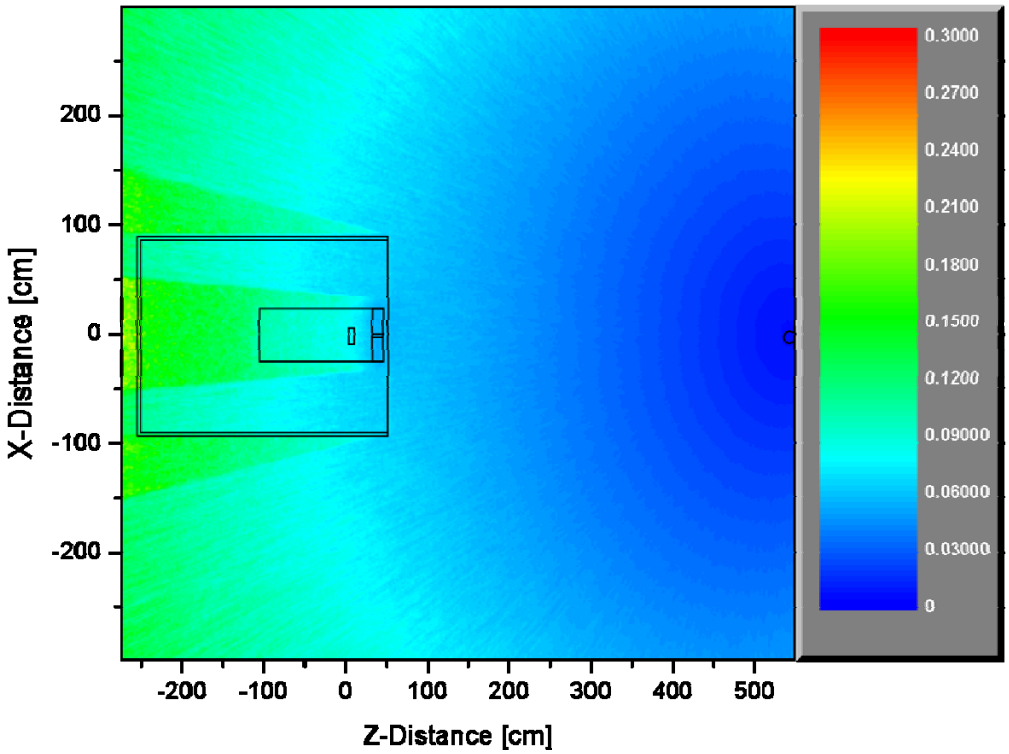

Figure H-4. Relative errors for the delayed neutron fluence map shown in Figure 54.

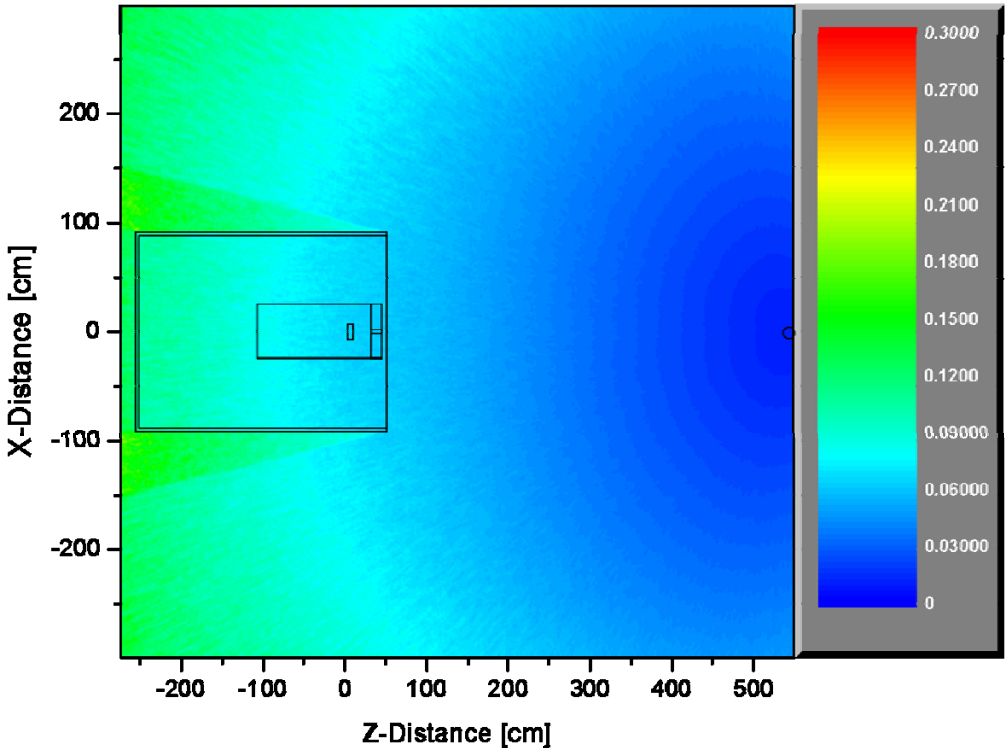

Figure H-5. Relative errors for the delayed neutron fluence map shown in Figure 55.

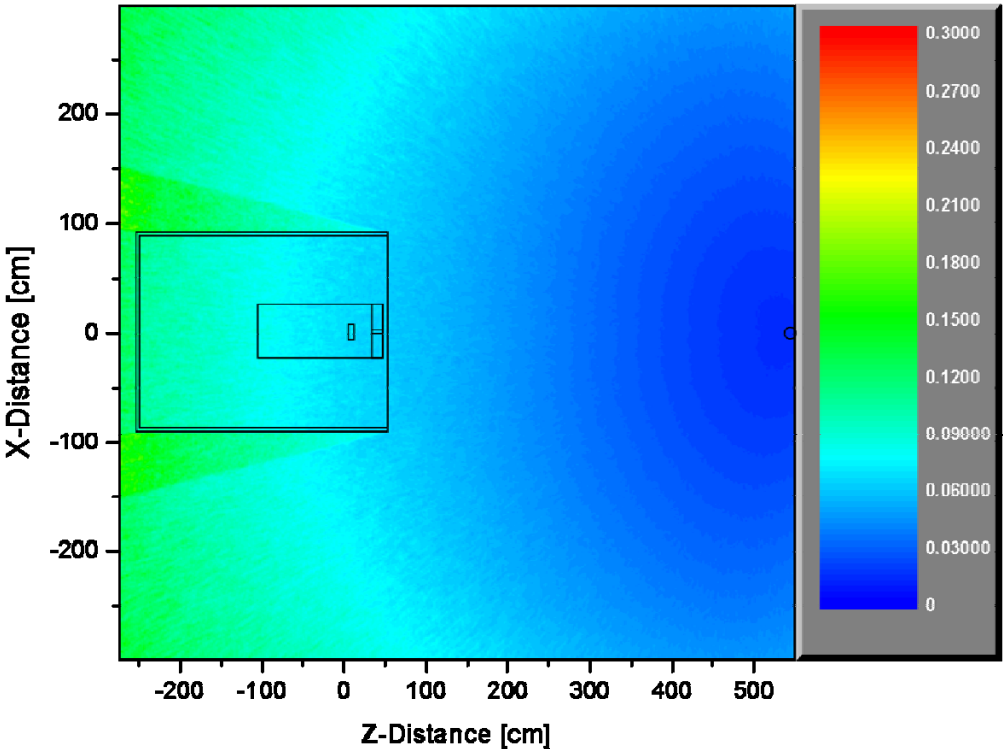

Figure H-6. Relative errors for the delayed neutron fluence map shown in Figure 56.

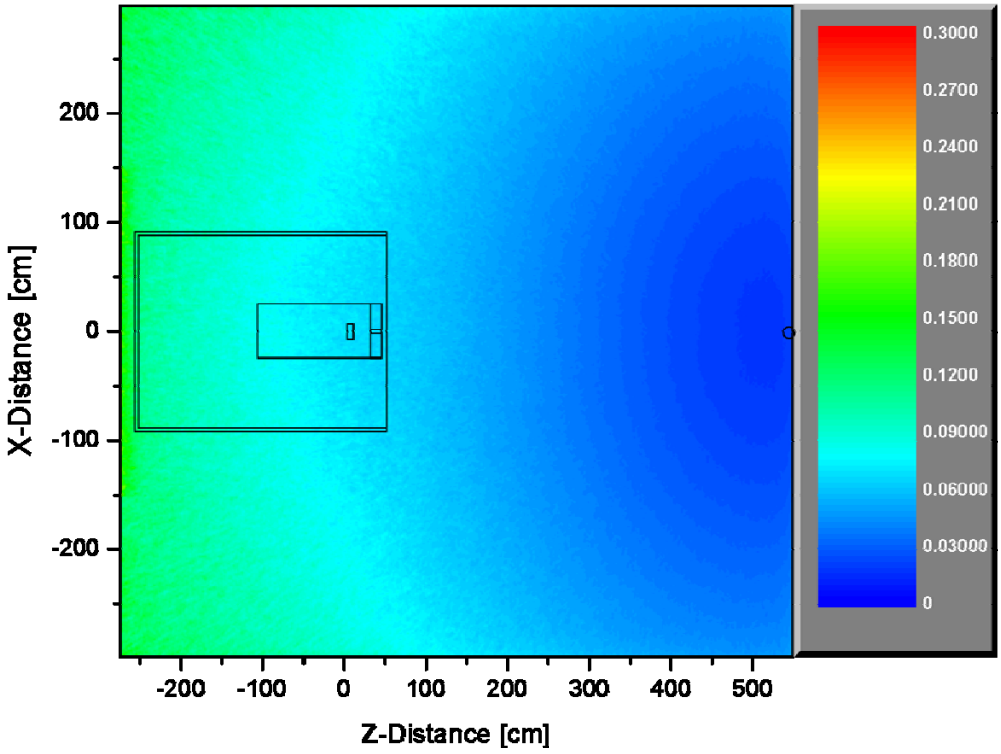

Figure H-7. Relative errors for the delayed neutron fluence map shown in Figure 57.

INTERNAL DISTRIBUTION

1. Sara Pozzi
2. Marek Flaska
3. Thomas Miller
4. Vladimir Protopopescu